VECTOR SUM PHASE SHIFTER USING A QUADRATURE MAGIC-T FOR APPLICATION IN POLARIZATION CONTROL

LU WEI JIA
(B.Eng. (Hons.), NUS)

A THESIS SUBMITTED

FOR THE DEGREE OF MASTER OF ENGINEERING

DEPARTMENT OF ELECTRICAL AND COMPUTER ENGINEERING

NATIONAL UNIVERSITY OF SINGAPORE

2014

Declaration

I hereby declare that this thesis is my original work and it has been written by me in its entirety. I have duly acknowledged all the sources of information which have been used in the thesis. This thesis has also not been submitted for any degree in any university previously

_____

LU WEI JIA
9 April 2014

Acknowledgement

I wish to express my sincere gratitude to my supervisor, Associate Professor Koen Mouthaan, for his support, encouragement, understanding and guidance that made this dissertation possible. Without him pointing me in the right direction, this project would not have been completed.

I would like to thank Mr Joseph Ting Sing Kwong and Dr. Chio Tan Huat from NUS Temasek Laboratories (TL). Without their understanding and support in my studies, it will not be possible for me to complete my part-time master of engineering while working.

Special thanks also to Madam Lee Siew Choo in the Microwave Research Lab (NUS) and Mr. Tan Peng Khiang in the Antenna Group (NUS TL). Without Madam Lee's technical support in fabricating the circuits and Peng Khiang's knowledge in the available fabrication technologies and proper handling of the test equipment, the prototype would not have been built and tested.

In addition, I also thank Mr. Tang Xingyi and Mr. Ray Fang for their valuable discussion and assistance in every aspect of this project. Their readiness to share their knowledge and expertise has greatly benefitted my learning.

I also appreciate my colleagues at NUS TL for their understanding and encouragement they have given to me along the way. Last but not least, I would like to take the opportunity to thank my parents and my little brother for their love and support through the whole journey.

Table of Contents

Summary

Polarization refers to the orientation of the electric field as electromagnetic (EM) waves propagate through space. The commonly used polarizations include vertical (V), horizontal (H), slant +/-45°, left hand circular polarization (LHCP) and right hand circulator polarization (RHCP). Its application can be found in both military and commercial systems. In military radar systems, it is used for target identification; in electronic warfare systems, it is used for jamming and counter-jamming. Commercial systems use it to increase the communication capacity through polarization diversity. Therefore, the ability to have polarization diversity is greatly desired.

An electromagnetic wave is transmitted or received in a polarization that is determined by the antenna. The polarization, however, can be controlled when a polarization controller is used with a dual-polarized antenna. The polarization controller changes the polarization by varying the amplitude and the phase of the signal feed to the antenna. It employs either an RF switch, or a hybrid circuit and phase shifters to control the signals to or from the antenna.

The aim of this thesis is to investigate and implement a wideband two-way vector sum phase shifter for the application in polarization control. A key novel development is the Quadrature Magic-T circuit discussed in Chapter 3. A typical magic-T produces 0° and 180° phase difference between the two collinear arms when the sum-port and the delta-port are excited respectively. In the Quadrature Magic-T circuit, besides having the typical magic-T response, the input phase

difference between the sum- and delta-ports needs to be 90° apart in order to achieve excitation in only one of the collinear arms. This feature ensures that the signals at the two outputs are vector summed together when both the sum-port and delta-port are excited in phase. The pair of output signals has equal amplitude but variable phase difference. As such, the Quadrature Magic-T is a crucial component in the proposed two-way vector sum phase shifter design.

The proposed two-way vector sum phase shifter with 180° phase tuning uses a power divider, a Quadrature Magic-T and two variable gain amplifiers. To extend the phase coverage, two broadband 90° phase shifters and four RF switches are included. The individual components are separately designed and tested to verify their performance. The final design of the two-way vector sum phase shifters has a 360° phase tuning from 2 GHz to 6 GHz. When connected to a dual-polarization antenna arranged in +/- 45°, the circuit is able to achieve the standard V, H, RHCP and LHCP polarizations with full RF power.

Besides polarization control, the circuit developed in this thesis is also useful for beam steering in a phased array antenna and phase modulation in a communication system. With further optimization and size reduction, the circuit has the potential of becoming a new device in the range of microwave and millimeter wave.

List of Tables

List of Figures

List of Symbols

Z_0	Characteristic impedance (Ω)
Z_{0e}	Even mode impedance (Ω)
Z_{0o}	Odd mode impedance (Ω)
ω	Angular frequency (rad s^{-1})
k	Wave number (m^{-1})
f	Frequency (Hz)
λ	Wavelength (m)
$\boldsymbol{E}$	Electric field intensity (V/m)
E_x	Electric field amplitude in x direction
E_y	Electric field amplitude in y direction
$\boldsymbol{H}$	Magnetic field intensity (A/m)
$\vec{x}$	Unit vector in x direction
$\vec{y}$	Unit vector in y direction
ADS	Advanced Design System
RHCP	Right hand circular polarized
LHCP	Left hand circular polarized

V	Vertical polarization
H	Horizontal polarization
EM	Electromagnetic
VGA	Variable gain amplifier
∀	For all

Chapter 1 Introduction

1.1   Background

Polarization of the electromagnetic (EM) wave has been widely exploited in communication systems and radars. There are many reasons for the need to control the polarization of the transmitted and received EM wave.

In geostationary communication satellites, polarization is used to double the channel capacity of the satellite link. This is achieved by broadcasting a signal in the vertical plane and another signal in the horizontal plane. Therefore, both signals can be transmitted at the same frequency without interfering with each other. When such systems are used, polarization alignment between the base station on earth and the satellite becomes important. The rejection of the undesired polarization must therefore be high [1]. As such, it is necessary for the base station on earth to have the ability to adjust its polarization.

Polarization is also important in the transmission of radar pulses and reception of radar reflections by the same or a different antenna. Radar determines the targets' speed, range, altitude, direction and characteristics by transmitting and measuring the wave reflected from the target. A complex scatterer has a unique polarization conversion characteristic that is used in target identification process [2]. In addition, some targets have very different radar cross sections (RCS) when they are illuminated with signals of different polarizations. As such, the radar's ability to identify the objects can be greatly enhanced if it is able to transmit and

receive in different polarizations [2]. In the presence of rain, it is desirable to transmit and receive in the same circular polarization. This is because the backscatter of the rain is in the opposite circular polarization while the return from the actual target is in a polarization that is similar to the transmitted signals [3]. In electronic warfare, radar jamming is used to conceal aircrafts from the radars that guide surface to air missiles. The attempt to jam the radar can be made difficult if the radar is able to operate in different polarizations and frequencies [2], [4].

1.1.1 Polarization of EM waves

For plane transverse electromagnetic waves travelling in free space, the electric field intensity, **E**, and magnetic field intensity, **H**, are orthogonal to each other and are always perpendicular to the direction of wave propagation. The polarization of uniform plane waves is defined as the direction of the time varying behavior of the electric field intensity vector, **E,** at some fixed point in space, along the direction of propagation [5].

There are two main types of polarizations – linear and elliptical. Linear polarizations refer to the cases when the electric field is always directed along a straight line. They include vertical polarization, horizontal polarization and slant polarization. The electric field of vertical polarization lies on the vertical plane and the electric field of horizontal field lies on the horizontal plane. For slant polarization, the most widely used cases are the slant +/-45° which have equal vertical and horizontal components.

For the case in which the direction of the electric field is changing with time, it is classified as elliptical polarization. Left handed circularly polarization (LHCP) and right handed circularly polarization (RHCP) are special cases of elliptical polarization. For any other cases (both time variant and invariant), the polarization can always decompose into either a pair of orthogonally linear polarizations or a pair of oppositely circular polarizations.

1.1.2 Mathematical representation of polarization

For the convenience of the discussion, let's assume that the wave is always propagating in the z-direction. The electric field of the electromagnetic wave propagating in the z direction is given by:

$$\vec{E}(x,y,z,t) = \left[E_x \vec{x} e^{j(\varphi_x)} + E_y \vec{y} e^{j(\varphi_y)} \right] e^{j(\omega t - kz)} \tag{1-1}$$
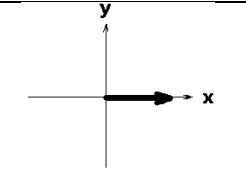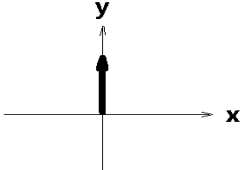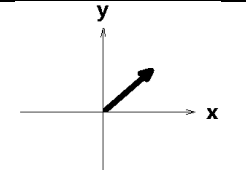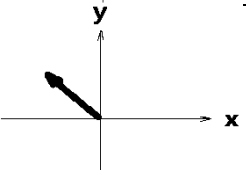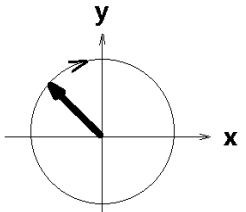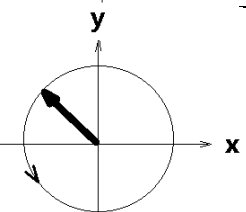
where E_x and E_y are the electric field amplitudes; φ_x and φ_y are the corresponding phases; $\omega = 2\pi f$ is the angular frequency and $k = 2\pi/\lambda$ is the wave number, $\vec{x}$ and $\vec{y}$ are unit vectors in x and y direction respectively. (1-1) can be represented in Jones vector as:

$$\vec{E} = e^{j(\omega t - kz)} e^{j(\varphi_x)} \begin{pmatrix} E_x \\ E_y e^{j(\varphi_y - \varphi_x)} \end{pmatrix} \tag{1-2}$$

The vector inside the big bracket indicates the amplitude in $\vec{x}$ and $\vec{y}$ direction and their relative phases. They are independent of time and are the absolute phase. It is more convenient to use it to represent the polarization of the wave. The commonly used polarizations include linear and circular polarizations. Table 1-1

lists the main polarizations and their mathematical and graphic vector representation.

Table 1-1: Main polarizations.

Polarization	Normalized Jone vector	Graphic Vector
Horizontal	$\begin{pmatrix} 1 \\ 0 \end{pmatrix}$	
Vertical	$\begin{pmatrix} 0 \\ 1 \end{pmatrix}$	
Slant 45°	$\frac{1}{\sqrt{2}} \begin{pmatrix} 1 \\ 1 \end{pmatrix}$	
-Slant 45°	$\frac{1}{\sqrt{2}} \begin{pmatrix} -1 \\ 1 \end{pmatrix}$	
LHCP	$\frac{1}{\sqrt{2}} \begin{pmatrix} 1 \\ -j \end{pmatrix}$	
RHCP	$\frac{1}{\sqrt{2}} \begin{pmatrix} 1 \\ j \end{pmatrix}$	

Circular polarization is a special case of elliptical polarization when the phase difference between $\vec{x}$ and $\vec{y}$ components of the electric field is 90°. Elliptical polarization can be obtained if the relative phase is different from 90°. The polarization of the wave is dependent on the relative amplitude and phase in $\vec{x}$ and $\vec{y}$ direction.

1.1.3 Polarization control methods

1.1.3.1 Polarization of antenna

The EM wave used for either communication or radar is transmitted through an antenna. The polarization of the EM wave is dependent on the polarization of the antenna. Antenna polarization is a characteristic of the antenna and its orientation [6]. Thus, a simple straight wire antenna will have one polarization when mounted vertically, and a different polarization when mounted horizontally. An antenna capable of transmitting one polarization is called single-polarized antenna while the antenna capable of transmitting in two orthogonal polarizations and their combinations is called dual-polarized antenna.

As examples, Fig. 1-1 shows a linearly polarized horn antenna, Fig. 1-2 shows a dual linear polarization horn antenna, Fig. 1-3 shows a circularly polarized spiral antenna, and Fig. 1-4 shows a dual linearly polarized array, which consists of large number of horizontally polarized elements and vertically polarized elements.

Fig. 1-1: Single polarization horn antenna.
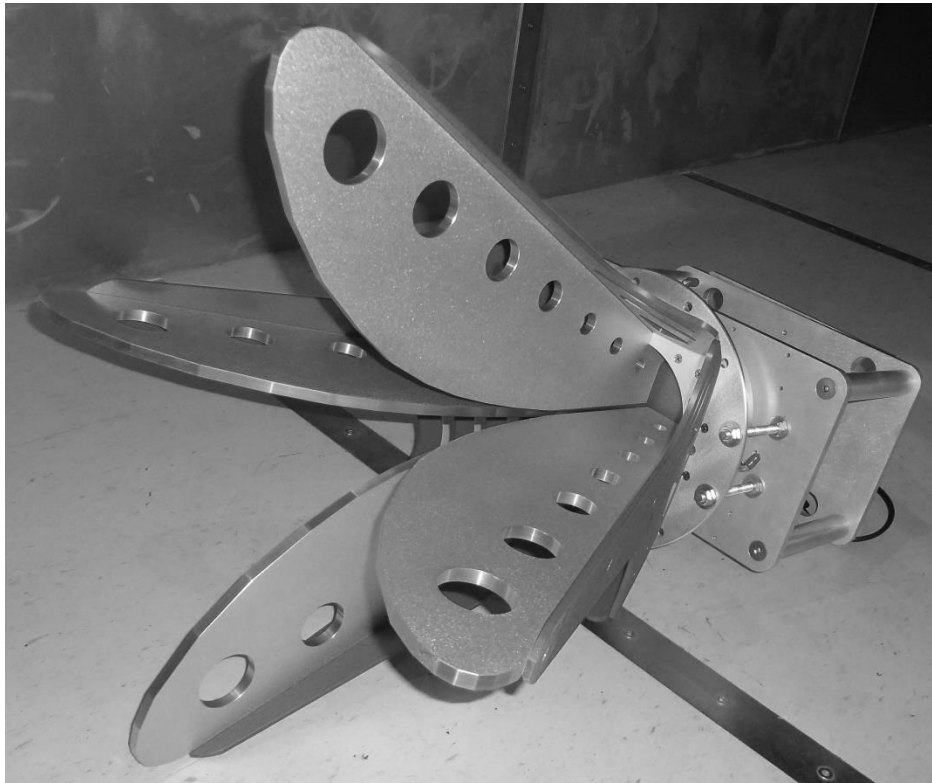
Fig. 1-2: Dual linear polarization horn antenna.
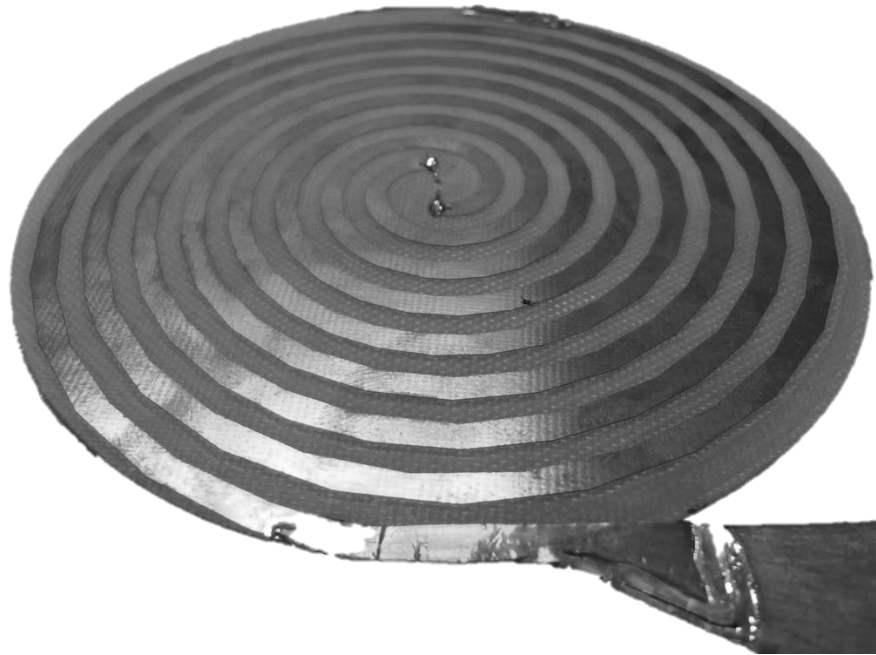
Fig. 1-3: Circular polarization spiral antenna.
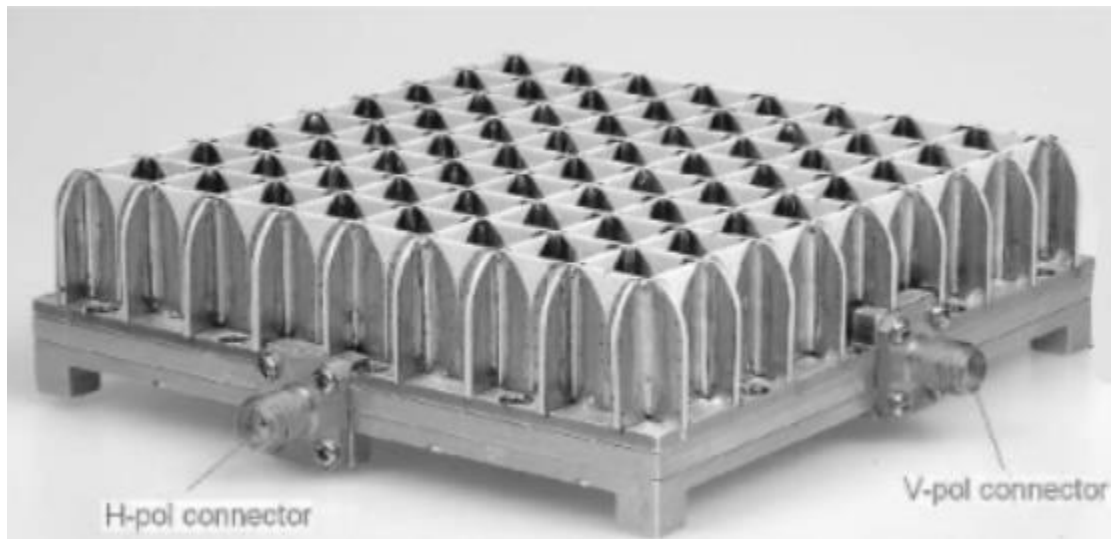
Fig. 1-4: Dual linear polarization array taken from [7].

It is important to note that the dual linear polarization antenna can also be converted into a circular polarized antenna by exciting them with a 90° phase difference, or a slant polarized antenna by exciting them in phase (slant +45°) or

out-of phase (slant-45°). Similarly, dual circular polarized antennas (RHCP and LHCP) are also able to achieve linear polarization (V, H, and slant +/-45°). As such, choosing the type of antenna is the first step in controlling the polarization of the electromagnetic wave.

1.1.3.2 Feeding circuit

From (1-2), the polarization of the EM wave can be varied by controlling its phase and the amplitude. The simplest way to control the amplitude is to switch on or off the excitation of a single-polarized antenna which is transmitting or receiving the EM wave. Using this method, one can achieve the targeted polarization depending on the type of the antenna used. For generating different polarizations, more than one antenna has to be used if the antenna used is not dual polarized. The drawbacks of this method include: a) occupy more space, b) lack of collocated phase center, c) may require high power switch for transmitting, d) less efficient for transmitting and poorer noise figure for receiving due to the insertion loss of the switch.

A more efficient way to control the polarization is to use a dual-polarized antenna and a polarization control circuit. Besides occupying a smaller space and having a collocated phase center, it is able to generate all the polarization states by using different pairs of excitation. The excitations to the orthogonally placed radiators of the antenna can be controlled using either switches, or variable gain amplifiers, or attenuators or phase shifters. [1], [8], [9].

Fig. 1-5 shows the architecture of a polarization controller proposed in [9]. A power divider splits the input signal equally. The phases of each signal are then adjusted using phase shifters and the power amplifier boosts up their amplitude. The signals, which normally have a relatively high power at this point, are summed by a 90° hybrid and fed to the feeds of the dual-polarization antenna.
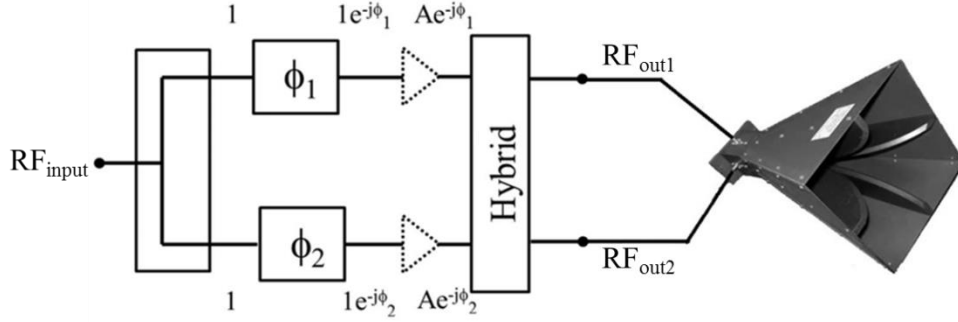
Fig. 1-5: Polarization controller architecture.

Assume the amplitude and the phase of the signal at each branch after the power divider to be 1 volt and 0°, respectively. The signals before entering the hybrid are $Ae^{-j\phi_1}$ and $Ae^{-j\phi_2}$. When a quadrature hybrid is used, the output signals are:

$$RF_{out1} = Be^{j(\frac{\pi}{4}-\frac{\phi_1}{2}-\frac{\phi_2}{2})}\left(2\cos(\frac{\pi}{4}+\frac{\phi_2}{2}-\frac{\phi_1}{2})\right) \tag{1-3}$$

$$RF_{out2} = Be^{j(\frac{\pi}{4}-\frac{\phi_1}{2}-\frac{\phi_2}{2})}\left(2\cos(\frac{\pi}{4}+\frac{\phi_1}{2}-\frac{\phi_2}{2})\right) \tag{1-4}$$

where $B = -\frac{1}{\sqrt{2}}A$. From the equations, it can be observed that the amplitude difference between the output signals is dependent on the phase difference between the input signals at the hybrids. There is no phase difference between the

9

two RF outputs. Hence, only four main polarization states can be achieved with full power, as listed in Table 1-2. For RHCP and LHCP, one of the paths has to be disconnected and the corresponding power cannot be utilized.

Table 1-2: Four main polarizations with full power.

Polarization	$\phi_1 - \phi_2$	RF_{out1}	RF_{out2}
V	$\pi/2$	*2B*	0
H	$-\pi/2$	0	*2B*
Slant 45°	0	$\sqrt{2}B$	$\sqrt{2}B$
Slant -45°	π	$\sqrt{2}B$	$-\sqrt{2}B$

For the four main polarization states, the circuit will make full use of the power amplifier in each path without using a high power RF switch, which is normally bulky, expensive, and easily damaged. The advantage will be more obvious if the circuit is used in an active antenna array.

1.2 Motivation

Polarization diversity is important to defense and communication applications. As such, there is a market for high performance polarization controller. In addition, with phased arrays gaining popularity, a large number of easily controllable and cheap polarization control circuits is needed.

The existing polarization control method using phasing (as highlighted in section 1.1.3.2) uses fixed phase shifters. The performance of the circuit depends heavily on the phase shifters and 90° hybrid. In addition, the circuit presented by

10

[9] can only achieve linear polarization control and has less than an octave bandwidth. Thus, there is a strong interest to improve the polarization control circuitry, especially for the application in phased arrays.

A question to ask is whether it is possible to get rid of the hybrid after the power amplifier for better efficiency and whether the polarization control circuit can be further improved for larger bandwidth with simpler circuitry. In addition, can the circuit achieve circular polarizations? In section 1.1.2, it has been shown that polarization can be changed by either adjusting the amplitude or the phase of the signals fed to the dual-polarized antenna. As such, a polarization controller circuit that focuses on changing the phase between the outputs is considered.

Vector sum phase shifters are known for their simple concept and wide phase shift coverage. They are good candidates to change the phase shift of the signals. While both 180° hybrid and a 90° hybrid can be used for summing the signals, the 90° hybrid is normally used because of its inherent ability to vector sum the signals. However, it is not easy to realize wideband 90° hybrid. Thus, a novel two-way vector sum phase shifter that uses broadband Quadrature Magic-T and spatial power combining is proposed, studied and implemented in this thesis. The design objectives for this quadrature Magic-T vector sum phase shifter include:

a) Broadband operation (targeting for 2~6 GHz)

b) Full microstrip structure for easy integration with active components

c) Polarization control for four main polarizations with full-power

11

d) Develop and validate all the sub-components

e) Demonstrate the full function of the circuitry

1.3   Thesis organization

The dissertation is organized in the following manner. In Chapter 2, a vector-sum 360° phase shifter is proposed. It consists of a two-way power divider, two variable gain amplifiers, two broadband 90° phase shifters and a proposed Quadrature Magic-T circuit.

In Chapter 3, the key component, a novel broadband Quadrature Magic-T circuit, will be presented. Agilent's ADS was used for the preliminary design of the component and Ansys HFSS was used for the detailed design. A prototype was fabricated and tested. Comparison of the measured results with the simulated results was performed to validate the design.

In Chapter 4, the investigation of a broadband 90° phase shifter is presented. The 90° phase shifter is required to broaden the phase coverage of the vector-sum phase shifter from 0° – 180° to 0° – 360°.

In Chapter 5, prototypes for both RF switch and variable gain amplifier are presented to validate the functions of the components.

In Chapter 6, an implementation of the vector sum phase shifter is shown. The circuit was fabricated and measured.

In Chapter 7, the use of vector sum phase shifter as a polarization controller will be presented and explained in detail. The vector sum phase shifter

is compared with another polarization controller architecture proposed in prior literature.

Last but not the least, Chapter 8 concludes the whole project. Future work and further applications of the circuit are proposed.

1.4   Original contributions

The original contributions of this thesis are as follows:

- Proposed and implemented a novel broadband polarization controller architecture using Quadrature Magic-T circuitry and spatial power combining concept. The circuit is able to:
  - o   Achieve four main polarizations with full power.
  - o   Generate two signals with good amplitude balance and continuous phase difference from 0° to 360°.
  - o   Independently control either the phase difference or the absolute amplitude.
- Proposed the Quadrature Magic-T circuit. The circuit, besides having the features of a normal Magic-T, has a quadrature phase relationship between the sum-port and delta-port. It is an ideal device to be used in broadband two-way vector sum type of phase shifter.
- Overcome the design challenges by locally increasing the thickness of the substrate in the coupled line area of the quadrature Magic-T. A thinner substrate will result in a width of the coupled line in the magic-T being too thin to be fabricated; a thicker substrate will result in the width of the 50 Ω

line in the circuit to be too wide for design. This issue was resolved through local increment of the substrate thickness.

- Magic-T implementation in microstrip requires jump wires similar to the Lange coupler. It has poor repeatability as the size and the shape of the jump wires are difficult to control. It was resolved through using $0 \ \Omega$ resistors as the jumper. This greatly simplifies the fabrication challenge for the microstrip magic-T circuit.

Chapter 2 Two-way vector sum phase shifter

2.1 Introduction

A vector sum phase shifter achieves the desired phase shift by summing two quadrature signals with different amplitudes. The concept of vector-sum phase shifter is not new and different ways have been explored to implement the circuit.

Vector sum phase shifter using VGAs and quadrature hybrid is proposed in [10]. Using this method, the phase shift can be digitally controlled. Chip implementations of the vector sum phase shifters have also been widely explored. In [11], active balun and high-speed CMOS operational transconductance amplifier achieving a full 360° vector sum phase shifter has been proposed. This circuit operates from 2 GHz to 3 GHz. A vector sum CMOS phase shifter IC which uses I/Q network and is able to cover full 360° in the 2.3–4.8 GHz range is also presented in [12]. The use of left-hand/right-hand transmission line as an I/Q generator in a CMOS vector sum phase shifter has been explored by [13]. Other methods such as using an acousto optic polarization coupler and MEMS have been used to implement the phase shifter [14]. A semi-integrated device which uses a differential off-chip LC network for quadrature summation and a fully integrated IC which uses a passive polyphase filter for quadrature summing network are presented in [15]. Among all the implementations, the challenges lie mainly in accurately implementing the key phases (0°, 90°, 180° and 270°) and broadband summation of the signals.

Normally, the vector sum phase shifters are two-port devices and the reported phase shifts are referenced to the signal at the input ports. However, in some application, such as in polarization controllers, it is more advantageous to have a two-way vector sum phase shifter. This two way vector sum phase shifter is a three-port device and the shift in the phase is between the two outputs. In this chapter, a novel two-way vector sum phase shifter using a Quadrature Magic-T is proposed. Analysis of the phase change along the circuit will be carried out. For this implementation, wideband performance can be achieved.

2.2 Novel two-way vector-sum phase shifter

2.2.1 Block diagrams
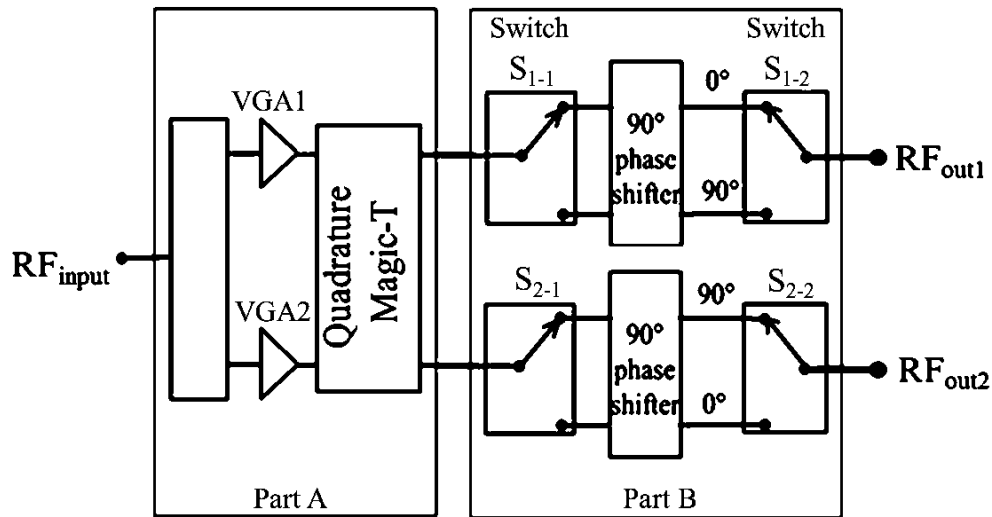
Fig. 2-1: Proposed block diagram of the two-way vector-sum phase shifter.

Fig. 2-1 shows the proposed block diagram of the two-way vector sum phase shifter. In Part A two signals are generated with equal amplitude and a variable phase difference from 0° to 180° using vector-sum phase shifter concept.

16

It consists of a broadband power divider, two variable gain amplifiers (VGAs) and a Quadrature Magic-T circuit.

For part A, the input signal is divided into two signals, equal in amplitude and phase, by the power divider. The amplitude of the two output signals from the power divider is varied by the two VGAs before being fed into the sum-port and delta-port of the Quadrature Magic-T. The signals will be vector-summed by the Quadrature Magic-T circuit when they reach the two output ports. The Quadrature Magic-T is a circuit proposed in this thesis. It is the key circuit for the two-way vector-sum phase shifter. The detailed operation, design and implementation of the Quadrature Magic-T will be presented in Chapter 3.

To achieve 360° coverage, Part B has to be included in the design. It consists of two sets of broadband 90° phase shifters and four RF switches. It is a trade-off between using two broadband 90° phase shifters and one 180° broadband phase shifter which is difficult to design and implement especially when it is in microstrip structure. Each set of broadband 90° phase shifter consists of a phase delay path and a reference path. The details of the phase shifter will be presented in Chapter 4. The four RF switches are grouped into two pairs. Each pair of switches is connected with one set of phase shifter, and responsible for the selection of either the phase delay path or the reference path. The details about the VGAs and RF switches will be presented in Chapter 5. At the two outputs of part B, the phase difference can be changed to any value within 360°.

2.2.2 Signal flow analysis
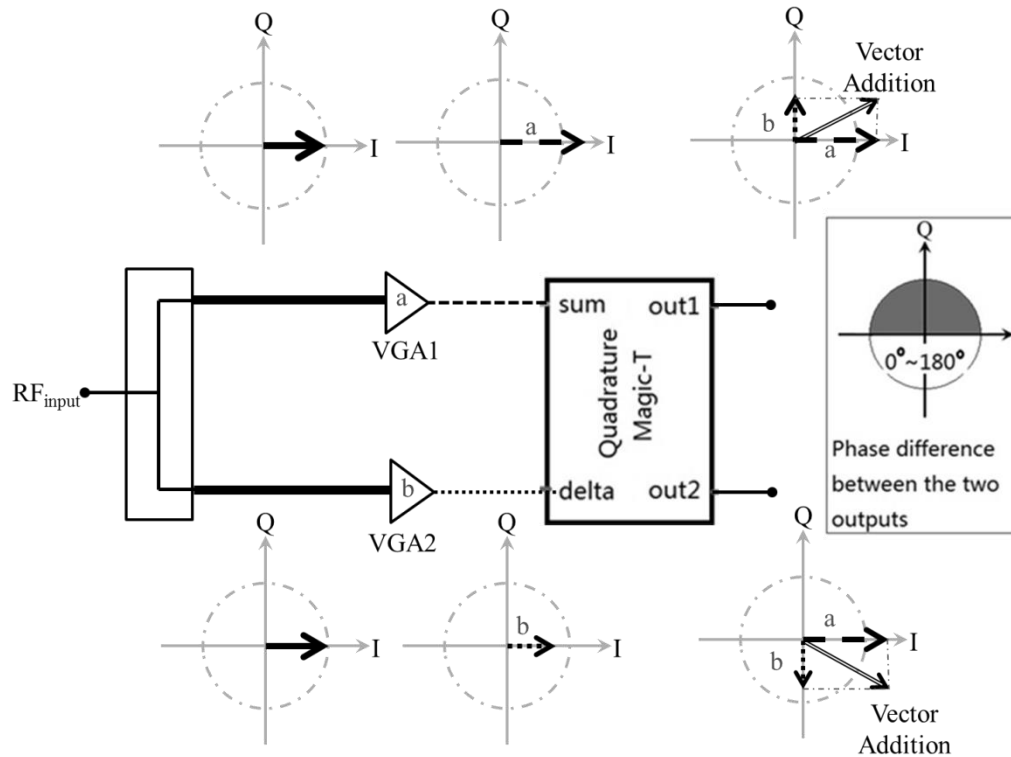
Fig. 2-2: Amplitude and phase changes in Part A.

Fig. 2-2 illustrates the amplitude and phase changes of the signals in part A. The vectors at the top of the figure correspond to the signals flowing in the upper branch of the circuit. The vectors at the bottom of the figure correspond to the signals that are flowing in the lower branch. Depending on the control of the two VGAs, the phase difference between the two output signals can be varied from 0° to 180° while keeping a low amplitude imbalance. The shaded half circle represents the phase difference range between the two outputs.

The key component in part A is the novel Quadrature Magic-T. The unique feature of this Quadrature Magic-T is its capability to perform vector

summation at the two output ports for the signals fed from the sum- and delta-ports. Due to the quadrature phase arrangement, the amplitude balance between the two output ports is inherently good regardless of the amplitude of the either input ports. Most importantly, the phase difference between the two resultant signals can be tuned by varying the gains of the two VGAs.
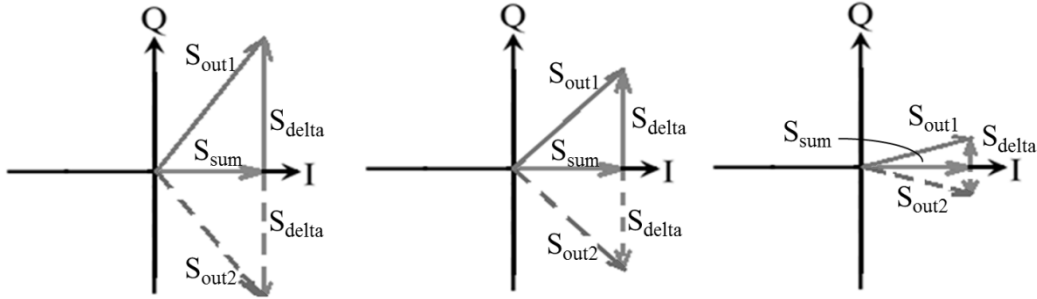
Fig. 2-3: Resultant signals at out1 (S_{out1}) and out2 (S_{out2}) versus amplitude of signals due to sum-port (S_{sum}) and delta-port (S_{delta}).

Fig. 2-3 illustrates the resultant vector of the signals at out1 and out2 when the amplitude of the signal applied at the delta-port is reduced. The phase difference between the two resultant vectors (S_{out1} and S_{out2}) decreases as the amplitude of the signals (represented by the length of S_{delta} arrow) due to excitation at the delta-port is decreased. The phase difference between the output signals can also be decreased by increasing the amplitude of the signal to the sum-port. Therefore, a smaller signal to the delta port and a larger signal to the sum-port will result in a smaller phase difference. The smallest phase difference is 0° when no signal goes to the delta port or when the signal to the sum-port is significantly later than that of delta-port. Contrary to that, the largest phase difference is 180° when only delta-port is excited or the excitation at delta port is significantly higher than that of sum-port. Hence, the phase difference between

19

the two output ports can be tuned from 0° to 180° by controlling the amplitude of either or both input ports. A special case occurs when the signal to the delta port is equal to that of the sum port. In this case, a 90° phase difference will be produced. The good isolation between the two input ports ensures that the signals can be controlled independently without affecting each other.
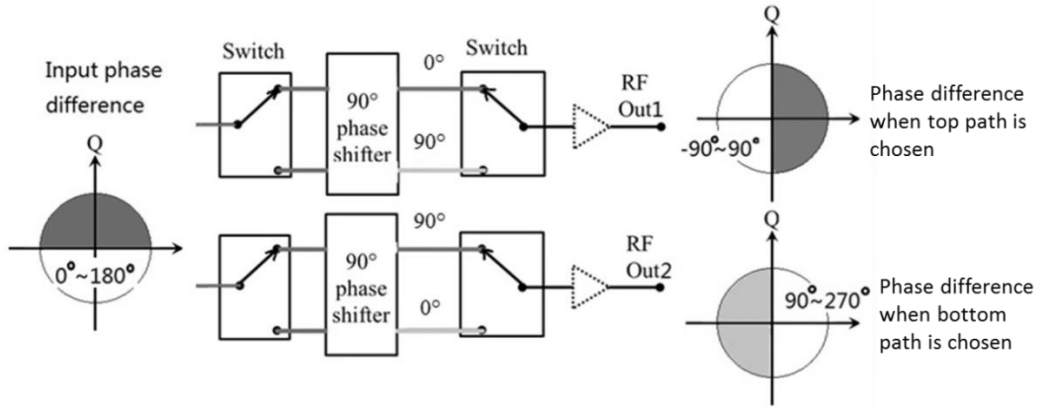
Fig. 2-4: Phase difference coverage before and after Part B circuit.

Fig. 2-4 illustrates the phase difference coverage before and after the Part B circuit. Depending on the required output phases, out1 and out2 of the Quadrature Magic-T are connected to either the phase delay circuit or the reference circuit of the 90° phase shifters. The connection of the circuit to the top path of the phase shifters corresponds to the case where -90° to 90° phase is required while the bottom path corresponds to the case where 90° to 270° phase is required.

2.2.3 Mathematic analysis

Assuming the signal at each branch after the power divider is W volt, the RF outputs for part A can be expressed as:

$$RF_{out1} = \frac{1}{\sqrt{2}} W(a + jb) \qquad (2\text{-}1)$$

$$RF_{out2} = \frac{1}{\sqrt{2}} W(a - jb) \qquad (2\text{-}2)$$

Where a and b are the gains of VGA1 and VGA2 respectively.

The signals can also be expressed as:

$$|RF_{out1}| = \frac{1}{\sqrt{2}} W \sqrt{a^2 + b^2} \qquad (2\text{-}3)$$

$$|RF_{out2}| = \frac{1}{\sqrt{2}} W \sqrt{a^2 + b^2} \qquad (2\text{-}4)$$

$$\Delta\theta = 2\arctan(\tfrac{b}{a}) \qquad (2\text{-}5)$$

(2-3) and (2-4) show that the resultant amplitude of the two branches is equal. (2-5) shows that the phase difference between the two branches dependents only on the amplitude ratio of the two input signals.

It is possible to control the resultant phase difference without changing the resultant amplitude or the other way round, control resultant amplitude without changing the resultant phase difference. For that to occur, the amplitudes of the two input signals to delta- and sum-port have to be changed concurrently. For the

21

case where only the resultant amplitude is changed, the following formula can be derived from (2-1) to (2-5)

$$b = a \cdot tan(\frac{\Delta\theta}{2}) \tag{2-6}$$

$$20\,log(b) - 20\,log(a) = 20\,log\left(tan\left(\frac{\Delta\theta}{2}\right)\right) \tag{2-7}$$

$$= constant$$

$$|RF_{out1}| = |RF_{out2}| = \frac{1}{\sqrt{2}}A \cdot a \cdot csc(\frac{\Delta\theta}{2}) \tag{2-8}$$

From (2-7), the resultant phase will be kept constant once the signal difference in dB between the two inputs is constant. For the case in which the resultant phase difference is changed, the following formula can be applied.

$$a = d \cdot cos(\frac{\Delta\theta}{2}) \tag{2-9}$$

$$b = d \cdot sin(\frac{\Delta\theta}{2}) \tag{2-10}$$

$$|RF_{out1}| = |RF_{out2}| = \frac{1}{\sqrt{2}}W \cdot d \tag{2-11}$$

Where d is a constant determining the resultant amplitude, and $\Delta\theta$ is the resultant phase difference to be changed to. These formulas are useful in determining the settings of the VGAs in the vector sum phase shifter.

The output at part B will introduce another j or $-j$ term to the phase of the output signals depending on the path chosen. The magnitude of the output signals will not be affected by the phase shift.

2.3   Ideal ADS simulations

To verify the feasibility of the vector sum phase shifter, an ADS simulation of the circuit (Fig. 2-1) using ideal components was carried out. The Quadrature Magic-T is represented by a 90° phase shifter and an ideal 180° hybrid. (The detailed performance of the Quadrature Magic-T can be found in Chapter 3.) V1 and V2 are the control voltages for the VGA1 and VGA2 respectively. S is the state of the RF switches. As all the components are ideal, the simulation results do not vary with the frequency. In addition, all the ports are well matched to 50 Ω.

The voltages V1 and V2 are varied from -1 V to 1 V with a step size of 0.2 V and 0.5 V respectively. The switch S is changed to direct the signal from the reference line to the phase delay line of the 90° phase shifter. When S = 0, S_{1-1} and S_{1-2} are connected the reference line while S_{2-1} and S_{2-2} are connected to the 90° phase shifter. When S= 1, S_{1-1} and S_{1-2} are connected the 90° phase shifter and S_{2-1} and S_{2-2} are connected to the reference line.

Fig. 2-5 shows the phase difference between the port 2 and port 3 when different V1 and V2 are applied. When the switch state S is 0, the phase coverage is from 90° to 270°; when S is 1, the phase coverage is from -90° to 90°. It is observed that there are more than one V1 and V2 setting that can achieve the same phase difference between the two output ports. Fig. 2-6 shows the $|S_{21}|$ and $|S_{31}|$ of the circuit. The $|S_{21}|$ and $|S_{31}|$ vary with V1 and V2. In addition, for each V1 and V2 voltage setting, the $|S_{21}|$ and $|S_{31}|$ are equal to each other. The

23

amplitude imbalance of the two ports is shown in Fig. 2-7. An amplitude imbalance of 0 dB is observed for port 2 and port 3.
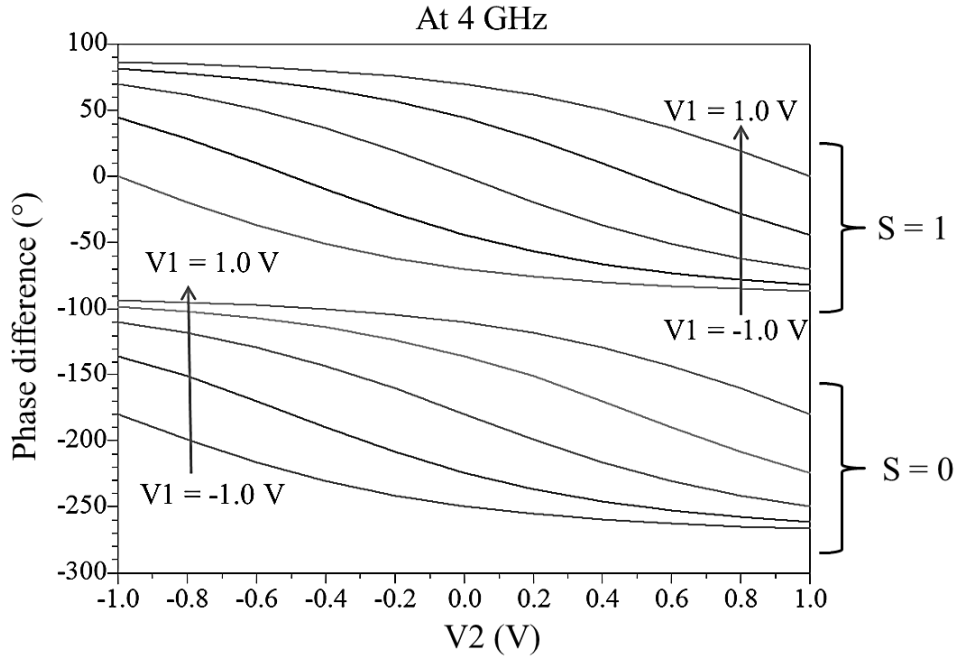
Fig. 2-5: Phase difference between port 2 and port 3 (ideal).
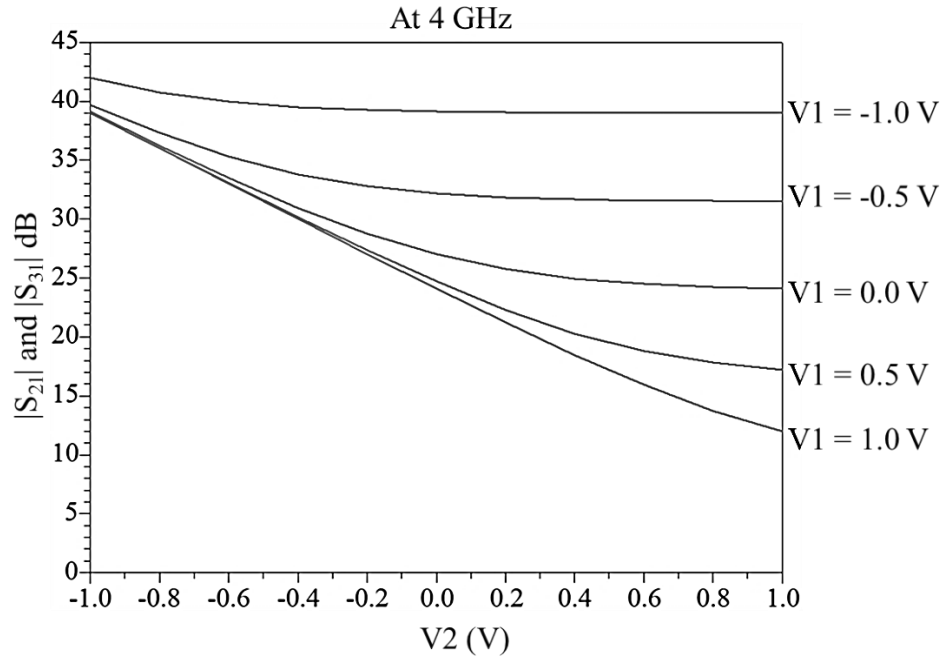
Fig. 2-6: $|S_{21}|$ and $|S_{12}|$ for all switch states (ideal).

24
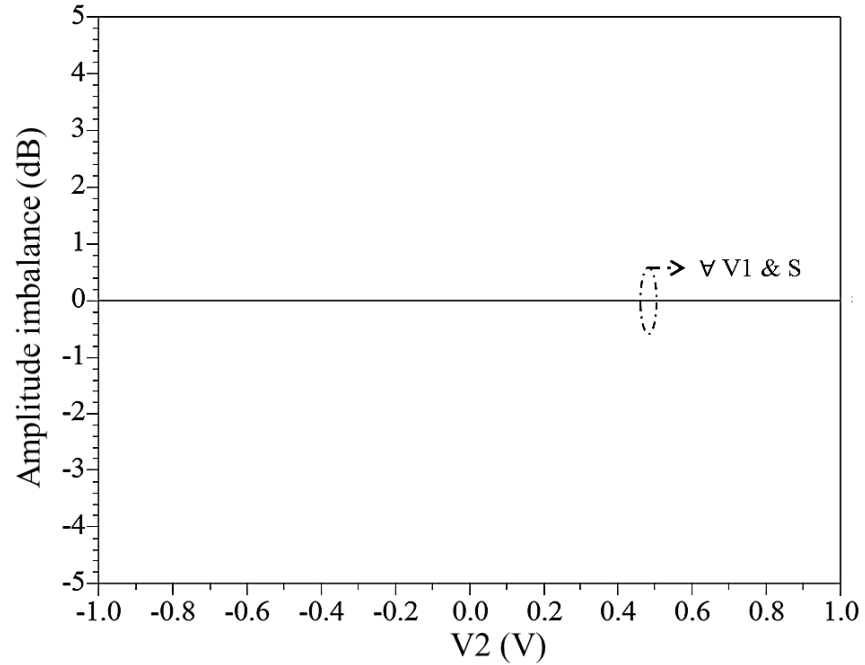
Fig. 2-7: Amplitude imbalance for all switch and V1 states (ideal).

2.4 Conclusions

A novel vector sum phase shifter using a Quadrature Magic-T is proposed and analyzed. The circuit consists of a novel Quadrature Magic-T circuit, broadband 90° phase shifters, VGAs and a power divider. Using this circuit, continuous 360° phase shift can be achieved and the output is two way. This circuit is suitable for application in polarization control.

Chapter 3 Quadrature Magic-T

3.1 Introduction

3.1.1 Classification of hybrids

A hybrid is either a 90° hybrid or a 180° hybrid. A 90° hybrid, also known as quadrature hybrid or direction coupler, has 90° phase difference between the two output ports. A 180° hybrid has a phase difference of 0° or 180° between the two output ports when the sum-port or the delta-port is excited respectively.

Hybrids can be implemented in waveguide, coaxial line, stripline and even in microstrip transmission line. Some of the common hybrid configurations include coupled lines, branch lines, rat-race and magic-T [16]. Their operating bandwidth can be narrow or wideband. The branch line hybrid and the rat-race hybrid are narrow band devices. Stripline multistage directional coupler and Lange coupler are for broadband applications.

A wideband hybrid normally requires heavily coupled transmission lines with equal even- and odd-mode phase velocities. Therefore, it is a challenge to design a wideband hybrid in microstrip which has different even- and odd-mode phase velocities. However, microstrip hybrid is preferred as it is easily integrated with other active electronic components.

3.1.2 Examples of a hybrid

As an example, Fig. 3-1 shows the schematic of a typical 3-dB directional coupler with 3:1 bandwidth. It requires three coupled lines with even- and odd-mode impedances of $Z_{0e1} = 59 \ \Omega$, $Z_{0o1} = 43 \ \Omega$, $Z_{0ec} = 162 \ \Omega$, $Z_{0oc} = 15 \ \Omega$ [17]. The coupled line at the centre is difficult to implement in practice due to its large impedance difference between the even- and the odd-mode. Additionally, stripline has to be used as the even and odd mode phase velocities must be as close to each other as possible to avoid performance degradation.
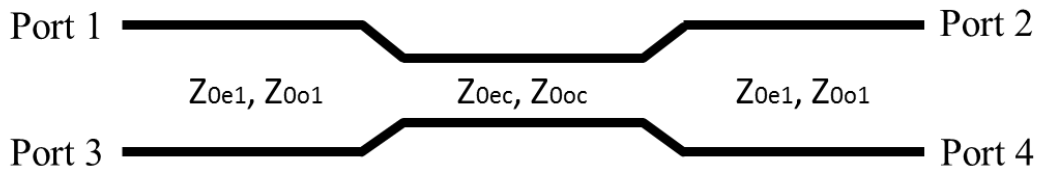
Fig. 3-1: Multistage directional coupler.

Another example is a Lange coupler. It achieves broadband performance by using interdigital coupled lines. However, its narrow line width, small gaps and bond wires increase the complexity and difficulty in implementation [16].

A 3-dB tandem coupler is shown in Fig. 3-2. It consists of two 8.34 dB couplers in cascade. Compared to the 3-dB directional coupler, the tandem coupler requires coupled lines with less coupling [18] but doubles the physical size. An issue with implementing the tandem coupler in microstrip is the difference between the even-mode and the odd-mode phase velocities. It significantly affects the directivity and isolation of the coupler. According to [19],

27

a 10% difference in phase velocities will cause the directivity of a 10 dB coupler to drop from a theoretical infinite value to 13 dB. In addition, directivity becomes worse if the coupling ratio is low. To compensate for the difference in the phase velocities, stubs or capacitors are added to the coupled line [20]. However, it is applicable only for narrow band coupler.
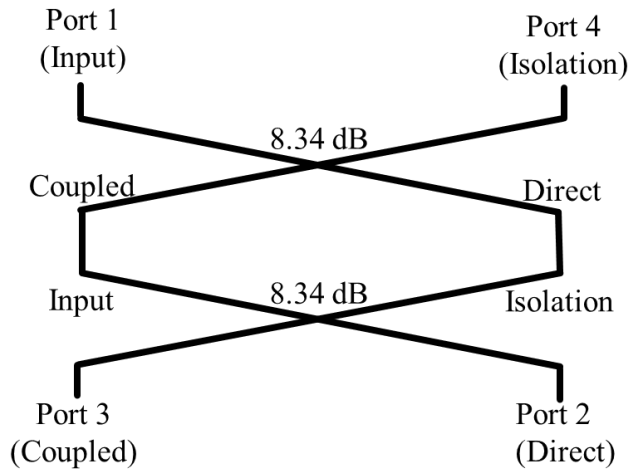
Fig. 3-2: 3 dB tandem coupler.
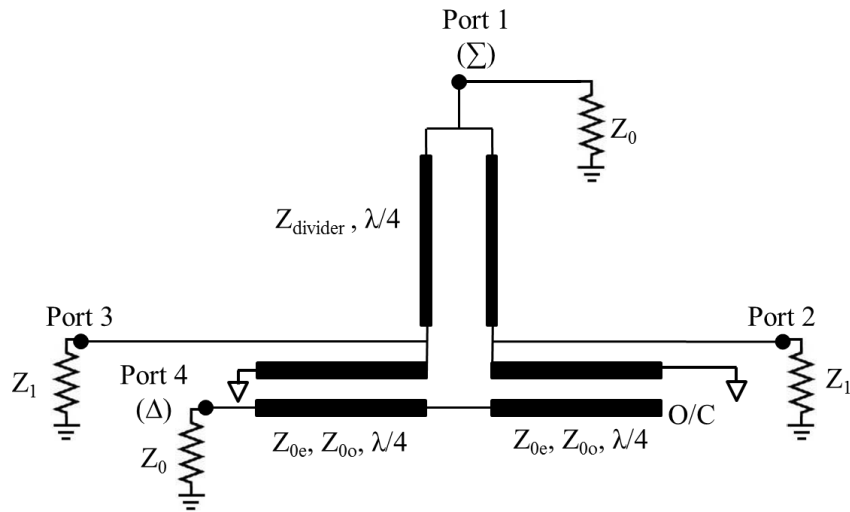
Fig. 3-3: Broadband 180° hybrid [21].

A broadband planar 180° hybrid consisting of a power divider and a broadband balun is proposed in [21]. Fig. 3-3 shows the topology of the circuit. The circuit is implemented in microstrip line and is able to achieve wide bandwidth with good amplitude imbalance of less than 0.5 dB and phase error of 5°. A good isolation between the sum- and delta-ports is also reported. According to [21], the required design parameters can be found using

$$Z_{divider} = \sqrt{2Z_0 Z_1} \tag{3-1}$$

$$Z_{0e} = Z_0 \sqrt{\frac{1+C}{1-C}} \tag{3-2}$$

$$Z_{0o} = Z_0 \sqrt{\frac{1-C}{1+C}} \tag{3-3}$$

Where $C = \sqrt{\frac{Z_0}{Z_0 + 2Z_1}}$

Assuming the port impedances for port 2 and port 3 are 50 Ω, the required $Z_{divider}$, Z_{0e} and Z_{0o} are 70.7 Ω, 97 Ω and 26 Ω respectively.

3.1.3 Definition of a 180° hybrid

The 180° hybrid has 4 ports as shown in Fig. 3-4. Port 1 is normally known as the sum-port, Port 4 is known as the delta-port and Port 2 and Port 3 are known as the collinear ports.
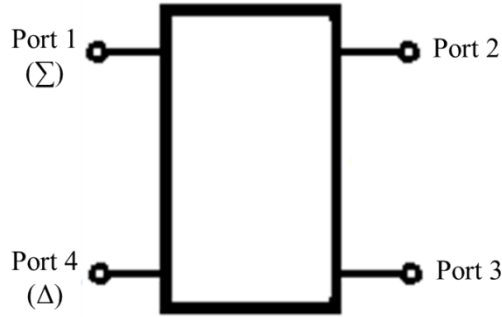
Fig. 3-4: Block diagram of a 180° hybrid and its port definition.

When discussing the 180° hybrid, it is common to report the phase difference between the collinear ports when either the sum-port or the delta-port is excited. However, the phase difference between the sum- and delta-ports when the collinear ports are excited is sometimes not reported. As we are interested only for the case where Port 2 and Port 3 are the output ports, two new terms will be introduced to ease the description of phase at the collinear ports when both sum- and delta ports are excited.

Cross-output phase difference: It is the phase difference between the two output ports when one of the input ports is excited, i.e. $\angle S_{31} - \angle S_{21}$ or $\angle S_{34} - \angle S_{24}$.

Cross-input phase difference: It is the phase difference at one of the output ports when both input ports are excited, i.e. $\angle S_{21} - \angle S_{24}$, or $\angle S_{31} - \angle S_{34}$. This phase difference determines how the signals are combined at the output port if both input ports are excited. Due to reciprocal relationship, it can also be interpreted as the phase difference between the two input ports if one of the output ports is excited.

30

3.1.4 Characteristics of a typical 180° hybrid
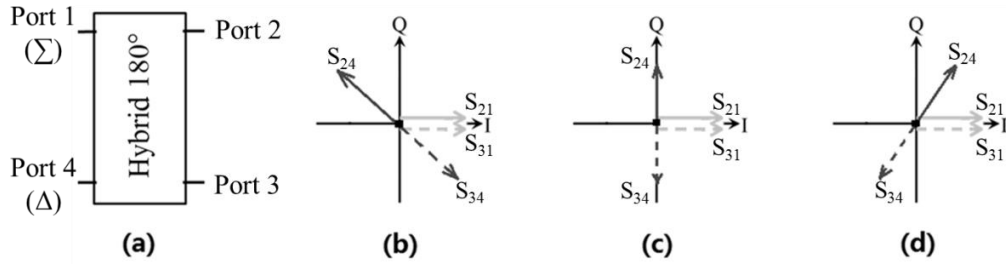
Fig. 3-5: (a) A typical 180° hybrid model and (b)-(d) its possible relative phases at Port 2 and Port 3 when both sum and delta ports are excited.

Fig. 3-5(a) shows a typical 180° hybrid circuit and its possible relative phase at the output ports when both sum-port (Port 1) and delta-port (Port 4) are excited in-phase. S_{21} and S_{31} represent the signals due to the sum-port excitation, and S_{34} and S_{24} represents the signal due to the delta port excitation. Solid line represents the signal at Port 2 and dashed line represents the signal at Port 3. The cross-output phase differences are maintained for all cases in Fig. 3-5(b) to (d), i.e. is 0° for sum-port excitation and 180° for delta-port excitation. However, in Fig. 3-5(b) the cross-input phase difference is greater than 90° at Port 2 and smaller than 90° at Port 3. Fig. 3-5(d) shows the opposite situation. Fig. 3-5(c) shows a special case where the phase difference at both output ports is 90°. Quadrature vector-sum occurs at both output ports under this special condition.

3.1.5 Objectives

For the 90° hybrid, it is difficult to achieve broadband performance, especially in microstrip line implementation. According to [21], for the 180° hybrid it is relatively easy to achieve broadband performance. Therefore, we ask the following questions:

a) Is it possible to achieve the required amplitude and phase of a polarization controller using 180° hybrid topology?

b) Is it possible to achieve a broadband performance for the quadrature vector-sum?

c) Is it possible to implement 180° hybrid using microstrip line?

The following sections will present the studies towards these objectives.

3.2   180° hybrid

The ideal circuit of Fig. 3-3 is simulated using ADS. Fig. 3-6 to Fig. 3-9 show the simulated results of the circuit. Fig. 3-6 shows that the circuit achieves more than 15 dB return loss for all the ports from 3.1 GHz to 4.9 GHz. Fig. 3-7 and Fig. 3-8 shows the insertion loss for sum-port and delta-port excitation, respectively. The signals are split equally between the two output ports.

Fig. 3-6: Simulated $|S_{11}|$, $|S_{22}|$, $|S_{33}|$ and $|S_{44}|$.
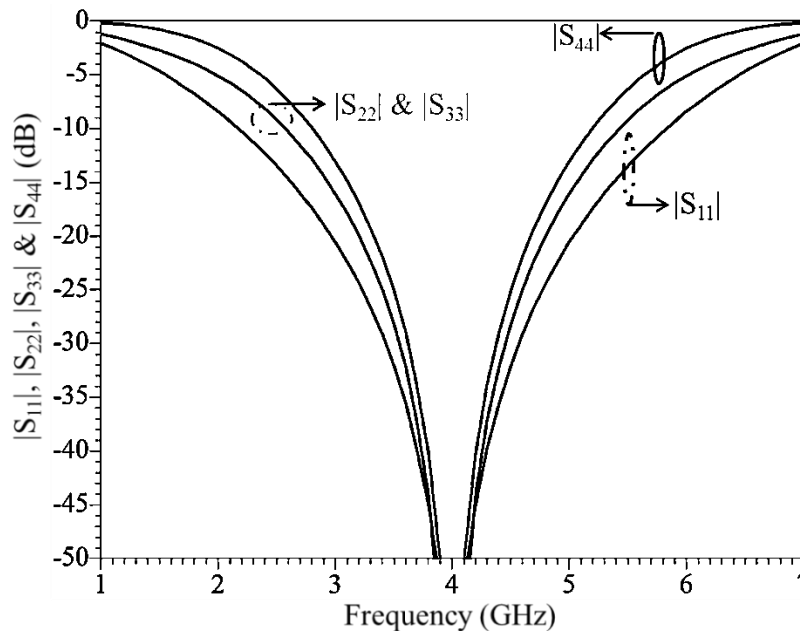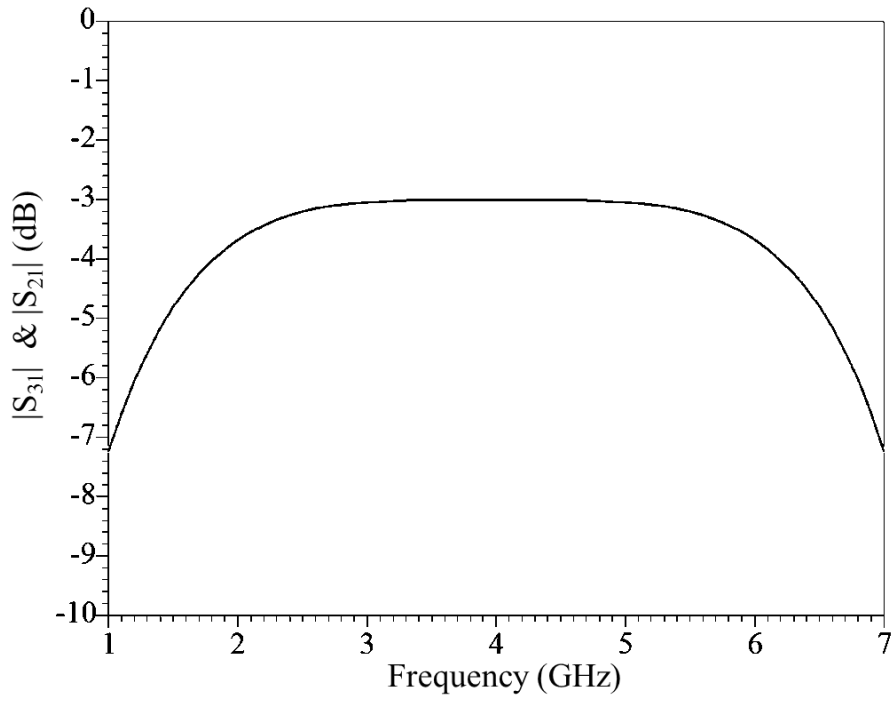
Fig. 3-7: Simulated $|S_{31}|$ and $|S_{12}|$ for sum-port excitation.
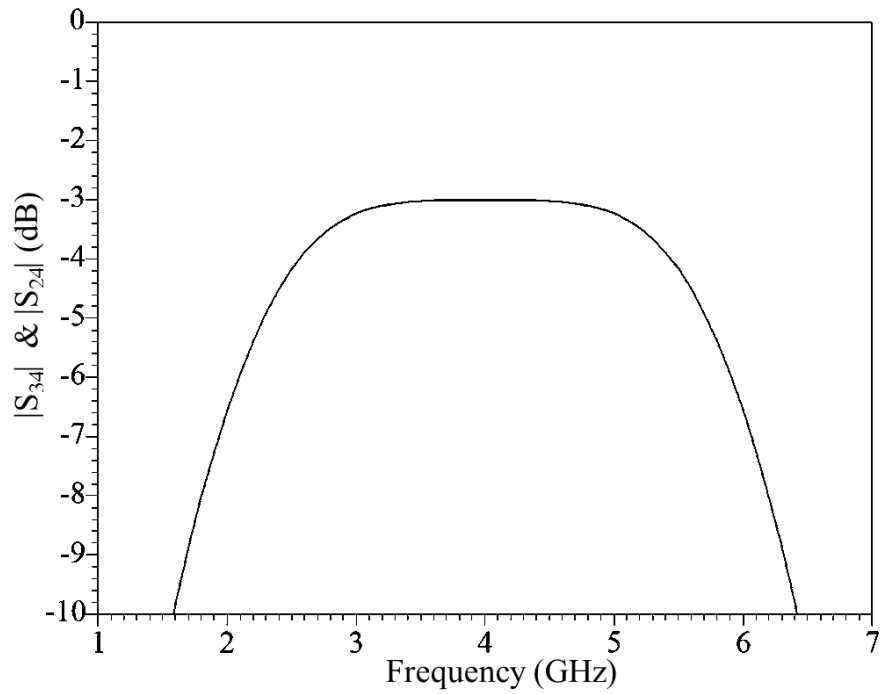
Fig. 3-8: Simulated $|S_{34}|$ and $|S_{24}|$ for delta-port excitation.
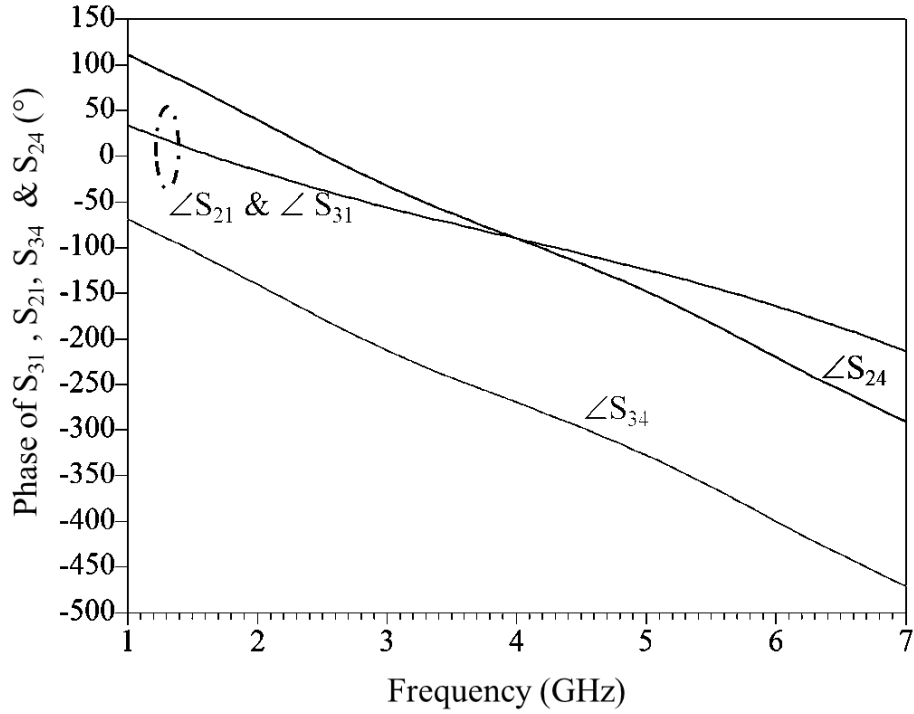
Fig. 3-9: Simulated insertion phase.
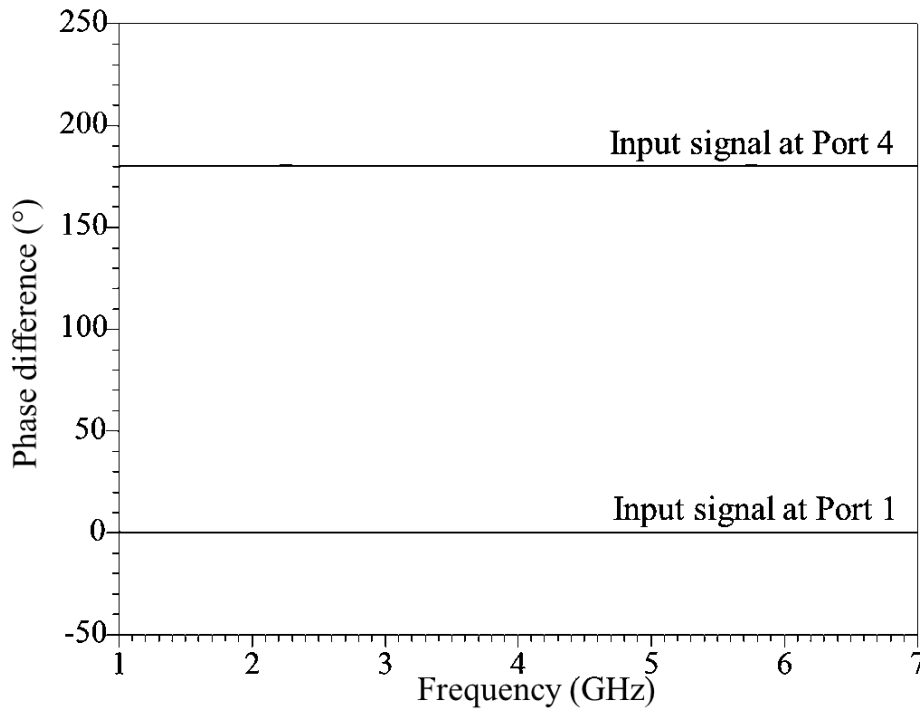
Fig. 3-10: Simulated phase difference between the two output ports.

Fig. 3-9 shows the simulated insertion phase. At every frequency, $\angle S_{21}$ and $\angle S_{31}$ are the same; $\angle S_{24}$ aligns well with $\angle S_{34}$ with an almost fixed phase difference of 180°. Fig. 3-10 shows the simulated cross-output phase difference. It is 0° for the signal from Port 1 (sum-port) and 180° for the signal from Port 4 (delta-port). These are fundamental features of 180° hybrid.

Fig. 3-9 also shows that the phase difference between S_{21} and S_{24} (or S_{31} and S_{34}) varies with frequency. At 4 GHz, the phase of S_{21} and S_{31} cross over with the phase of S_{24}. Their difference is not a constant. Therefore, a typical 180° circuit does not have a predefined cross-input phase difference.

It is worth to point out that the isolation between Port 1 and Port 4 is better than 50 dB from 1 GHz to 7 GHz. Unlike the 90° coupler, whose isolation is affected by the return losses, the isolation of the 180° hybrid remains very good even when the return losses are worse than 10 dB. This is one of the reasons that this 180° hybrid is favoured over the 3 dB directional coupler.

3.3   Novel Quadrature Magic-T

3.3.1 Definition of Quadrature Magic-T

Magic-T is the waveguide form of the 180° hybrid (which is usually planar is structure). To reduce confusion and complexity in naming the proposed circuit, magic-T will be used to represent the planar form of 180° hybrid from here onwards. Quadrature Magic-T is defined as a special magic-T circuit whose cross-input phase difference is 90° (quadrature) across the operation band. Fig.

35

3-11 shows the phase relationship. The ports assigned to Quadrature Magic-T are the same as that shown in Fig. 3-4.

(a)   (b)
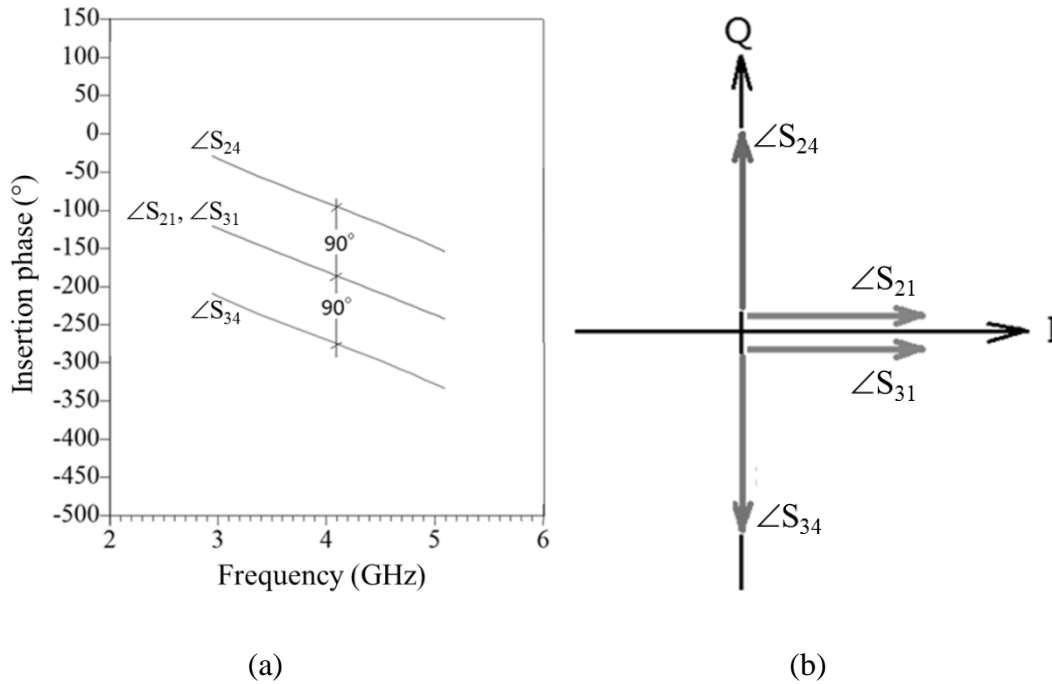
Fig. 3-11: Definition of Quadrature Magic-T
(a) Insertion phase relationship (b) Vector representation

The unique feature of Quadrature Magic-T is its capability to perform vector summation at the two output ports for the signals from sum-port and the signal from delta-port. The resultant signals have equal amplitude and variable phase difference. Its usage as a vector sum phase shifter can be found in Chapter 2.

3.3.2 Preliminary design of a Quadrature Magic-T

By including an extra section of transmission line to the sum-port as shown in Fig. 3-12, the magic-T circuit can be transformed into a Quadrature Magic-T. The transmission line has a characteristic impedance of Z_0 Ω which is

matched to the port impedance and has a specific electrical length. Therefore, the return losses and insertion losses of the circuit will not be affected when the insertion phase is changed. Fig. 3-12 is also simulated in ADS. The phase response of the circuit is shown in Fig. 3-13. Fig. 3-14 shows the cross-input phase difference. The outputs due to sum-port excitation are 90° apart and with a deviation less than ±1° from that of the outputs due to the delta-port excitation from 3.1 GHz to 4.9 GHz. These simulation results show that the Quadrature Magic-T not only retained the characteristics of a normal Magic T but also has a wider bandwidth and inherent quadrature phase characteristics.
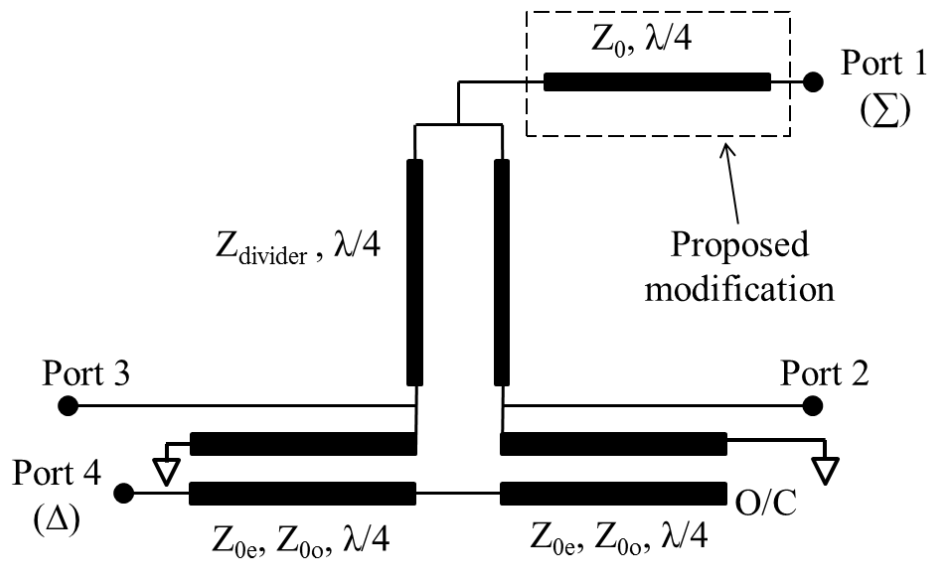
Fig. 3-12: Quadrature Magic-T.
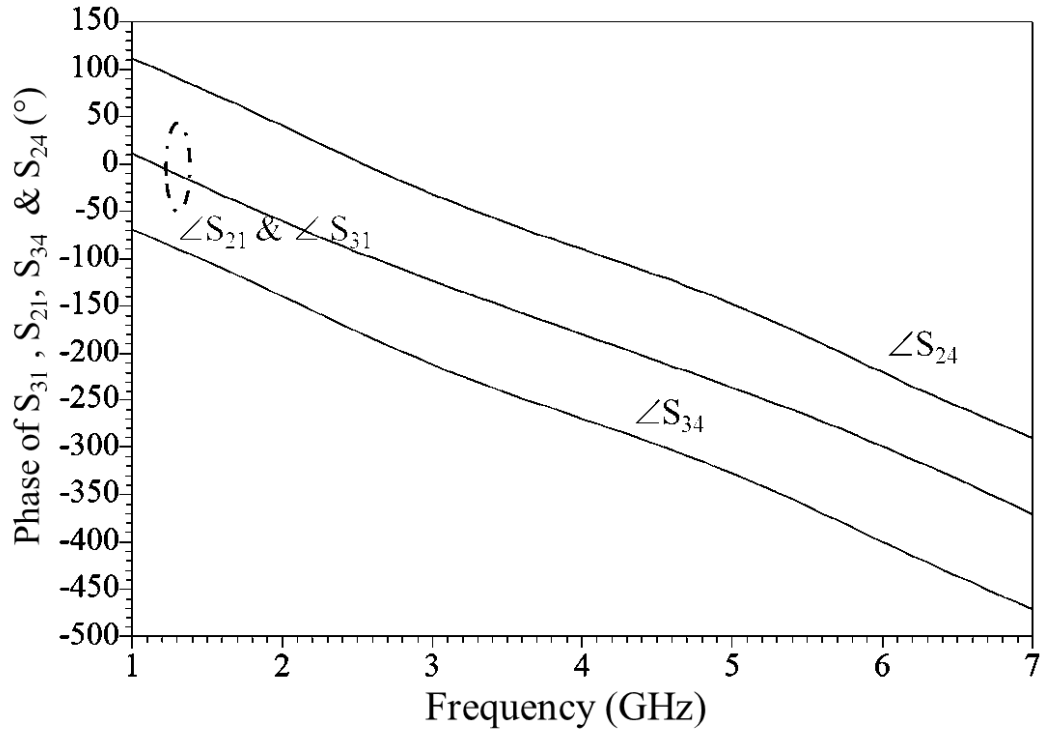
Fig. 3-13: Phase response of the Quadrature Magic-T.
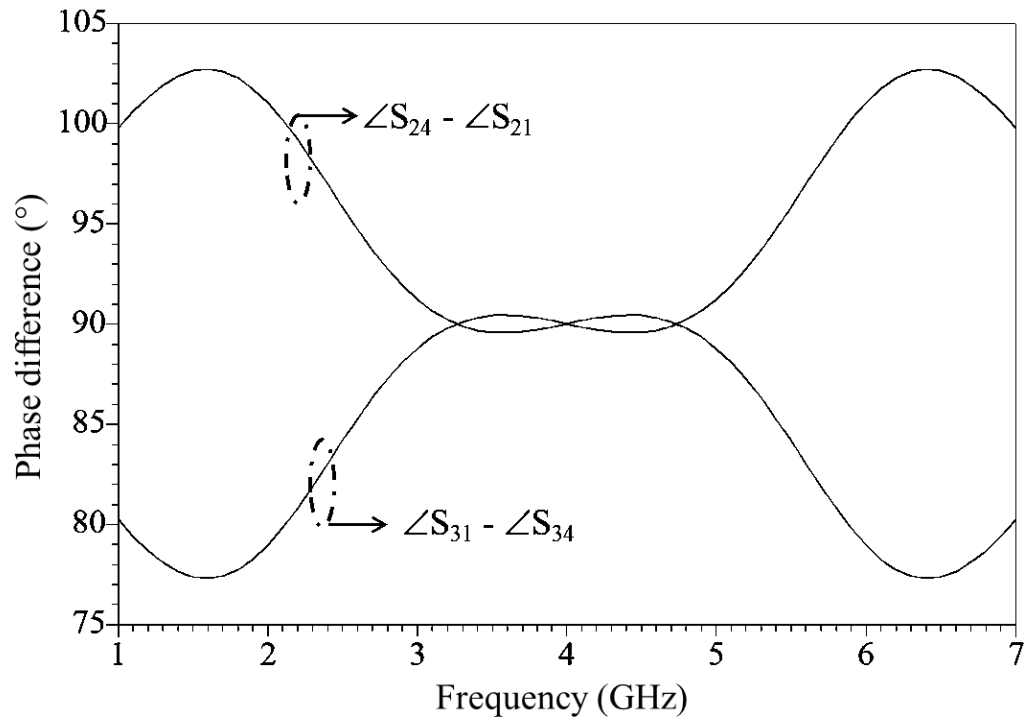
Fig. 3-14: Cross-input phase difference of the Quadrature Magic-T.

3.3.3 Improved Quadrature Magic-T

The circuit shown in Fig. 3-12 has the S parameter performance of a Quadrature Magic-T. However, compared to the design target, its bandwidth is not sufficiently large. Further improvement on the circuit through tuning and optimization was carried out. The tuned/optimized values for $Z_{divider}$, Z_{0e} and Z_{0o} are 70.7 Ω, 110 Ω and 23 Ω respectively.
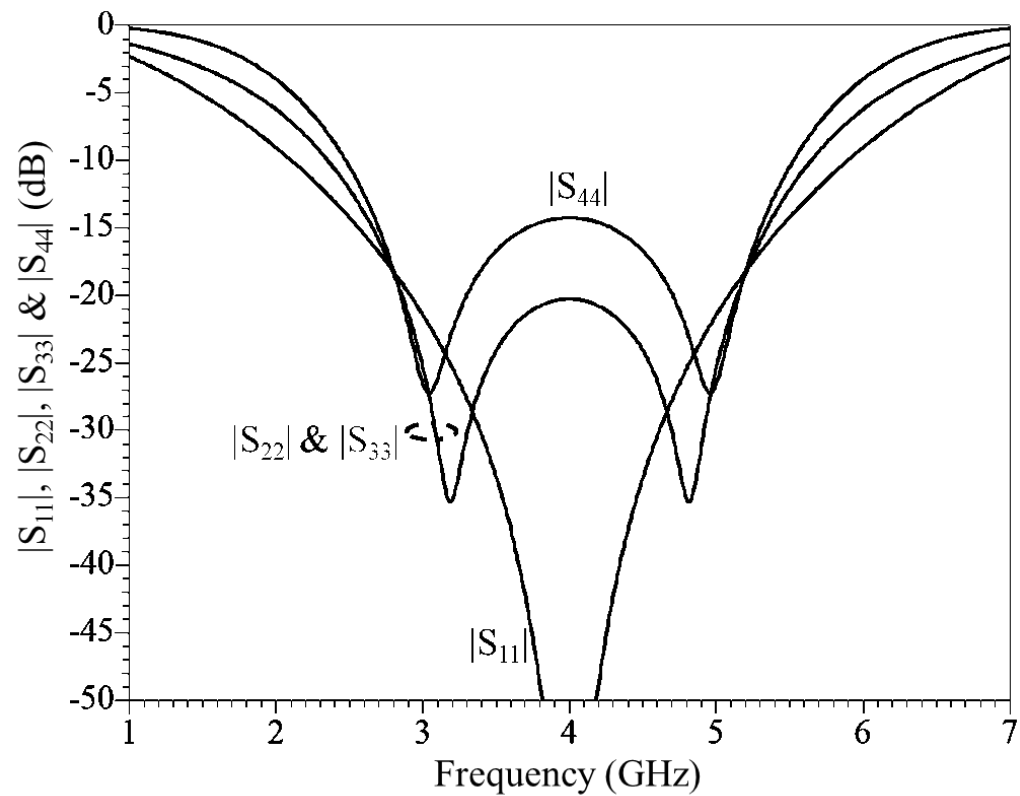
Fig. 3-15: Simulated $|S_{11}|$, $|S_{22}|$, $|S_{33}|$ and $|S_{44}|$ of the improved Quadrature Magic-T.
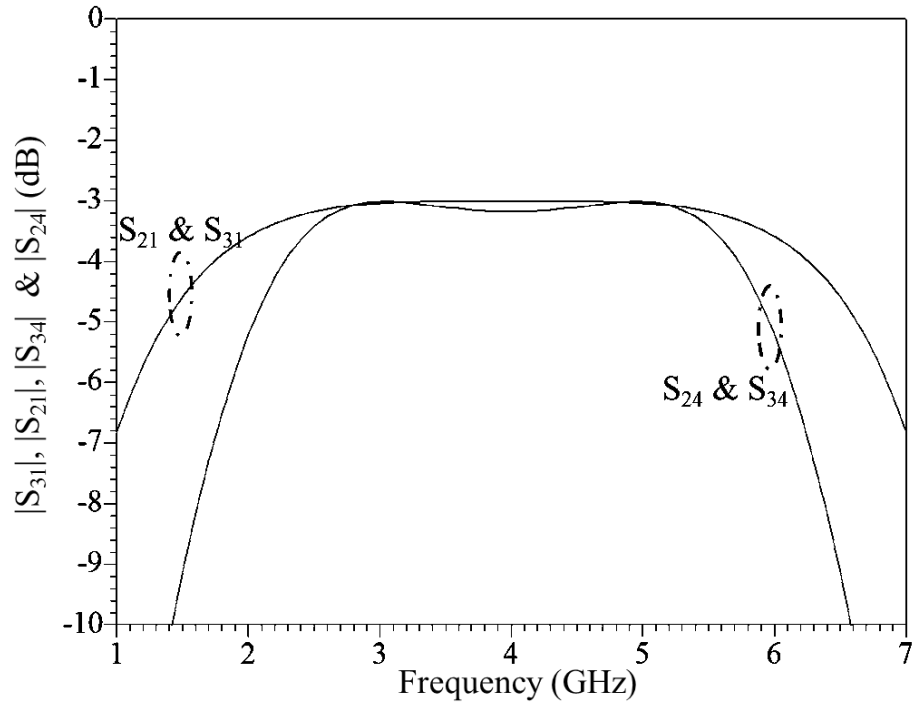
Fig. 3-16: Simulated $|S_{31}|$, $|S_{21}|$, $|S_{34}|$ and $|S_{24}|$ of the improved Quadrature
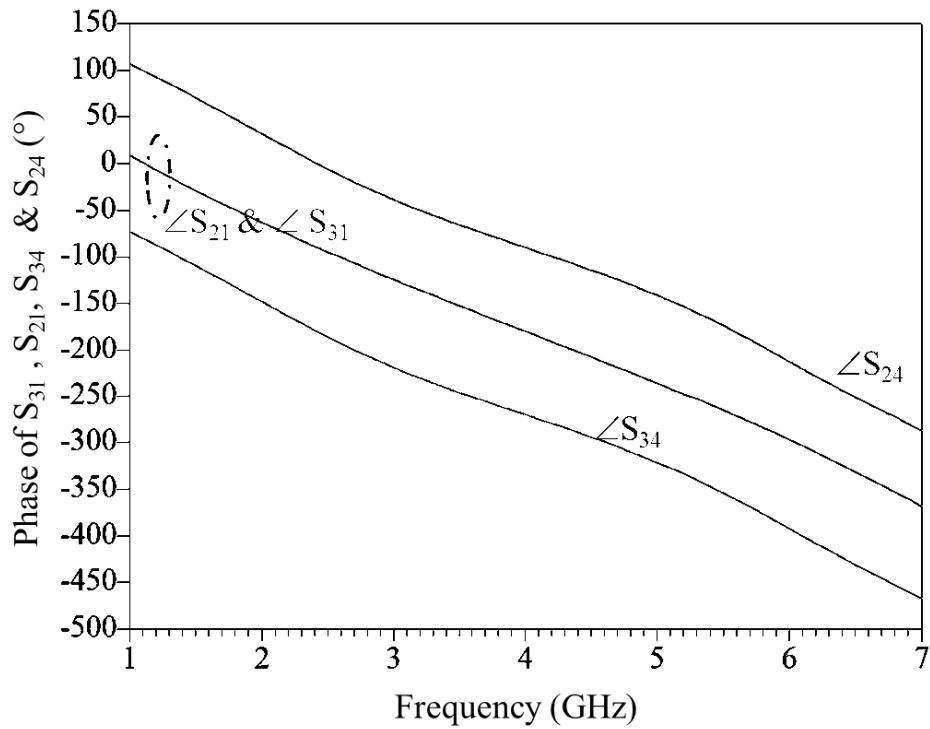
Magic-T.

Fig. 3-17: Simulated insertion phase for the improved Quadrature Magic-T.
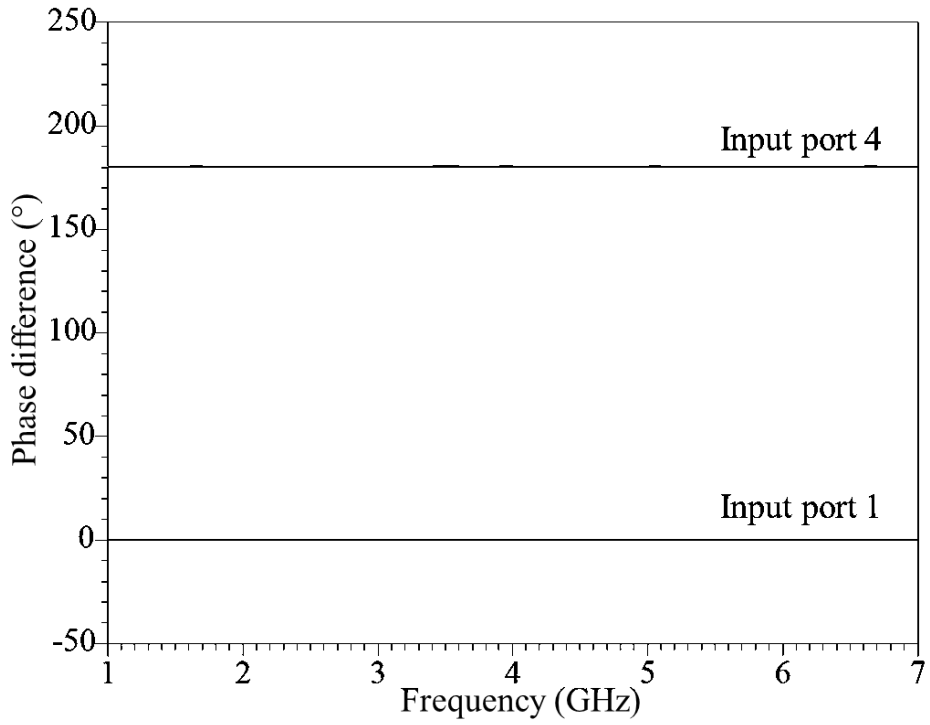
Fig. 3-18: Simulated improved cross-output phase difference.
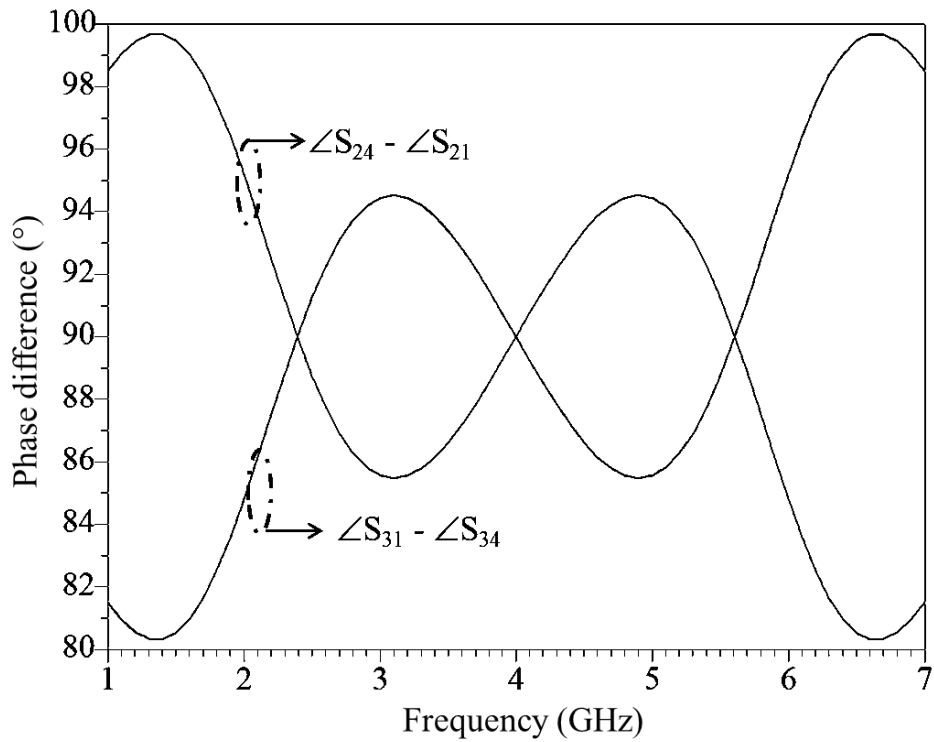
Fig. 3-19: Simulated improved cross-input phase difference.

41

Fig. 3-15 to Fig. 3-19 show the simulated results of the optimized Quadrature Magic-T circuit. Return losses for all the ports are larger than 10 dB from 2.5 GHz to 5.5 GHz. Instead of observing a single reflection zero, double reflection zeroes are observed in Fig. 3-15. Low amplitude imbalance is observed between the two output ports for the signal from either input. When the sum-port is excited, the power division is about 3.6 dB from 2 GHz to 6 GHz; when the delta-port is excited, the power divider is about 3.6 dB from 2.4 GHz to 5.6 GHz. The cross-output phase differences between port 2 and port 3 are 0° for the signals from the sum-port, and 180° for signal from the delta-port respectively. The cross-input phase difference at either of the output ports between the signal from sum and delta-ports is between 85° to 95°. Good isolation (above 40 dB) is observed even though the return losses are only larger than 10 dB. The improved circuit shows that a bandwidth of at least 2:1.

3.4   HFSS simulation

The proposed design shown in the previous section is only at schematic level. For actual implementation, the physical structure of the circuit has to be taken into consideration. Ansys HFSS simulation was used for this task. Fig. 3-20 shows the HFSS model of the circuit in microstrip structure. The structure consists of a balun portion for generating anti-phase signals and a power divider portion for generating in-phase signals.

Based on the previous ADS simulation, the coupled line in the balun portion requires high even-mode impedance and low odd-mode impedance. This

means that the gap and the width of the coupled lines have to be small and the thickness of the substrate has to be thick. As the smallest gap and width of the coupled lines are limited by the fabrication techniques, which is 0.1 mm and 0.2 mm respectively, the only parameter that can be varied is the thickness of the substrate. However, a thick substrate will result in the width of 50 ohm line to become very large, which is not acceptable due to high order mode considerations and difficulties in bending and matching with connectors. With these considerations, the substrate used is 32 mils RO4003 from Rogers Corporation. The 50 Ω line has a width of 1.8 mm. The thickness of the substrate will be locally increased from 32 mils to 64 mils for the balun area by stacking another 32 mil RO4003 to the main PCB. This will ease the challenge in meeting the strong coupling requirement.
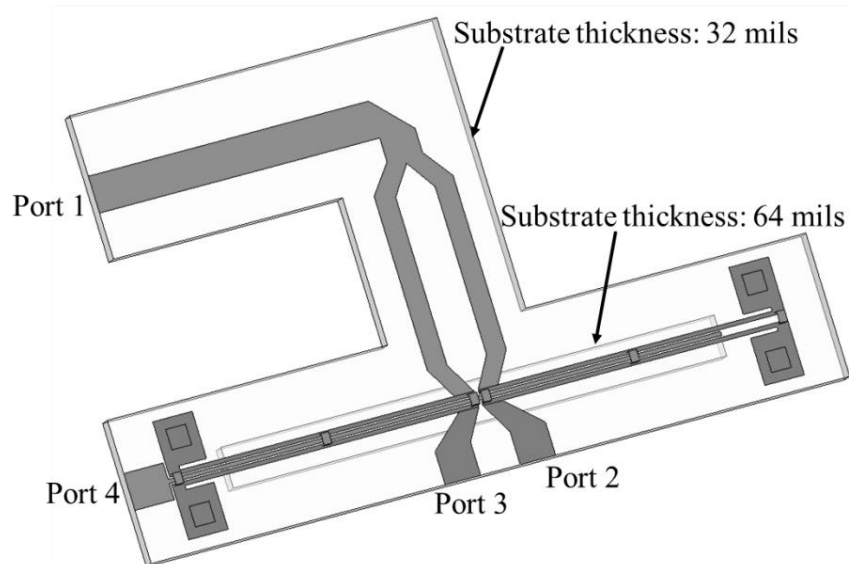
Fig. 3-20: HFSS model of a Quadrature Magic-T.

Fig. 3-21 to Fig. 3-24 show the HFSS simulation results of the Quadrature Magic-T. Port 2 and port 3 have achieved return losses larger than 10 dB from 2.1 GHz to 5.9 GHz. Port 4 achieves a return loss larger than 10 dB from 2.1 GHz to about 5.6 GHz. Except from 4 GHz to 5.2 GHz where the return loss is better than 9 dB, Port 1 has return losses larger than 10 dB from 2 GHz to 6.4 GHz. A reason for the difference may be due to the difference in even and odd mode phase velocities at the coupled line.

Fig. 3-22 shows the insertion losses when the signal enters from either Port 1 or Port 4. The amplitude imbalance between the two outputs is shown in Fig. 3-23. Between 2 GHz to 6 GHz, the amplitude imbalance is between -0.2 dB to 0.9 dB when Port 1 is excited; the amplitude imbalance is -1.4 dB to 0.3 dB when the signal enters from Port 4. Fig. 3-24 shows the isolation between the two input ports of the circuit. The isolation between Port 1 and Port 4 is larger than 29 dB.
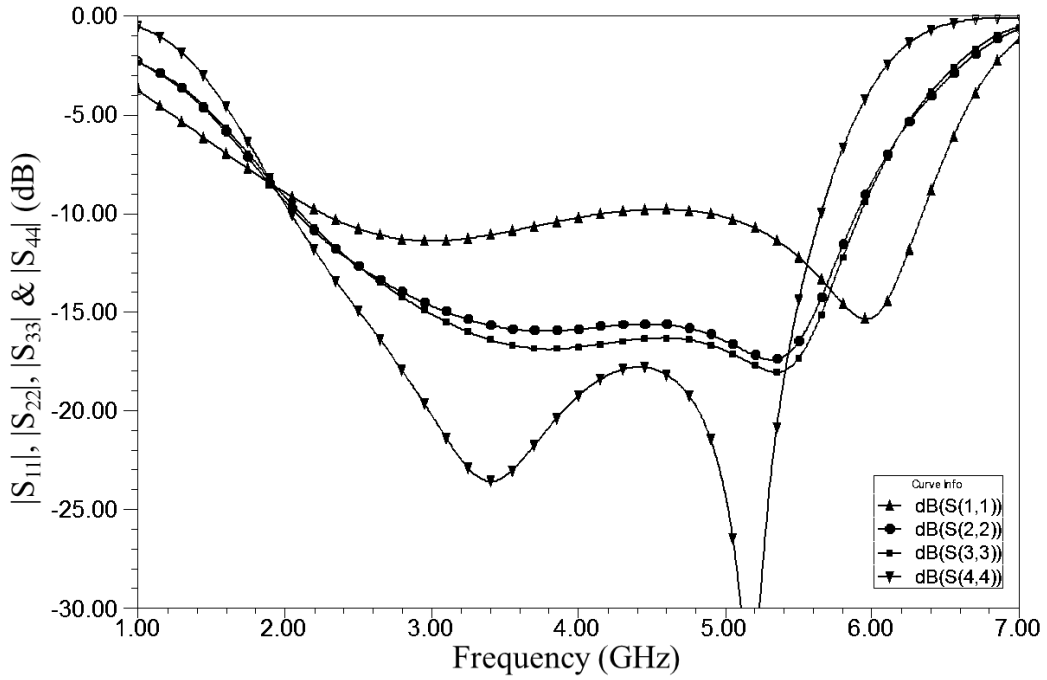
Fig. 3-21: $|S_{11}|$, $|S_{22}|$, $|S_{33}|$ and $|S_{44}|$ simulated in HFSS.
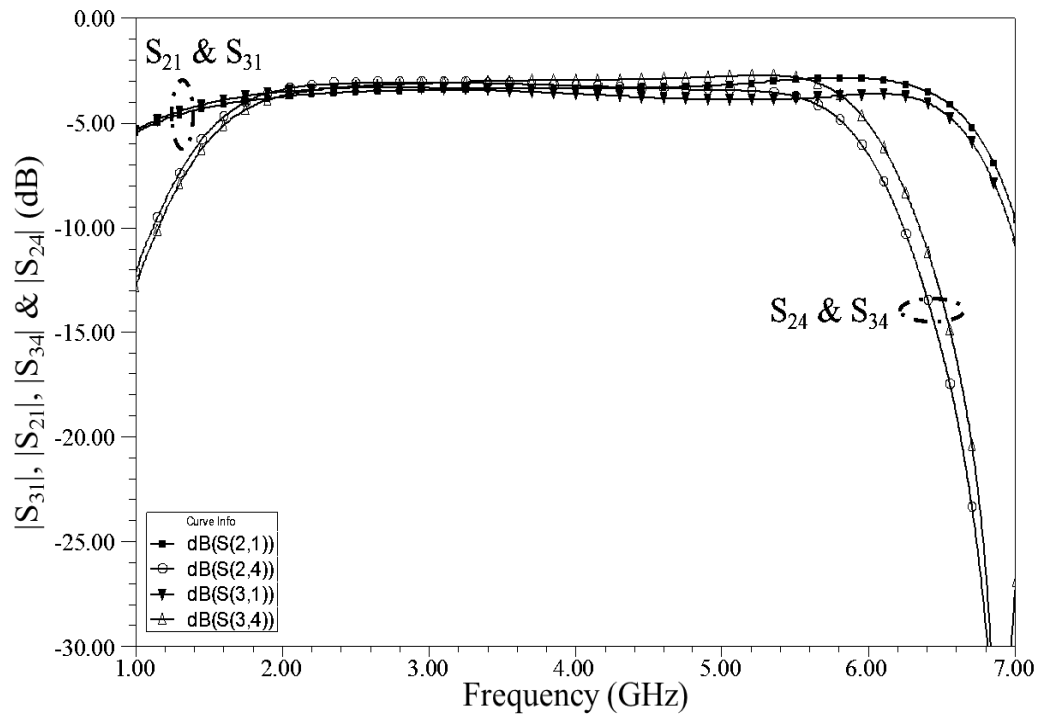
Fig. 3-22: $|S_{31}|$, $|S_{21}|$, $|S_{34}|$ and $|S_{24}|$ simulated in HFSS.

45
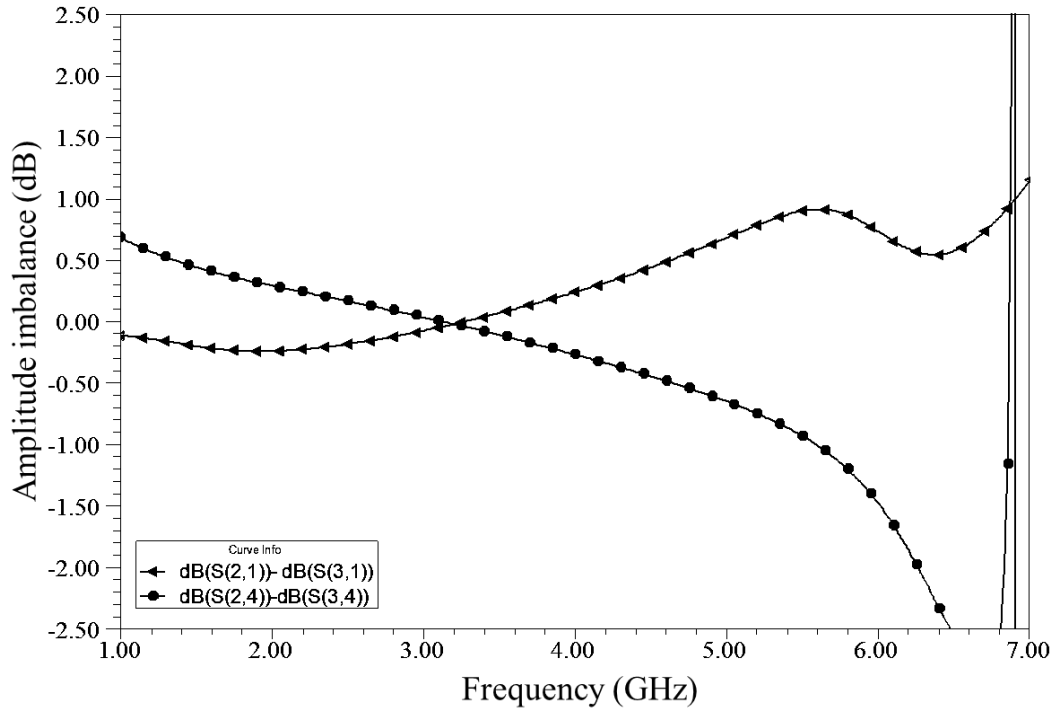
Fig. 3-23: Amplitude imbalance simulated in HFSS.
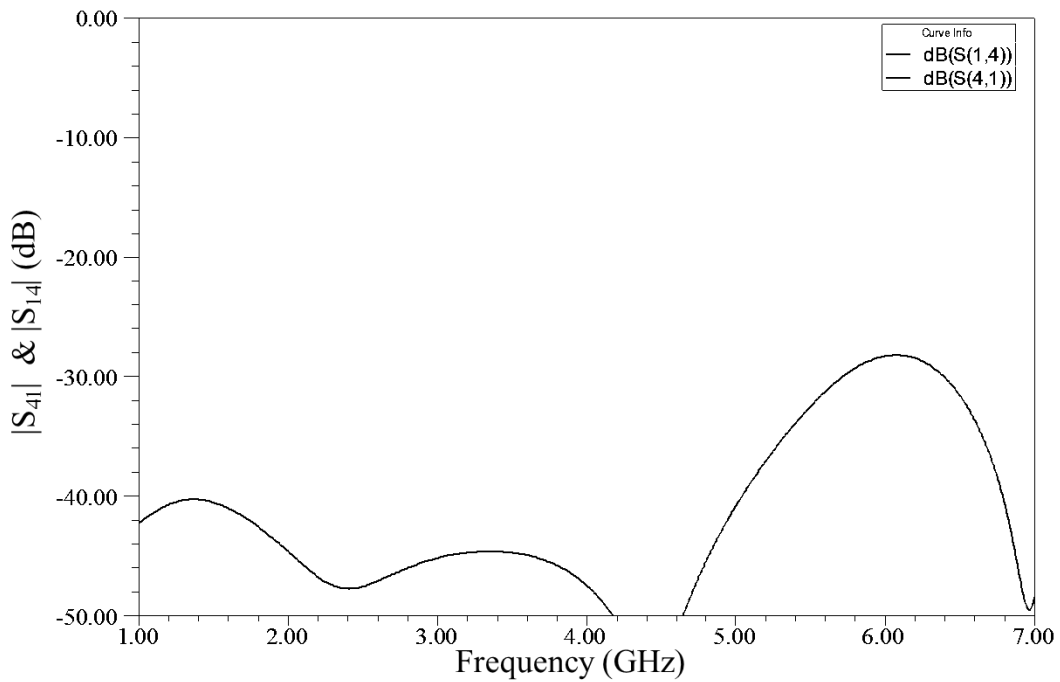
Fig. 3-24: $|S_{41}|$ and $|S_{14}|$ simulated in HFSS.
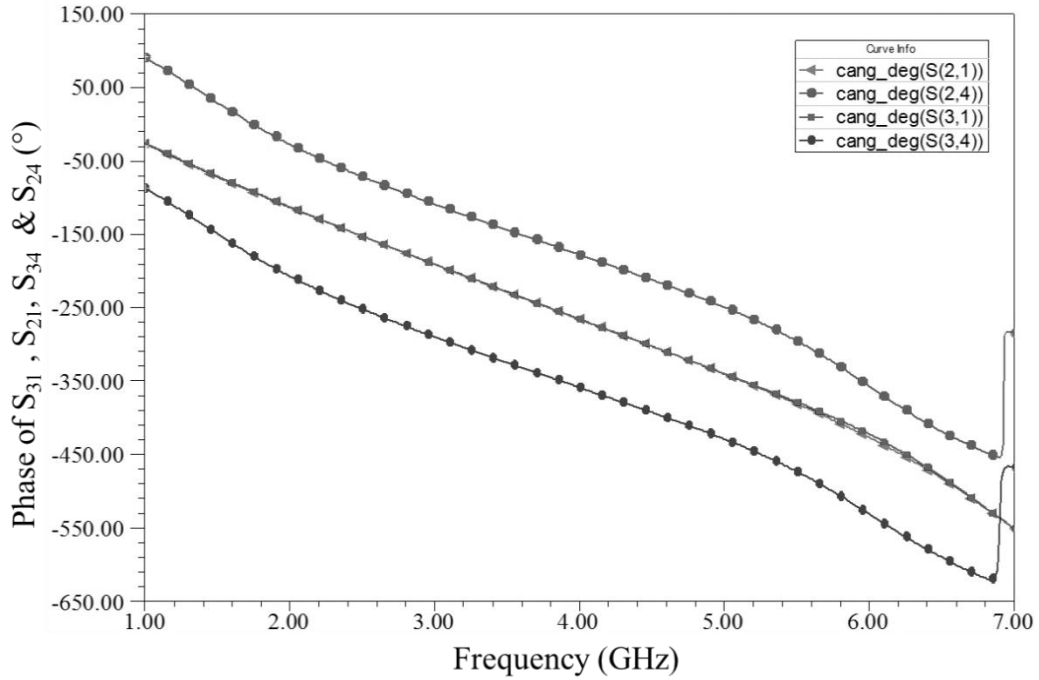
Fig. 3-25: Insertion phase simulated in HFSS.
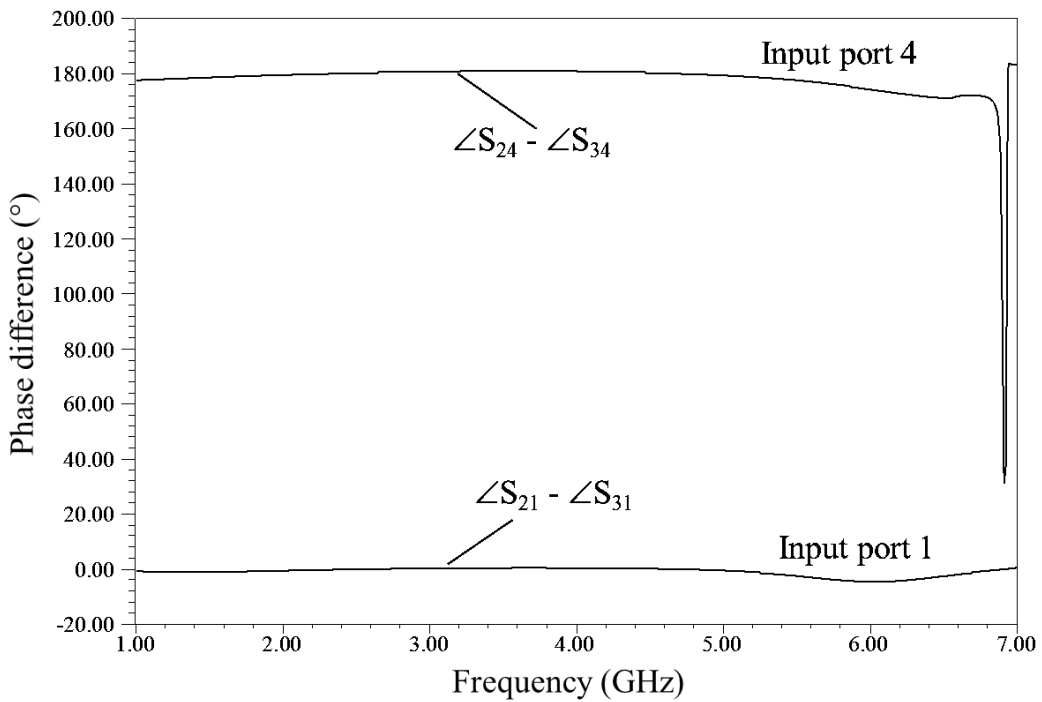
Fig. 3-26: Cross-output phase difference simulated in HFSS.
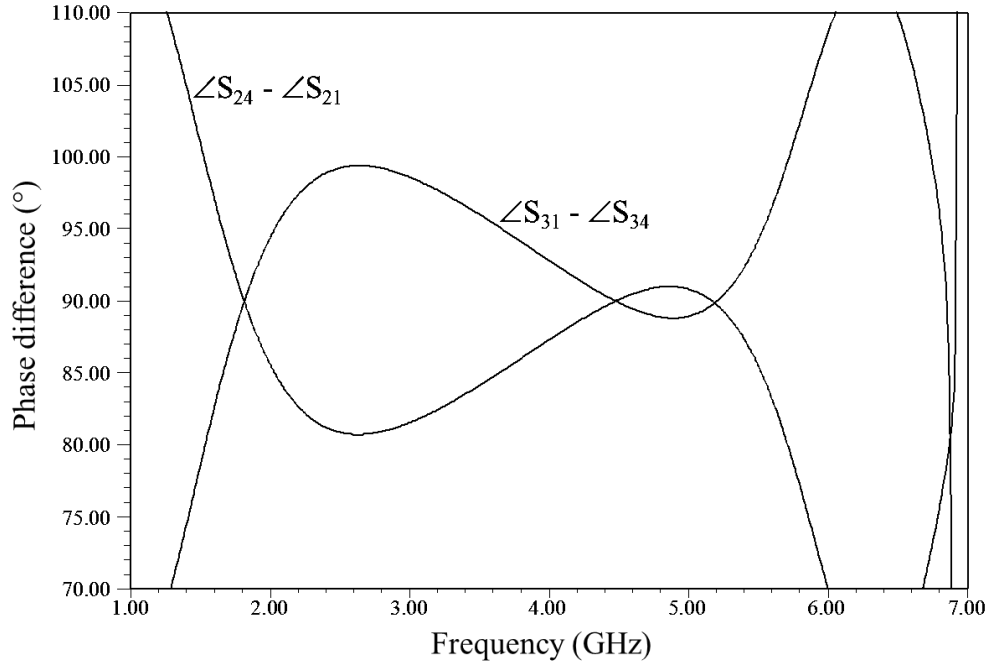
Fig. 3-27: Cross-input phase difference simulated in HFSS.

Fig. 3-25 shows the phase response of the circuit and Fig. 3-26 shows the cross-output phase difference between Port 2 and 3, respectively. For the sum-port input, the phase difference between Port 2 and Port 3 varies between -0.6° to 0.5° from 2 GHz to 5 GHz; the phase difference varies from 0.5° to 4.5° from 5 GHz to 6 GHz. For the delta-port input, the phase difference varies between 179° to 181° from 2 GHz to 5 GHz. The phase difference is between 173° to 179° from 5 GHz to 6 GHz. These results confirm the basic functions of a Magic-T circuit.

Fig. 3-27 shows the cross-input phase difference at each output port between the signals from sum and delta input ports. Between 2 GHz to 5.2 GHz, the phase difference is between 80.1° to 99.3°. This confirms the ability to perform quadrature summation of the input signals at the outputs for Quadrature Magic-T.

48

3.5 Fabrication and measurement results

The circuit was fabricated for testing. Fig. 3-28 shows the photo of the fabricated circuit. The PCB was milled using a LPKF S100 milling machine. The milling machine is capable of fabricating a minimum gap width of 0.1 mm. The X-Y resolution is about 0.25 μm. Excluding the connectors, the PCB board is about 40 mm by 28 mm. 0 Ω resistors are used to replace the jumper bond wires to connect the two transmission lines together. A slot on the bottom copper layer of the PCB was made and covered by a single-sided PCB so as to double the thickness of the substrate locally. The single-sided PCB takes the same size as the slot and was soldered to the larger PCB. The circuit was measured using an Agilent PNA and a TRL calibration was used. The circuit was measured from 1 GHz to 7 GHz and 401 data points were collected. The extra ports were terminated with 50 Ω loads during the measurement. The measurement includes the effect of the connectors. Six data sets were collected and combined into one S parameter file using ADS.
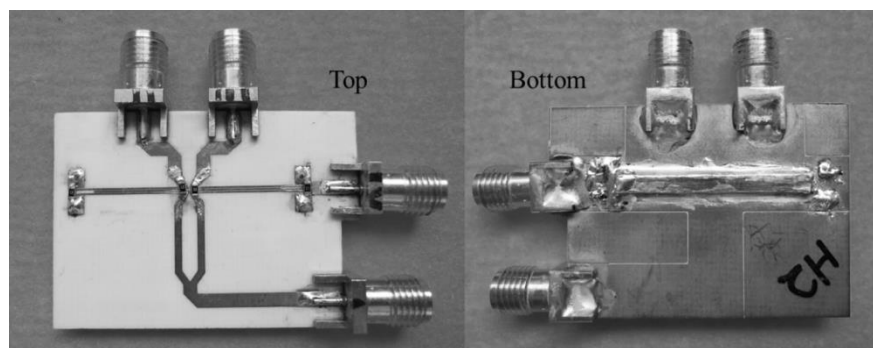
Fig. 3-28: Photo of the fabricated Quadrature Magic-T circuit.
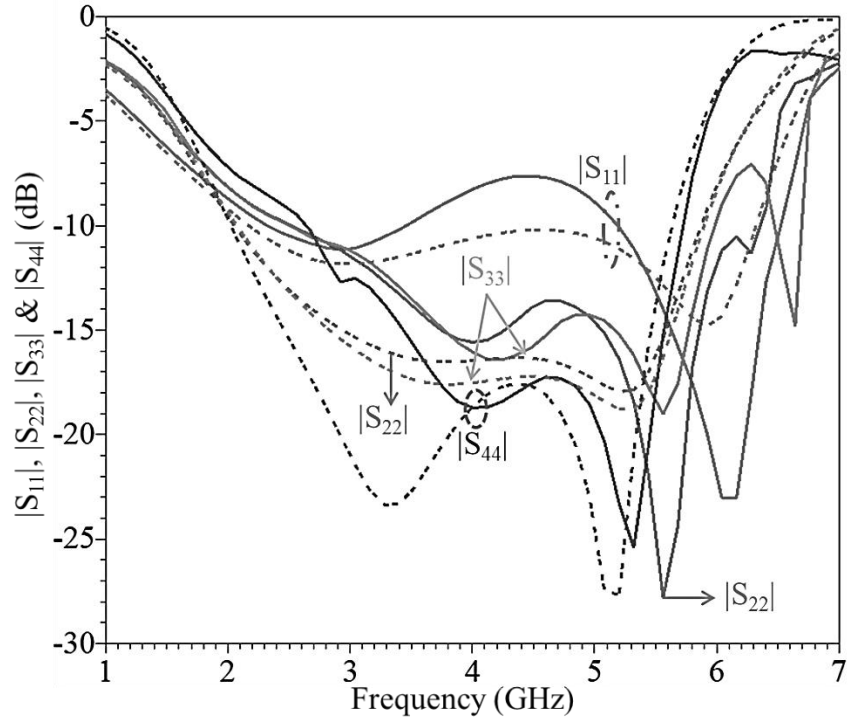
Fig. 3-29: Measured (solid line) and simulated (dotted line) $|S_{11}|$, $|S_{22}|$, $|S_{33}|$ and $|S_{44}|$ of the Quadrature Magic-T.
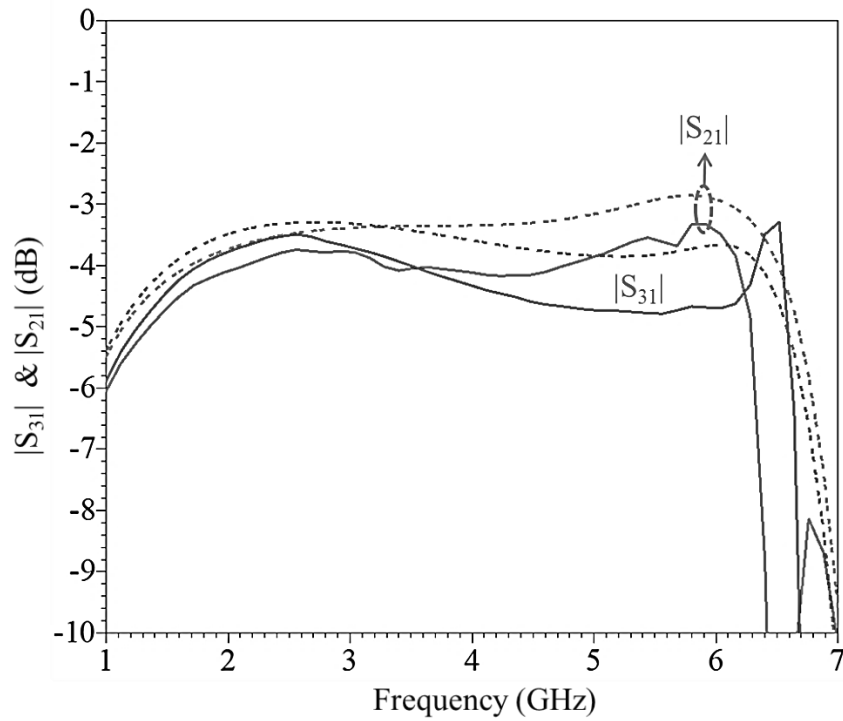
Fig. 3-30: Measured (solid line) and simulated (dotted line) $|S_{31}|$ and $|S_{21}|$ for the sum-port excitation.
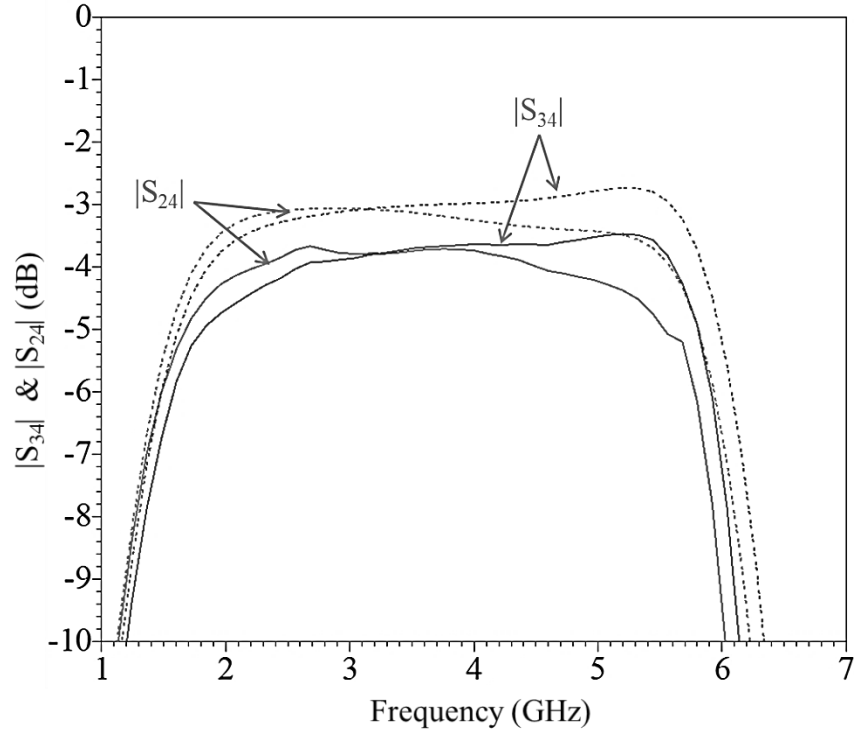
Fig. 3-31: Measured (solid line) and simulated (dotted line) $|S_{34}|$ and $|S_{24}|$ for the delta-port excitation.
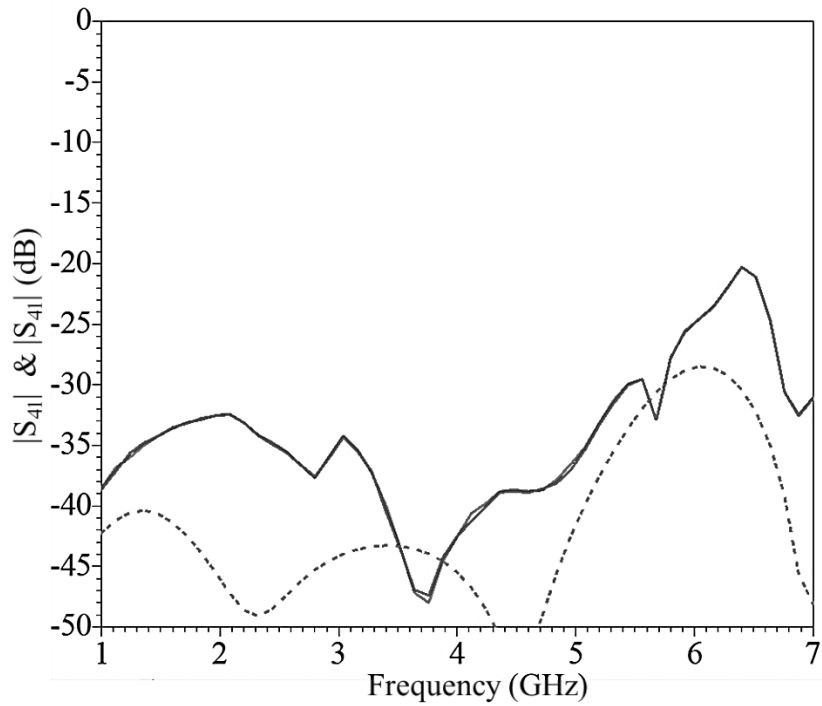
Fig. 3-32: Measured (solid line) and simulated (dotted line) $|S_{41}|$ and $|S_{14}|$.
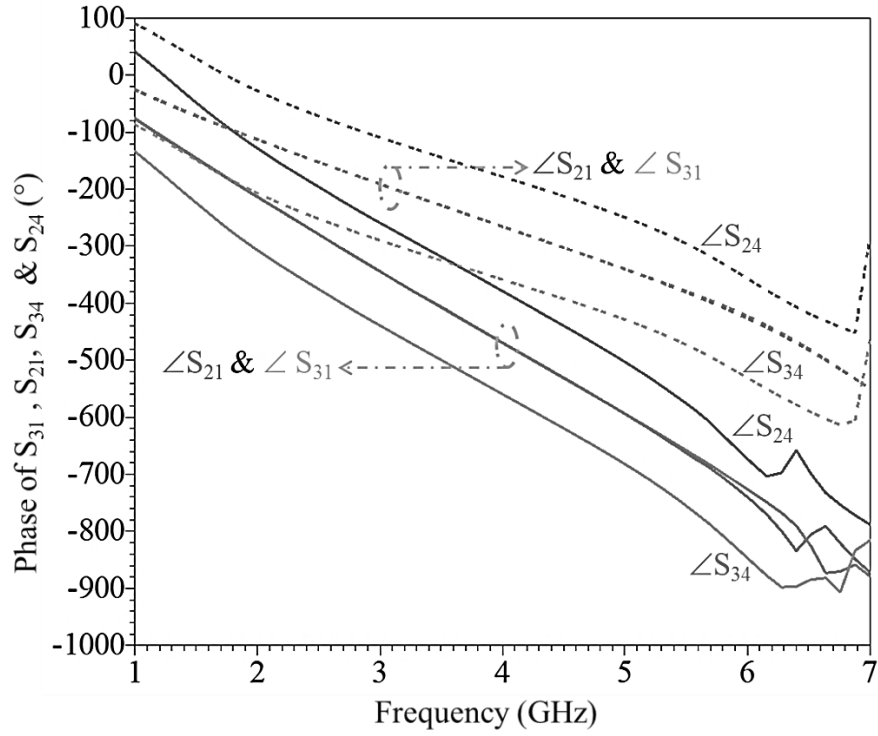
Fig. 3-33: Measured (solid line) and simulated (dotted line) insertion phase response.
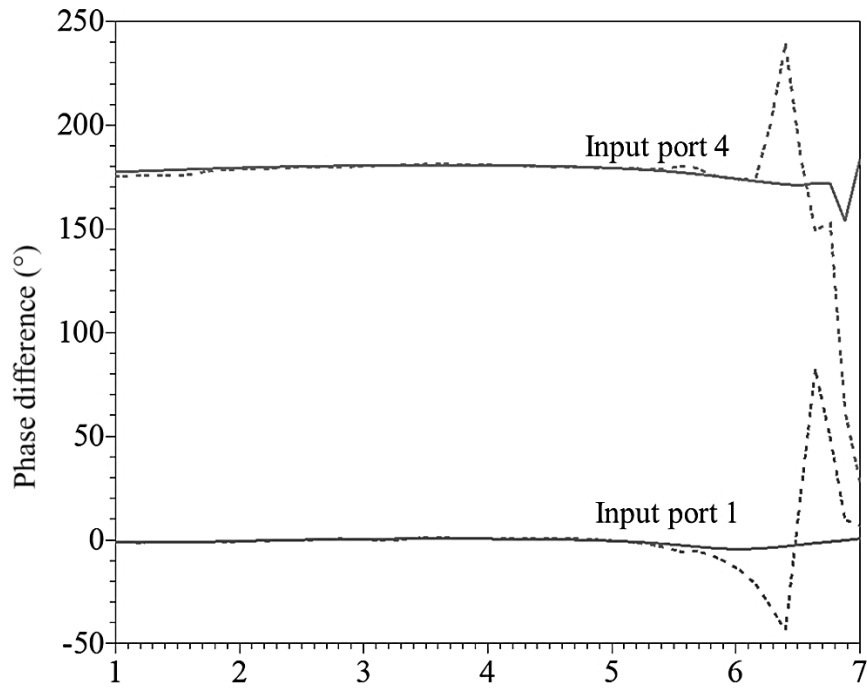
Fig. 3-34: Measured (solid line) and simulated (dotted line) cross-output phase difference.

52
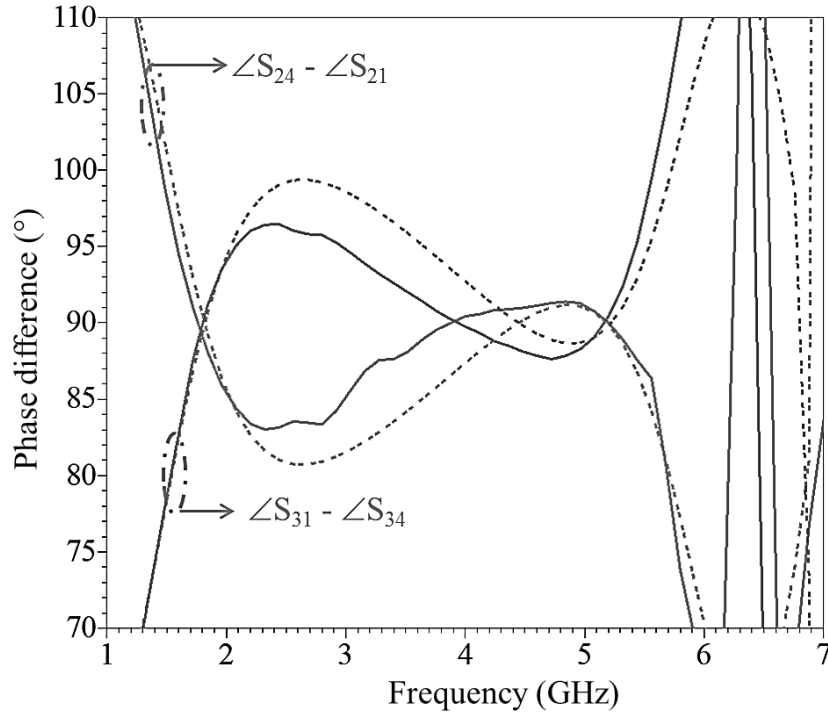
Fig. 3-35: Measured (solid line) and simulated (dotted line) cross-input phase difference.

Fig. 3-29 shows the measured return losses of the circuit. The return loss is larger than 10 dB from about 2.5 GHz to 6 GHz for Port 2 and Port 3. The return losses are larger than 10 dB from 2.7 GHz to 5.7 GHz for Port 4 (Fig. 3-12), and larger than 7.5 dB from 2 GHz to 6.5 GHz for the sum-port. Fig. 3-30 and Fig. 3-31 show the insertion losses of the circuit. The insertion losses of the circuit are about 4 dB. A greater amplitude variation is observed at higher frequencies. Fig. 3-32 shows that the isolation between sum and delta-port is more than 25 dB for frequencies below 6 GHz. Fig. 3-33 shows the phase response of the circuit and Fig. 3-34 shows the cross-output phase difference between Port 2 and Port 3. When the signal is applied at the delta-port, the phase difference is between 178° to 181° from 2 GHz to 5.4 GHz and between 173° and 180° from 5.4 GHz to 6 GHz. When the signal enters from the sum-port, the phase difference is

between -1.1° and 0.824° from 2 GHz to 5 GHz and between 0.4° and 13.2° from 5 GHz to 6 GHz. This confirms the basic function of a magic-T circuit.

Fig. 3-35 shows the cross-input phase difference. From 2 GHz to 5.4 GHz, the phase difference is between 87° and 97° at port 3 and between 83° and 92° at Port 2. This confirms the function of Quadrature Magic-T circuit.

3.6   Analysis and conclusions

Compared to the HFSS simulation results, the measured bandwidth is smaller and the frequency band has shifted up. In addition, a greater amplitude imbalance is observed for frequencies above 3.5 GHz. However, the phase performance of the simulated results is close to the measurement results.
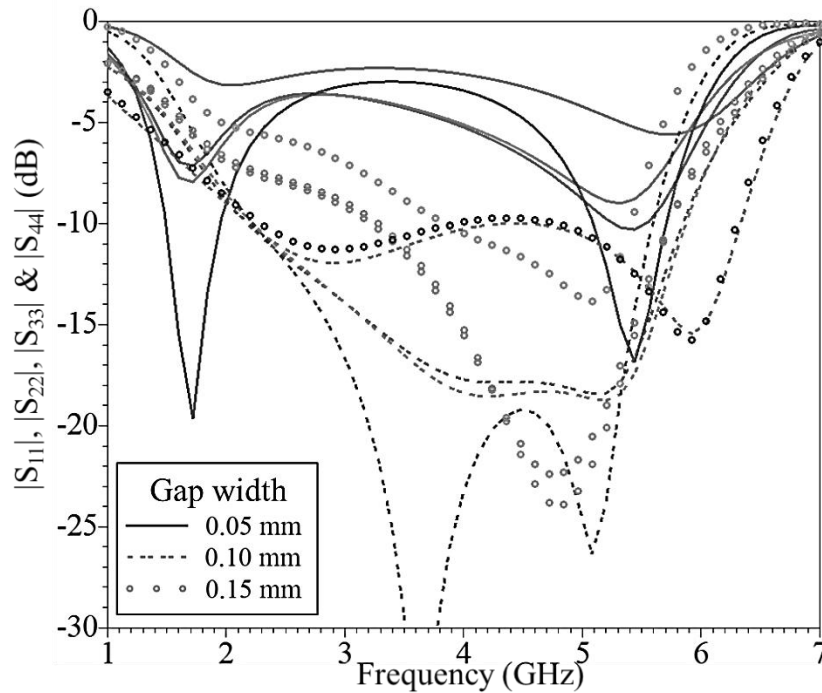
Fig. 3-36: Simulated $|S_{11}|$, $|S_{22}|$, $|S_{33}|$ and $|S_{44}|$ for different coupled line gap width.
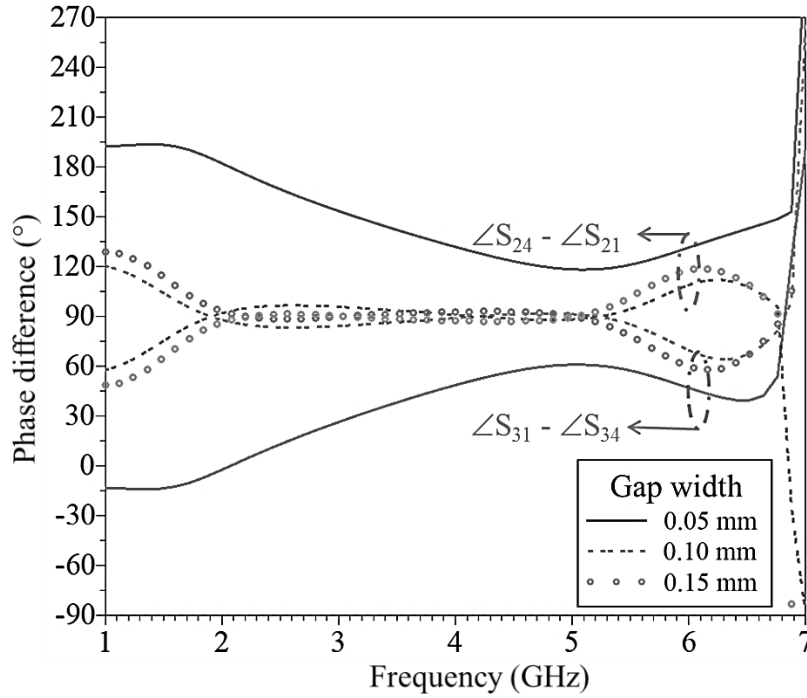
Fig. 3-37: Simulated cross-input phase difference for different coupled line gap width.

The discrepancies between the HFSS simulation and measurement results are probably due to the variation in coupled line section. Fabrication errors in the line width and the gap of the coupled line will greatly affect the performance of the circuit. Fig. 3-26 and Fig. 3-27 are the simulated results of the circuit when the gap between the coupled-line is varied. The return losses of the circuit deteriorate significantly even when the change is only 0.05 mm.

Though the circuit performs worse than expected, the concept to realize a Quadrature Magic-T by introducing an additional section of transmission line to the normal planar magic-T circuit is proven. This circuit will be used to achieve the broadband two-way vector-sum phase shifter for the polarization controller.

55

Chapter 4 Broadband 90° Phase shifter

4.1   Introduction

To extend the phase shift to full 360°, fixed value phase shifters with broad bandwidth are required. A prototype phase shifter will be designed, fabricated and tested before it is used in the final circuit design.

Phase shifters are used to change the phase of the reflected or transmitted signals. They are widely used in beam scanning phased arrays and phase modulators. Common types of passive phase shifters include loaded line, reflection type and switched network [22].

In the loaded-line phase shifter the insertion phase is changed through the load admittance attached to the transmission line. An advantage is that it does not have any spurious resonances. However, its drawback is that it is only suitable for small relative phase shifts [22]. A 90° loaded line phase shifter with 21% bandwidth and a phase error of ±2° is reported in [23].

Reflection type of phase shifters normally consist of a 3 dB directional coupler and two reflective terminations [22]. When tunable terminations, such as a varactor, are used, it is possible to achieve 360° phase shift [24]. In addition, reflection type of phase shifters is able to achieve relatively wideband performance [25]. However, the bandwidth of the phase shifters is affected by the bandwidth of the terminations and the coupled line [22], [25].

The switched network phase shifter includes switched line network, high pass/low pass network and all-pass network (e.g. Schiffman phase shifter). The phase shift of the switched line phase shifter depends on the insertion phase of the reference line and the delay line. It is normally used to implement large phase shifts. However, the required phase shift can only be accurately achieved at the center frequency [22].

The high pass/low pass phase shifter uses a low pass filter to achieve a phase lag and a high pass filter to achieve a phase lead. Typically, lumped elements are used to implement the circuit. A relatively wide bandwidth and compact layout can be achieved using this design. However, larger phase errors are observed in the larger phase bits when the bandwidth increases [26].

The Schiffman phase shifter achieves phase shift through a tightly coupled transmission line which is referenced to a normal transmission line. It has a few variant topologies such as double Schiffman phase shifter, cascaded Schiffman phase shifter, and parallel Schiffman phase shifter [27]. The bandwidth of such phase shifters can be increased by either increasing the coupling ratio of the coupled line or using multi-section of coupled lines. However, the design requires equal phase velocity for both even and odd mode in the coupled-line section [28]. Degradation in performance will be observed if there is a mismatch in phase velocities. Therefore, it is very challenging to implement the Schiffman phase shifter using microstrip line.

A variation to the Schiffman phase shifter was reported in [29]. The layout is similar to a parallel schiffman phase shifter except that one of the coupled lines is shorted to ground. It achieves 180° phase shift with 90% bandwidth. The phase deviation is within ±6° and the amplitude imbalance is within 0.5 dB.

Due to bandwidth consideration, this circuit is chosen over other topologies to extend the phase coverage of the vector sum phase shifters to 360°. To ease the challenge in implementing the circuit in microstrip line, instead of an 180° phase shifter, a 90° phase shifter will be designed, fabricated and tested.

4.2   Broadband 90° Phase shifter

A differential phase shifter that is similar to all-pass structures can be achieved using band-pass topologies [30]. The phase error produced by a C-section all-pass structure is opposite to that of a bandpass structure. As such, when the two circuits are combined together, it is possible to achieve smaller phase errors. Fig. 4-1 shows the topology of the phase shifter [30]. The diagram on the left is the phase delay circuit. It consists of two ports (Port 1 and Port 2) and two sections of coupled lines. The two C- section coupled lines are connected in parallel. The C-section coupled lines are connected to each other in parallel at the non-short circuited ends. At the short circuited end, one of the coupled line is connected to the ground. The right side of the diagram is the reference line. It consists of port 3, port 4 and a transmission line. When the circuit is used, Port 1 and Port 3 are excited in phase. The output signals at Port 2 and Port 4 will have a phase difference of 90°.

58
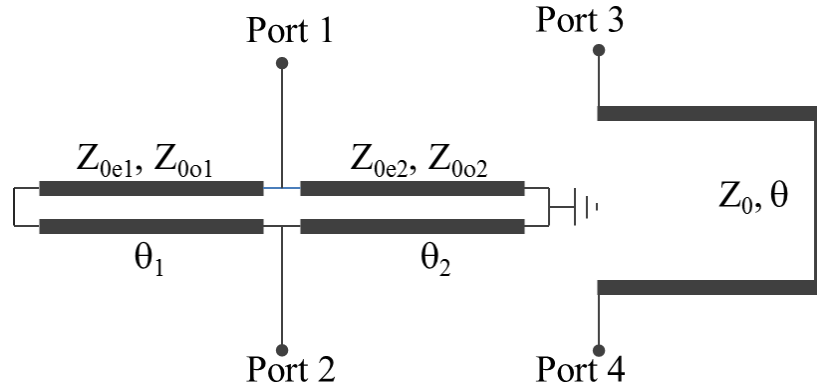
Fig. 4-1: Topology of the bandpass and all-pass phase shifter [30].

4.3   ADS simulation and design

To verify the functionality of the circuit, Fig. 4-1 was simulated using Agilent ADS. The required even and odd mode impedances for the two coupled line are Z_{0e1} = 64 Ω, Z_{0o1} = 57 Ω, Z_{0e2} = 108 Ω and Z_{0o2} = 50 Ω. The electrical length of the reference line, θ, is 270° at 4 GHz and its impedance is 50 Ω. The θ_1 and θ_2 are both 90° at 4 GHz.

Fig. 4-2 to Fig. 4-6 show the simulation results. The ideal circuit is able to achieve return losses larger than 15 dB for Port 1 and Port 2 and a perfect match for Port 3 and Port 4. Fig. 4-3 shows the insertion loss of the circuit. The insertion loss between Port 2 and Port 1 is smaller than 0.14 dB. Fig. 4-4 shows the amplitude imbalance between the two paths with the maximum imbalance of 0.14 dB from 2 GHz to 6 GHz. Fig. 4-5 and Fig. 4-6 show the phase response and the phase difference between the two paths respectively. The phase error is less than ±1.5° between 2 GHz and 6 GHz.

59
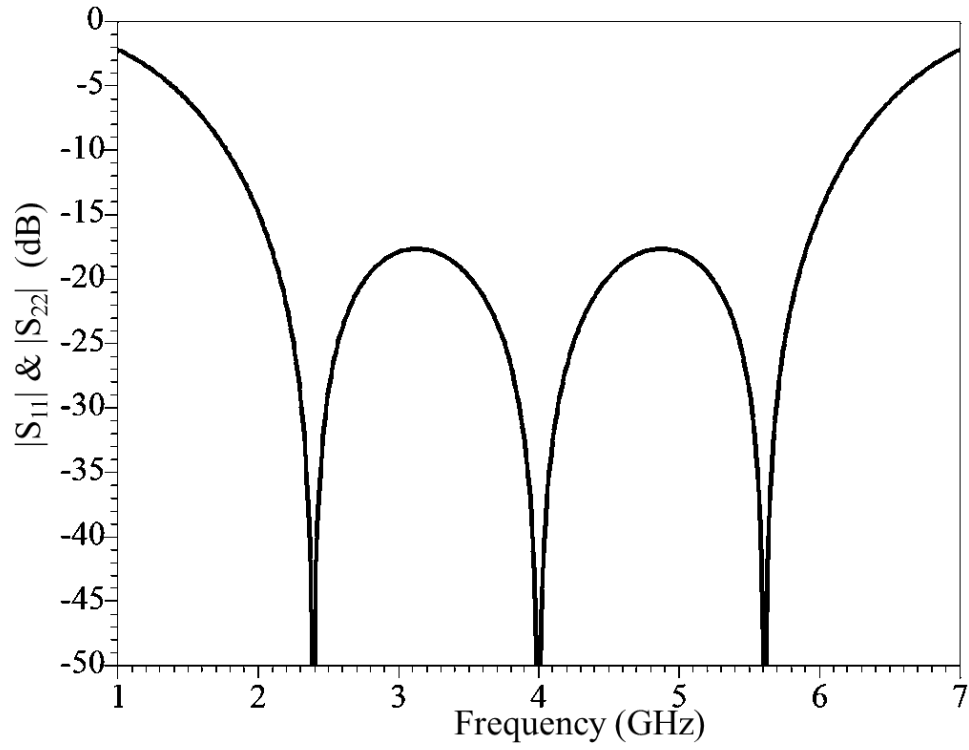
Fig. 4-2: Simulated |S$_{11}$| and |S$_{22}$| of the phase shifter.
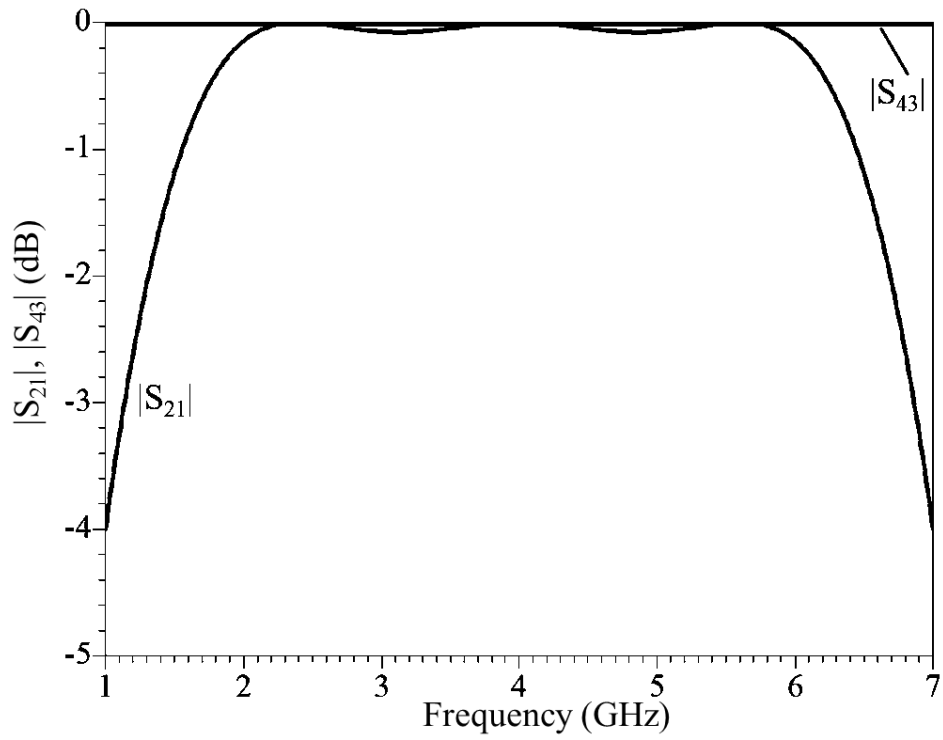
Fig. 4-3: Simulated |S$_{21}$| and |S$_{43}$| of the phase shifter.

60
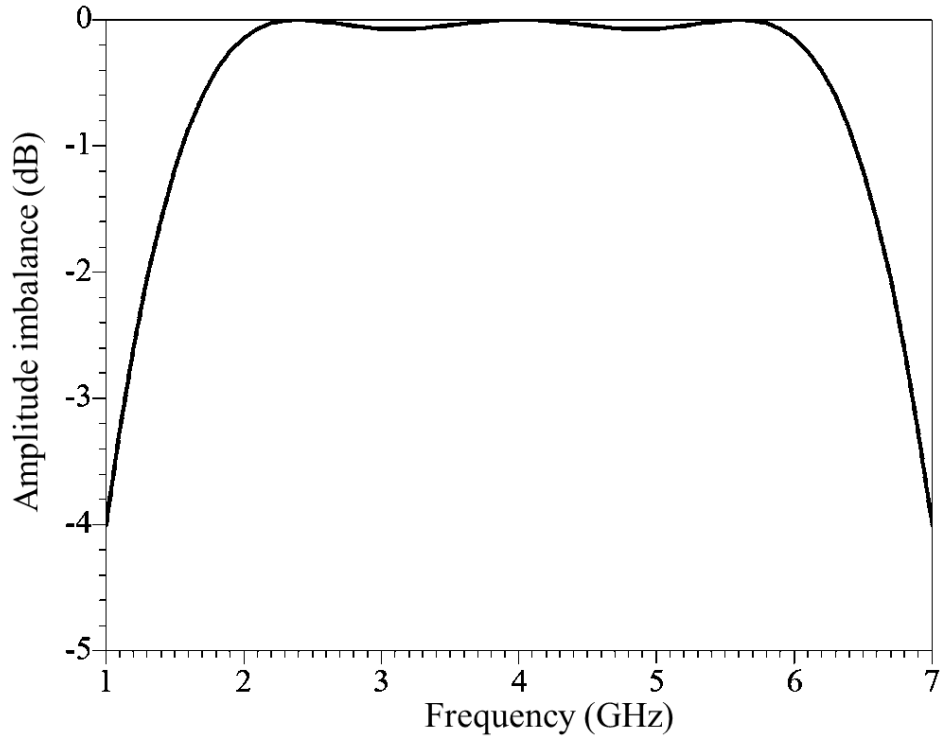
Fig. 4-4: Amplitude imbalance between the two paths.
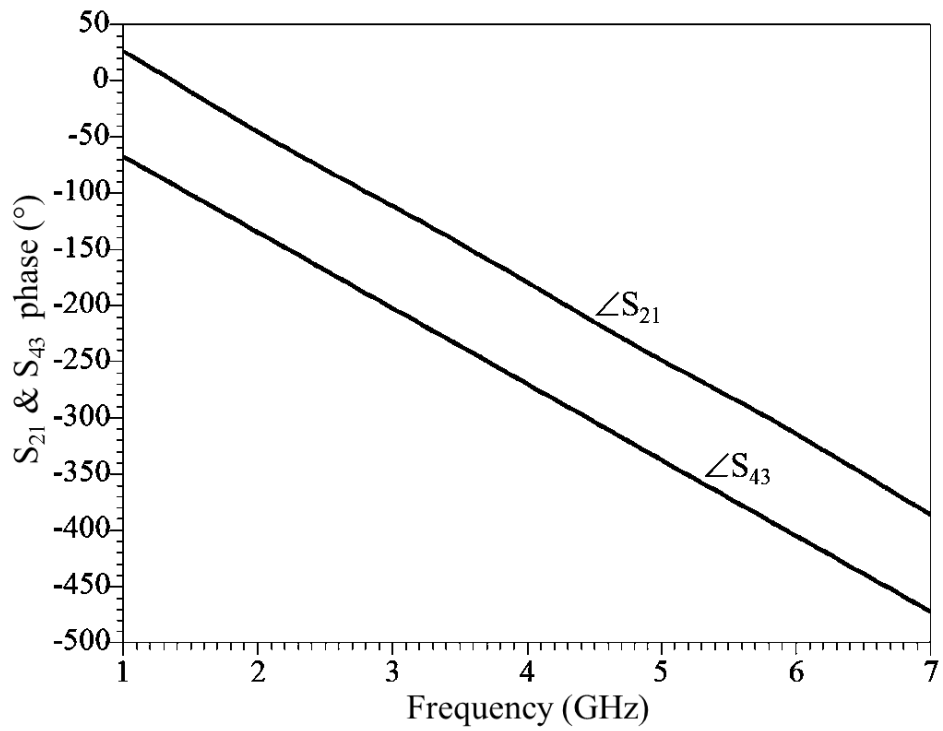
Fig. 4-5: Simulated phase response of the phase shifter.
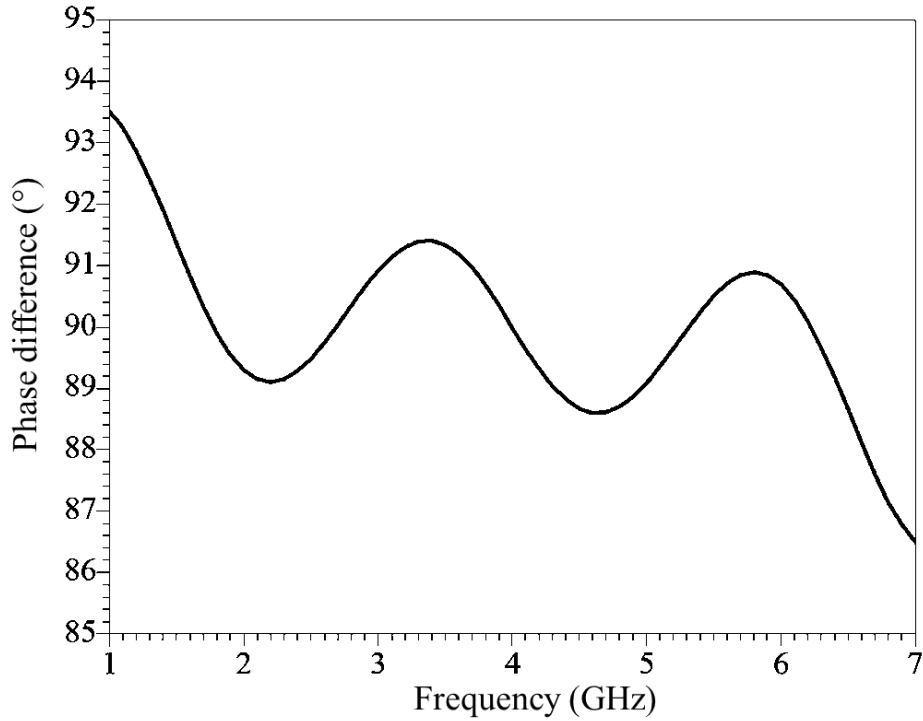
Fig. 4-6: Phase difference between the two paths.

4.4 HFSS simulation and implementation

The circuit was simulated using Ansys HFSS. Fig. 4-7 shows the HFSS model of the circuit. The circuit was implemented on 32 mils RO4003 substrate. The overall size of the circuit is 55 mm by 19 mm. The weakly coupled lines have a width of 1.4 mm and a gap width of 2 mm. The strongly coupled lines have a width of 0.7 mm and a gap width of 0.1 mm. L1 and L2 are about 9.9 mm and 9.8 mm respectively. The length L3 is 10 mm and L4 is about 14.21 mm. These design parameters were tuned to take into consideration of the minimum gap width that can be fabricated.

Fig. 4-8 shows the fabricated phase shifter. In the prototype, via holes were implemented by soldering a wire from the end to the ground. This may not perform as good as plated through via.
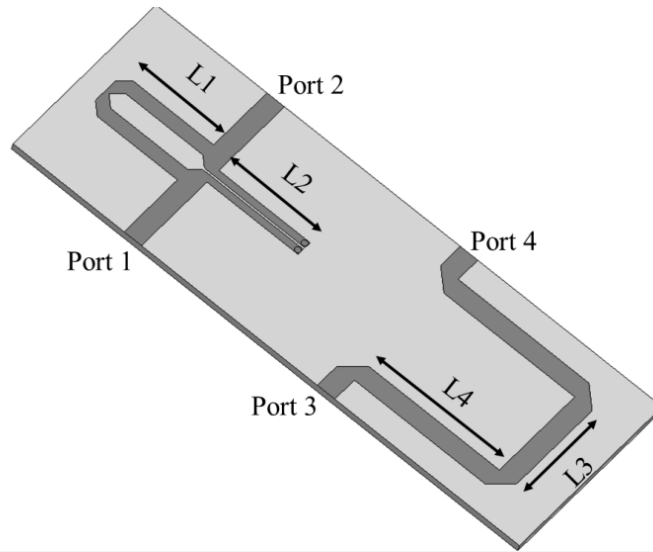
Fig. 4-7: HFSS simulation model of the phase shifter.
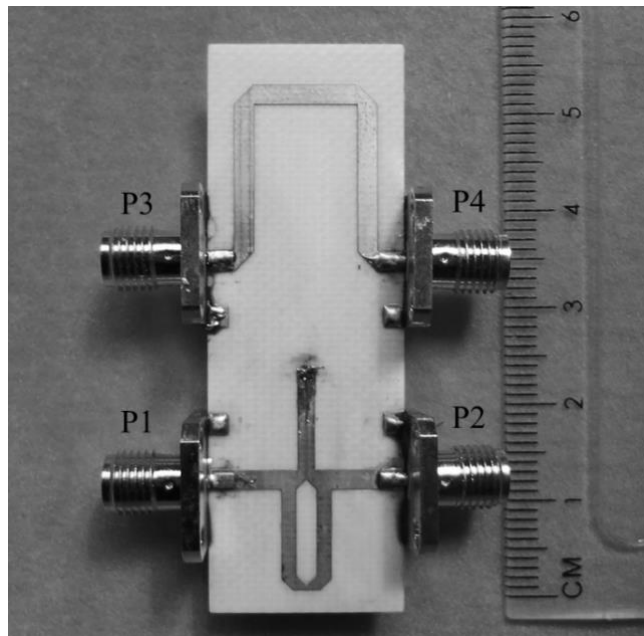
Fig. 4-8: Fabricated phase shifter.

4.5 Results and analysis

The circuit was measured using an Agilent PNA from 1 GHz to 7 GHz. The measurement results were compared with the simulation results. Fig. 4-9 and Fig. 4-13 show the measured and simulated results. Fig. 4-9 shows the $|S_{11}|$ and $|S_{22}|$ of the phase delay path. Fig. 4-10 shows the $|S_{33}|$ and $|S_{44}|$ of the reference path. The simulated results of the delay line achieve a return loss larger than 15 dB from 2 GHz to 6 GHz. Three reflection zeroes were found in the simulated results. In the measurement, the circuit only achieves a return loss larger than 15 dB and only two reflection zeroes are observed. The difference between the simulated and measured results is partially due to the missing reflection zero which is the direct result of some implementation errors such as the fabrication error in the gap width of tightly coupled line and the grounding vias.

For the reference line path, the measured return loss is larger than 14 dB from 2 GHz to 5.9 GHz. This shows that the connector is not properly matched with the transmission line. This mismatch may be due to the variation in the PCB thickness caused by the difficulty in controlling the milling depth. The uncertainty can be removed when an etching method is used to fabricate the PCB.
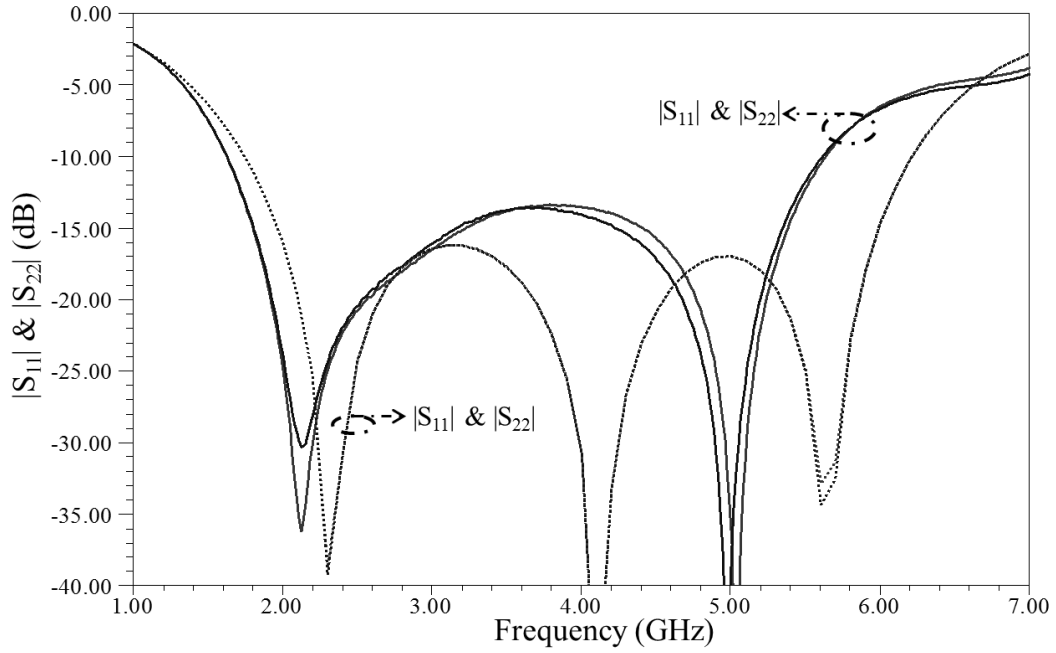
Fig. 4-9: Simulated (dotted line) and measured (solid line) $|S_{11}|$ and $|S_{22}|$.
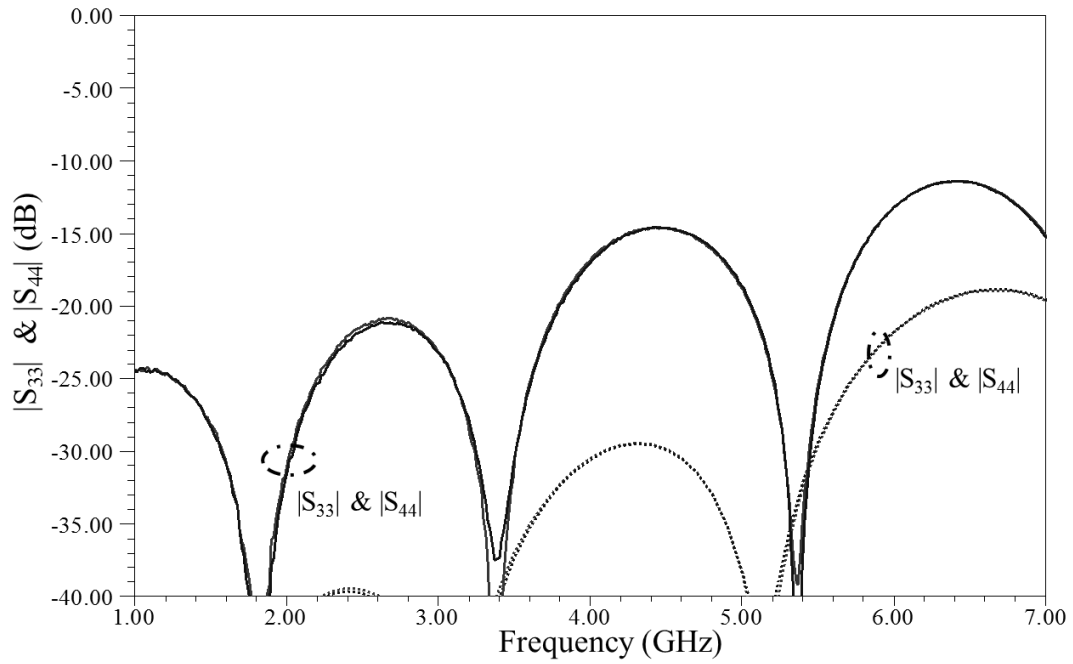
Fig. 4-10: Simulated (dotted line) and measured (solid line) $|S_{33}|$ and $|S_{44}|$.
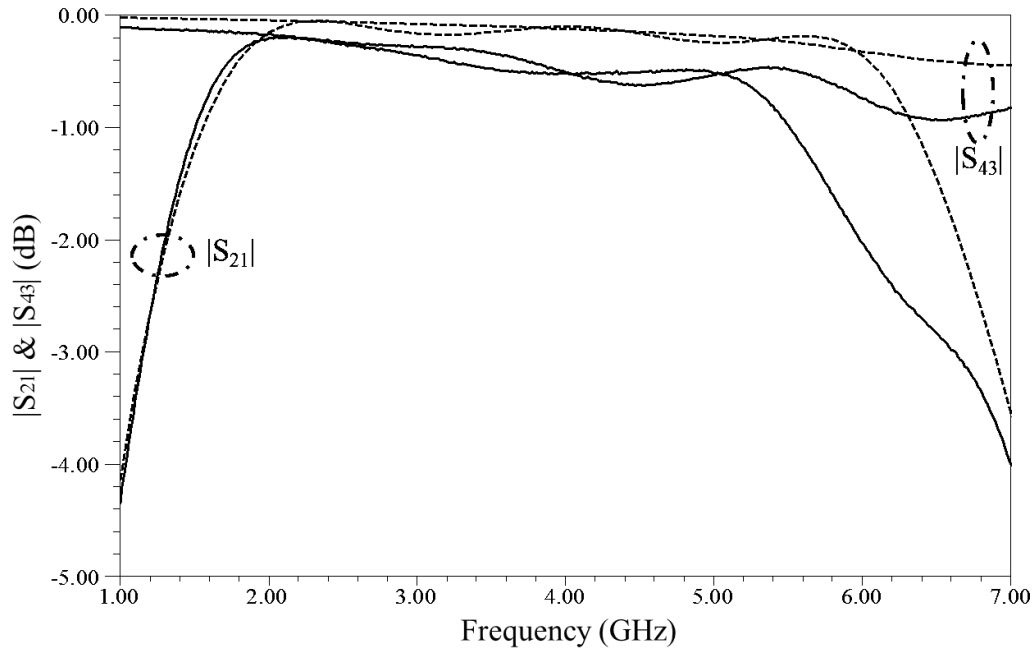
Fig. 4-11: Simulated (dotted line) and measured (solid line) $|S_{21}|$ and $|S_{43}|$.
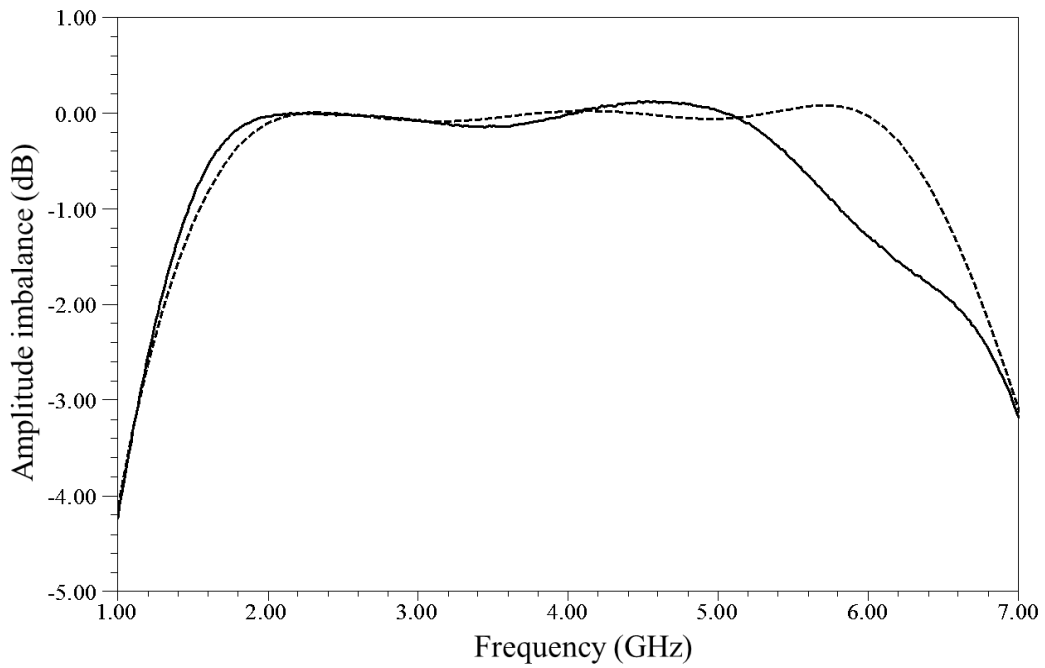
Fig. 4-12: Simulated (dotted line) and measured (solid line) amplitude imbalance.
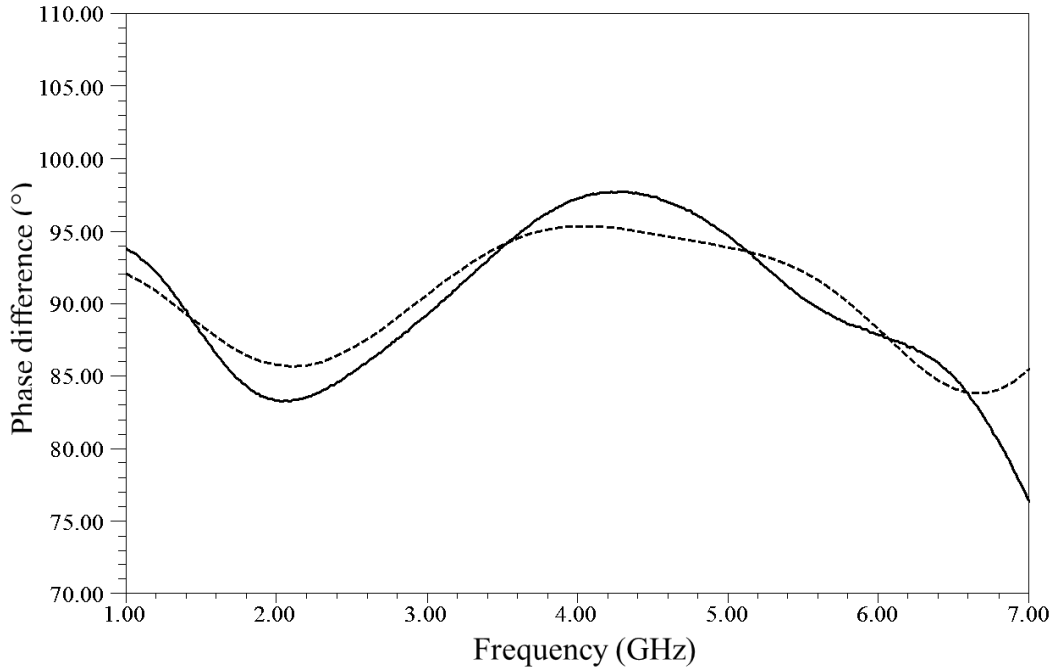
Fig. 4-13: Simulated (dotted line) and measured (solid line) phase difference.

Fig. 4-11 shows the insertion losses and Fig. 4-12 shows the amplitude imbalance of the circuit for the two paths. The simulated amplitude imbalance is ±0.08 dB from 2 GHz to 6 GHz. However, the measured amplitude imbalance is between -0.15 dB and 0.11 dB from 2 GHz to 5.2 GHz and between -0.15 dB and -1.3 dB from 5.2 GHz to 6 GHz. The increase in amplitude imbalance is probably due to the low return loss achieved by the delay line. Fig. 4-13 shows the phase difference between the two paths. The simulated phase difference is 90° with an error of about ±5°, while the measured phase difference is 90° with an error of about ±7.5°. These performance differences between the simulated and measured results are due to the issues as that of the poor return loss.

4.6　Conclusions

A broadband 90° phase shifter was designed and implemented for 2 GHz to 6 GHz. Though there are some differences between the simulated and the measured results, the objective to validate the performance of the circuit through building a prototype is achieved. With better fabrication procedure, the circuit can be integrated in the final polarization control circuit.

The design is able to achieve 90° phase shift with a phase error of ±5°, amplitude imbalance of ±0.08 dB and a return loss larger than 15 dB from 2 GHz to 6 GHz. The prototype has achieved 90° phase shift with phase error of about ±7.5°, amplitude imbalance from -0.15 dB to 0.11 dB and a return loss larger than 13 dB from 2 GHz to 5.2 GHz.

Chapter 5 Control circuits

5.1 Introduction

As variable gain amplifiers and RF switches are required in the two-way vector sum phase shifter design, it is necessary to verify these components' performance before they are used. In this chapter, commercially available variable gain amplifiers and RF switches will be chosen and separately tested.

5.2 Variable gain amplifier prototype

A variable gain amplifier (VGA) is an amplifier where the gain depends on the applied control voltages. It is widely used for automatic gain control and amplitude modulation. Recently, it was used in vector-sum phase shifters to change the phase of a signal by adjusting the relative amplitude of the vector signals [10], [31].

There are two main types of variable gain amplifiers commercially available: analog and digital. The analog VGA is able to achieve continuous gain variation while the digital VGA has a limited number of gain states which depends on the number of control bits.

For the application in the continuous vector sum phase shifter, the analog VGA is preferred as its gain can be continuously changed. Additionally, a VGA should have a flat gain performance and a predictable phase variation across the whole frequency band. Practically, however, these requirements are difficult to

fulfill as there are always phase dispersion and gain fluctuations. As such, a VGA with a bandwidth that is greater than the requirement will be preferred so that for the desired frequencies, a flat gain can be observed.

Table 5-1: VGA performance comparison.

Model	Frequency (GHz)	Gain (dB)	Bias (V)	Noise Figure (dB)	P1dB (dBm)	OIP3 (dBm)
Hittite - HMC972LP5	0.5 – 6	-35 – 15	5	7.5	21	28
Avago - VMMK-3503	0.5 – 18	-11 – 12	3-5	4.2	8	8

Two possible candidates, Hittite HMC972LP5 [32] and Avago VMMK-3503 [33] are identified. The parameters of the two VGAs are shown in Table 5-1. Based on the datasheets, the Avago VGA has significantly larger bandwidth and less gain variation from 2 GHz to 6 GHz compared to the Hittite VGA. Therefore, the Avago VGA is chosen for further study.

Two prototype circuits using the VGA IC components are implemented and measured. Fig. 5-1 is a drawing of the recommended biasing network for the VGA. Fig. 5-2 shows the photograph of the fabricated prototype which is implemented on 32 mils RO4003 substrate. Due to in house fabrication, rivets were used to implement the vias on the prototype PCB. A PNA is used to measure the circuits. During the testing, two DC power supplies were used. One of them supplied a constant 5 V to the V_{dd} pin; the other supplied a control voltage from 0 V to 1.8 V to the V_c pin. The V_c voltage is changed with a step size of 0.1 V.
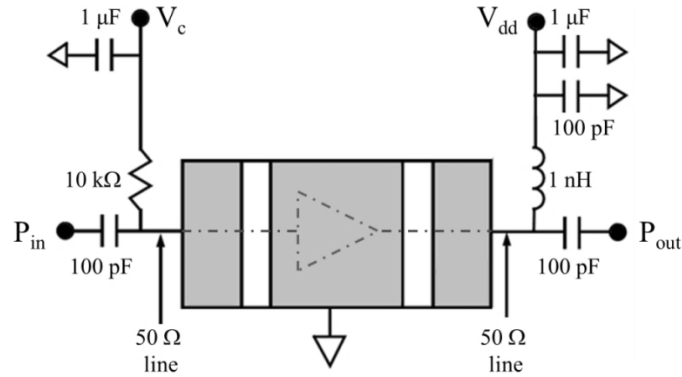
Fig. 5-1: Suggested VGA biasing network [33].
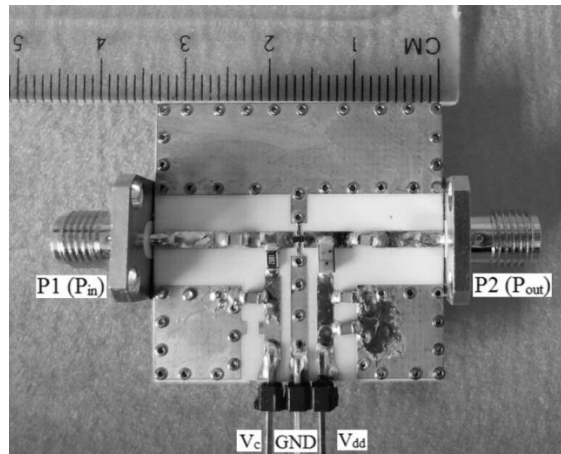
Fig. 5-2: Photograph of the fabricated VGA prototype.

Fig. 5-3 to Fig. 5-12 show the measured results for the two prototype VGA circuits. Fig. 5-3 and Fig. 5-4 show the measured return losses at the P1 (P_{in}) of the two VGAs. The return losses are larger than 7 dB before the VGAs are switched on and are larger than 13 dB when saturation points have been reached. The result agrees with the data reported in the datasheet.

Fig. 5-5 and Fig. 5-6 show the measured gain for different control voltages. A gain of 0 dB occurs roughly at the control voltage of 0.9 V for both amplifiers. The gain increases with the increase in control voltages. The gain is more

71

sensitive to the control voltage at lower frequencies. The gain ranges from -28 dB to 10 dB at 2 GHz and ranges from -17 dB to 7 dB at 6 GHz. In general, the gain performance is relatively flat without any sharp changes especially when the control voltage is high. The gain performance of VGA1 and VGA2 are very similar to each other. This important feature allows the vector sum phase shifter to have a more predictable performance.

Fig. 5-7 and Fig. 5-8 show the return losses for P2 (P_{out}). Both VGAs have a return loss larger than 9 dB from 2 GHz to 6 GHz. Fig. 5-9 and Fig. 5-10 show the reverse isolation of the VGAs. Within the required bandwidth, the reverse isolation is better than 16 dB. Both the port 2 return losses and reverse isolation did not meet the performance reported in the datasheet. A possible reason is that the top and bottom grounds are not well connected. The large-sized rivet vias connecting the top and bottom ground are located too far apart from the VGA chip. Better results can be expected if plated through vias are used instead. Sharp spikes are also observed in Fig. 5-7 to Fig. 5-10. A closer inspection of the results has shown that these spikes appear for V_c below 0.5 V and the signals are reverse fed into the VGAs. Further investigation is needed to confirm the cause of these spikes.

Fig. 5-11 and Fig. 5-12 show the measured phase response of the circuit. The maximum phase difference between the minimum and maximum control voltage is about 43°. No abrupt changes are observed in the phase for different control voltages.

Fig. 5-3: Measured $|S_{11}|$ of VGA1 under different control voltages.

Fig. 5-4: Measured $|S_{11}|$ of VGA2 under different control voltages.

Fig. 5-5: Measured $|S_{21}|$ of VGA1 under different control voltages.

Fig. 5-6: Measured $|S_{21}|$ of VGA2 under different control voltages.
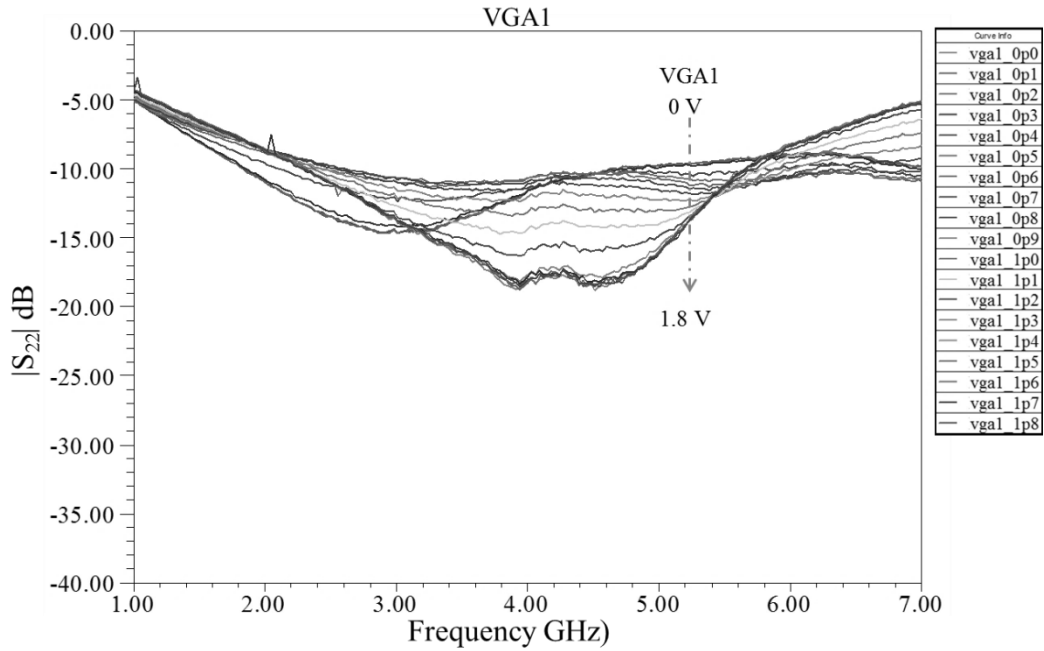
Fig. 5-7: Measured $|S_{22}|$ of VGA1 under different control voltages.
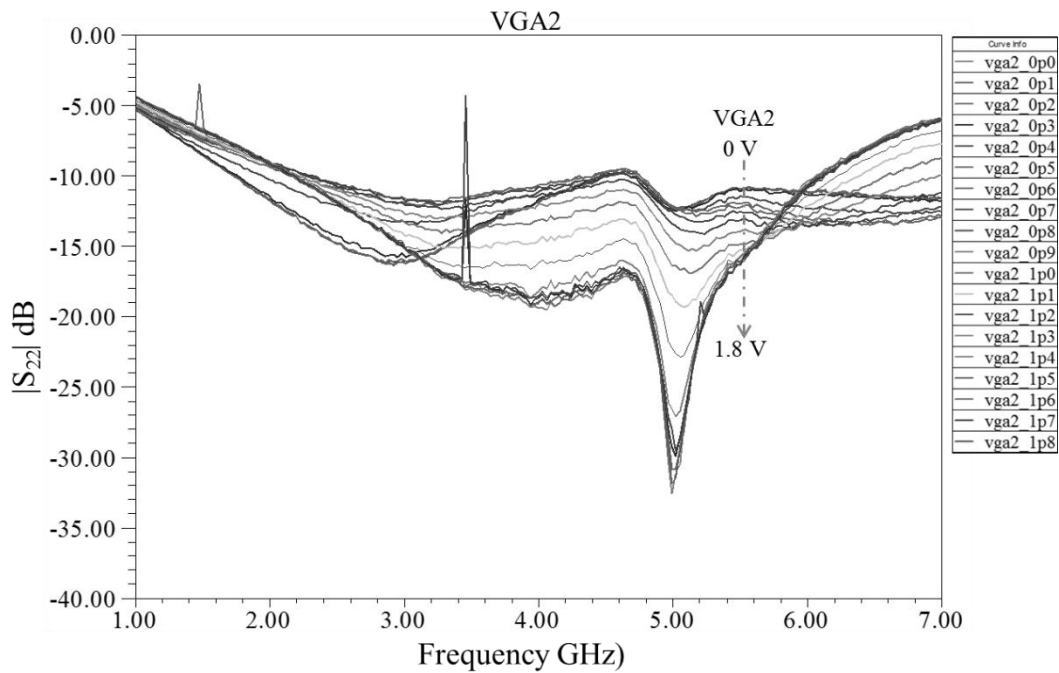
Fig. 5-8: Measured $|S_{22}|$ of VGA2 under different control voltages.
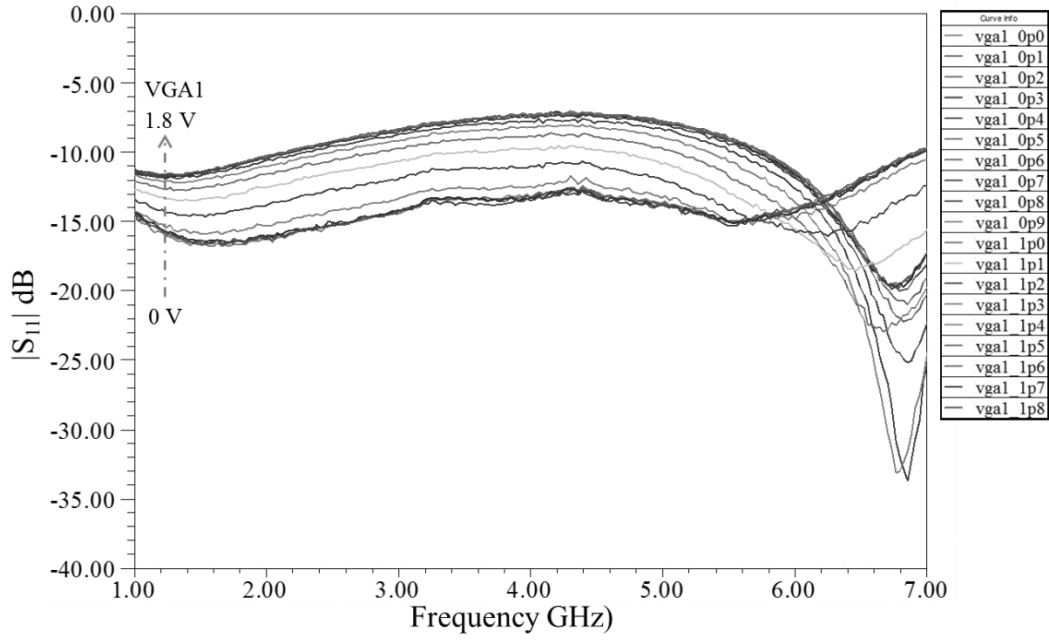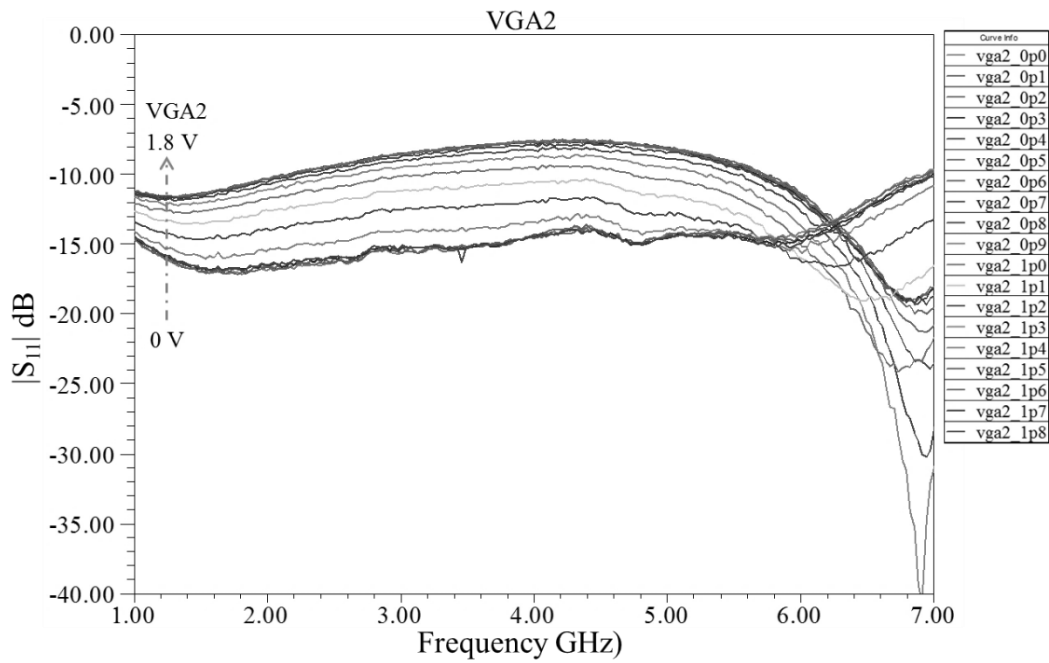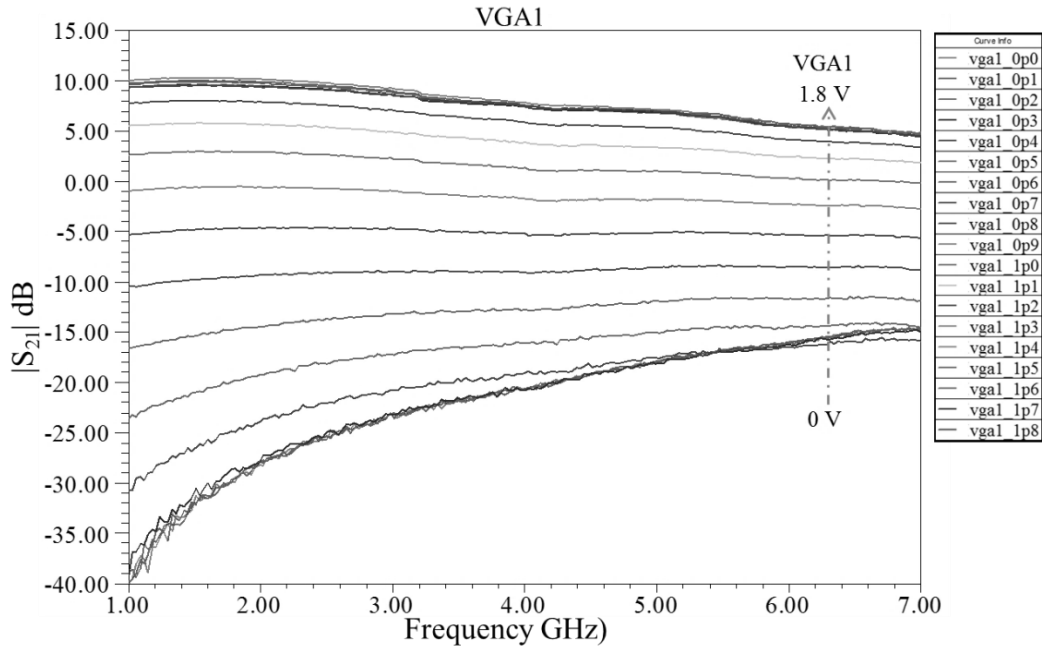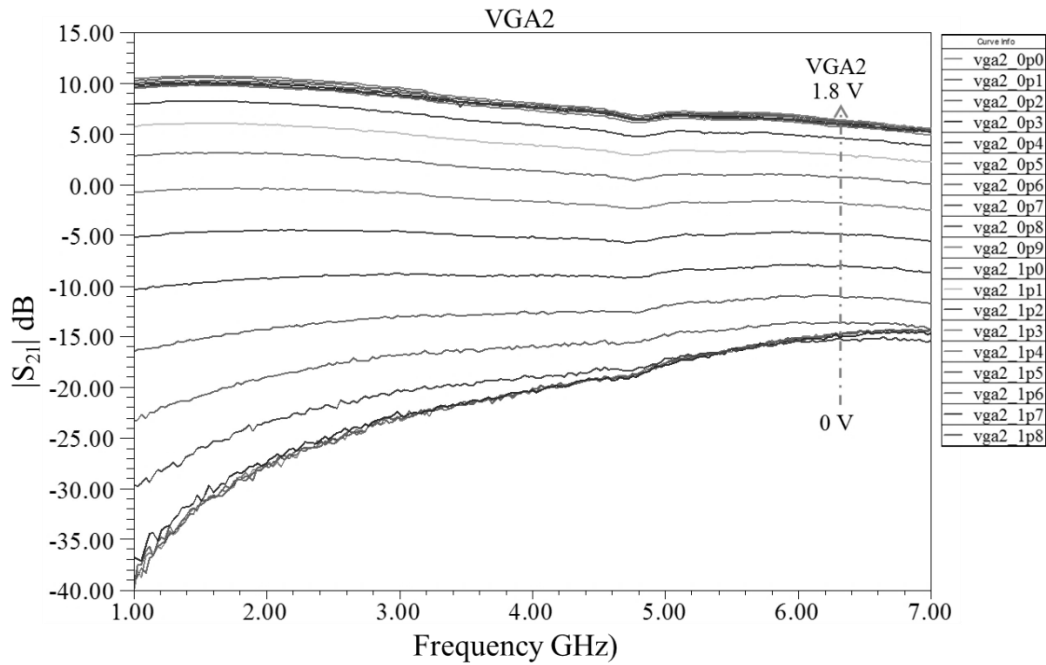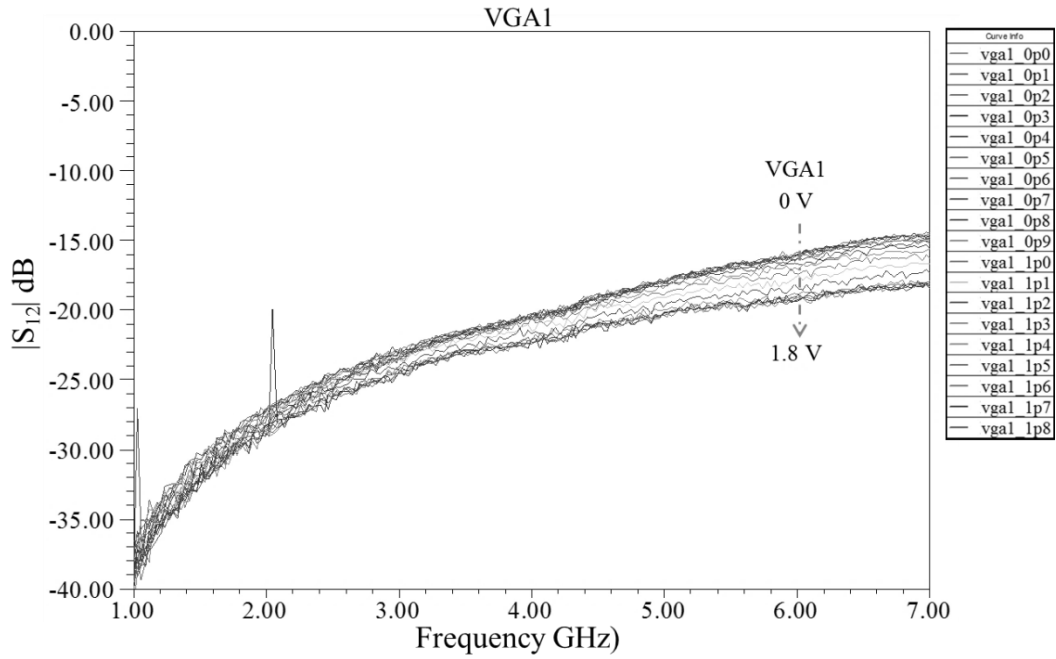
Fig. 5-9: Measured $|S_{12}|$ of VGA1 under different control voltages.
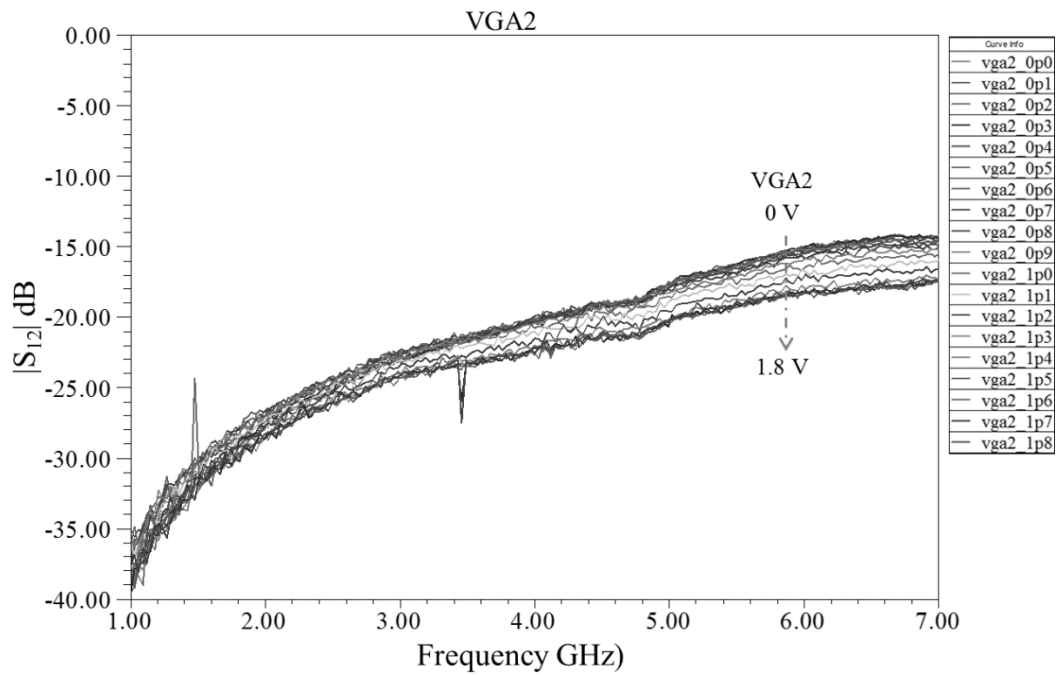
Fig. 5-10: Measured $|S_{12}|$ of VGA2 under different control voltages.
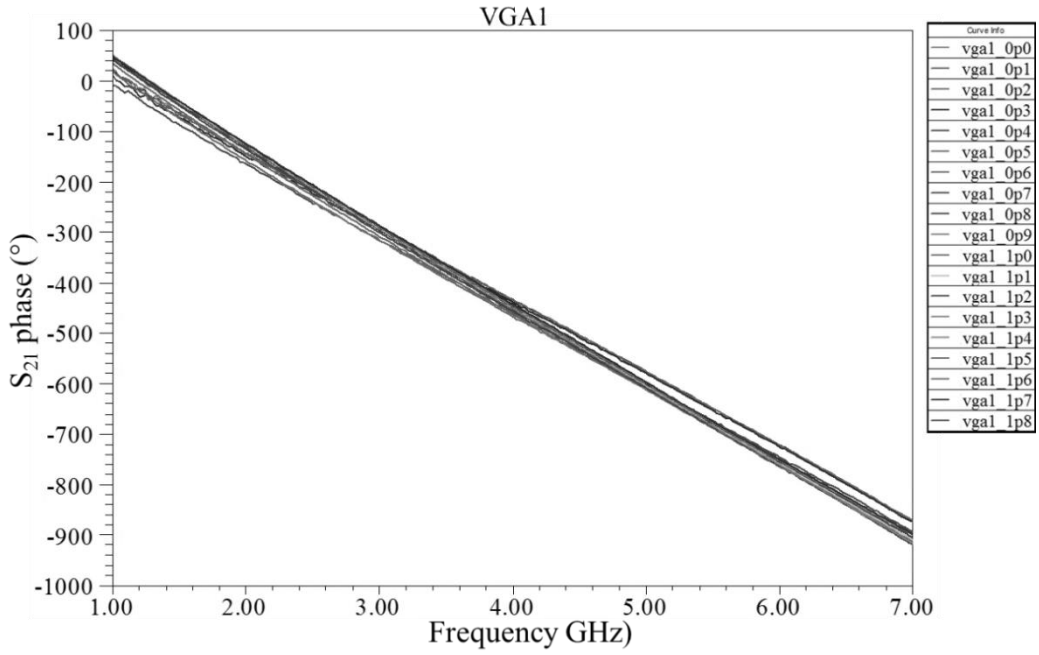
Fig. 5-11: Measured S_{21} phase for VGA1.
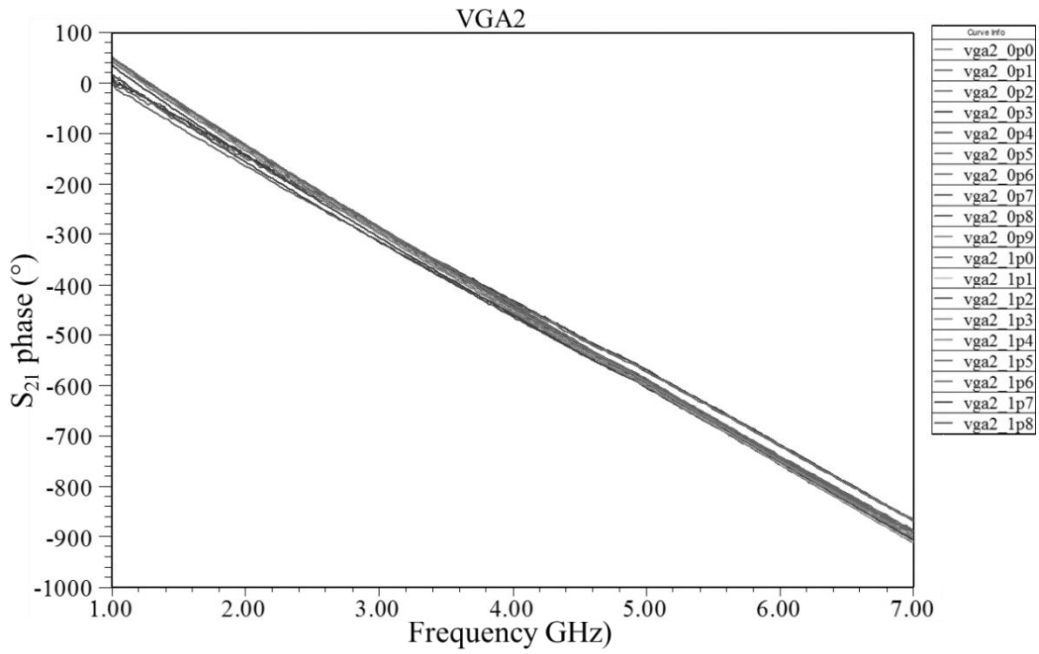
Fig. 5-12: Measured S_{21} phase for VGA2.

5.3 RF switch prototype

As extra 90° phase shifters are needed to extend the phase coverage of the vector sum phase shifter, RF switches have to be used to switch the signals between the reference and phase delay paths. A single-pole double-throw absorptive RF switch is identified, purchased and implemented for the objective.

Normally, RF switches can be classified into reflective type and absorptive type [34]. Reflective switch reflects the RF signal back to the source when it is disconnected. It uses either an open circuit or a short circuit to switch off a signal path. This results in a mismatch in the circuit, causing the entire signal to be reflected back to the source. Absorptive type switches, on the other hand, terminates the circuit with a matching load when disconnected. The incident signal energy is absorbed and dissipated as heat by the matching load. No energy is reflected back to the source. To ensure proper matching of the whole circuit, absorptive switches are used and Skyworks' SKY13286-359LF is selected. Fig. 5-13 is the block diagram of the switch. This switch is ideal for the application as it has a bandwidth of 0.1 GHz to 6 GHz. In addition, it is easy to use as it has a built-in decoder and uses a 5 V power supply. The detailed information about the IC can be found in the datasheet [35].

To validate the performance of the RF switch, a prototype circuit was fabricated and measured. Fig. 5-14 shows the photograph of the implemented switch mounted on a PCB. The switch is powered by a DC power supply and controlled by the voltage applied at the V_{ctl} pin. The control voltage is set to either

5 V or 0 V. The signal flows from port 1 to port 3 (path 1) when the switch is ON

(5 V); the signal flows from port 1 to port 2 (path 2) when it is OFF (0 V). The S

parameters of the prototype are measured using a VNA in the ON/OFF states.
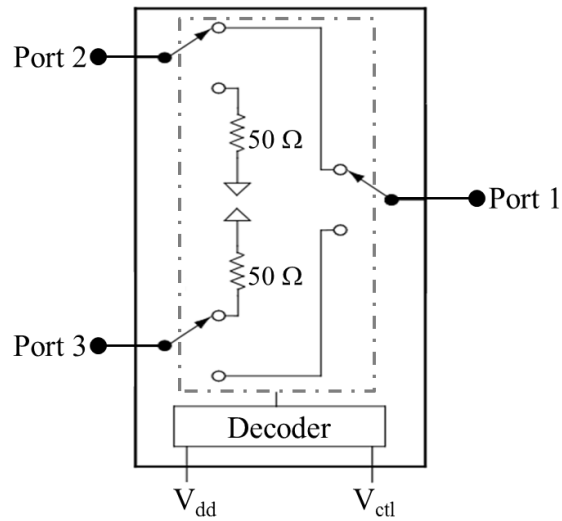
Fig. 5-13: Block diagram of SKY13286-359LF switch [35].
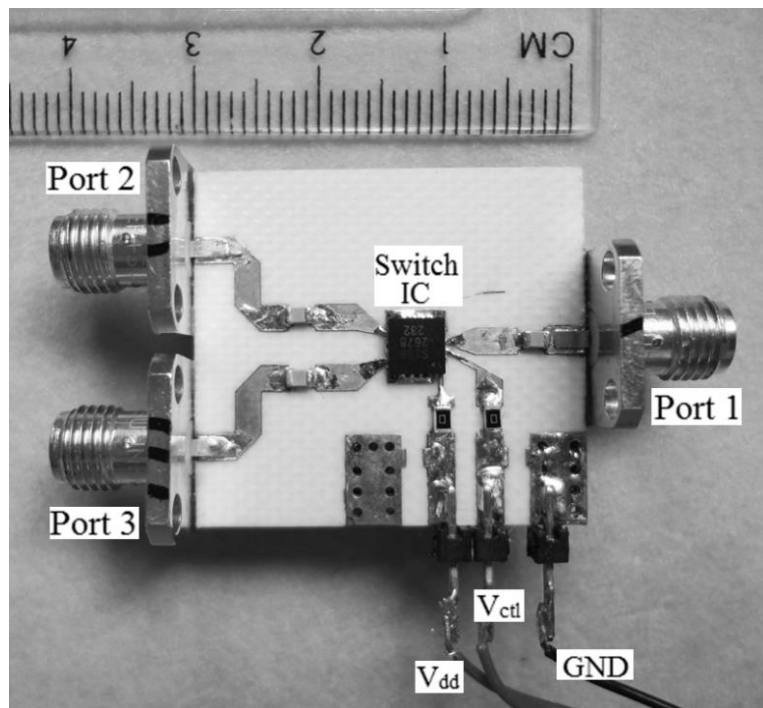
Fig. 5-14: Fabricated RF switch test board.

Two switches (S1 and S2) were fabricated and measured to confirm the repeatability of circuit. Fig. 5-15 and Fig. 5-16 show the measured return losses of the two switches. The return loss for Port 1 is better than 9 dB and consistent for both states. The return losses for Port 2 and Port 3 are better than 14 dB when the corresponding path is switched on and better than 9 dB when the corresponding path is switched off. Both switches have similar return losses performance. The measured return losses are poorer than given in the datasheet.

Fig. 5-17 and Fig. 5-18 show the insertion losses of the two switches at different states. When the path is turned on, the insertion losses are between 1.2 dB and 2.7 dB from 2 GHz to 6 GHz. When the path is off, the insertion loss is better than 20 dB. Fig. 5-19 and Fig. 5-20 show the amplitude imbalance between path 1 and path 2 when they are switched on. The amplitude imbalance is better than -0.38 dB for S1 and better than 0.22 dB for S2.

Fig. 5-21 and Fig. 5-22 show the output isolation between port 2 and port 3. The isolation is greater than 20 dB for both circuits. $|S_{32}|$ has the same results as $|S_{23}|$ as expected. Fig. 5-23 and Fig. 5-24 show the phase response of the two switches. Fig. 5-25 and Fig. 5-26 show the phase difference between the insertion states. The phase difference for S1 is less than 5.8° while for S2 is less than 1°.
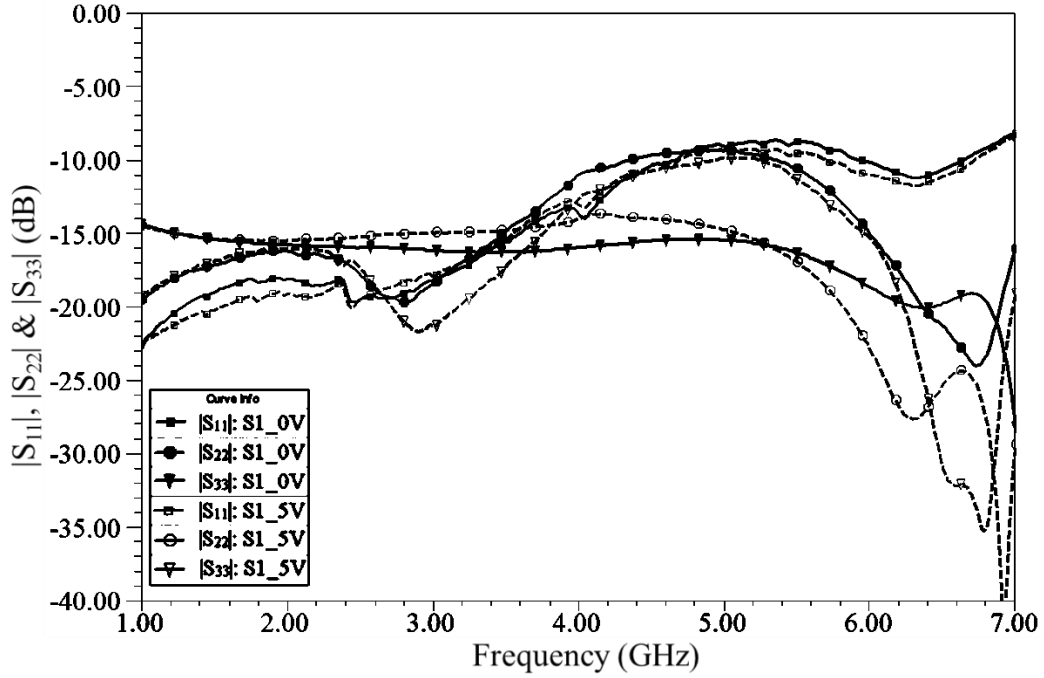
Fig. 5-15: Measured $|S_{11}|$, $|S_{22}|$ and $|S_{33}|$ for S1.
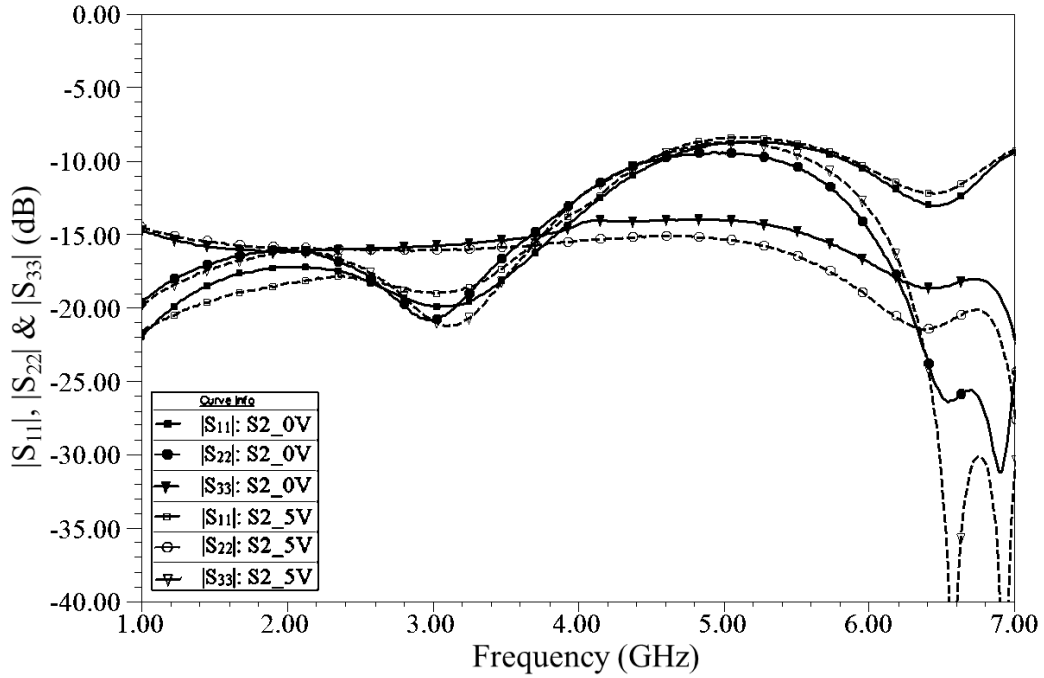
Fig. 5-16: Measured $|S_{11}|$, $|S_{22}|$ and $|S_{33}|$ for S2.
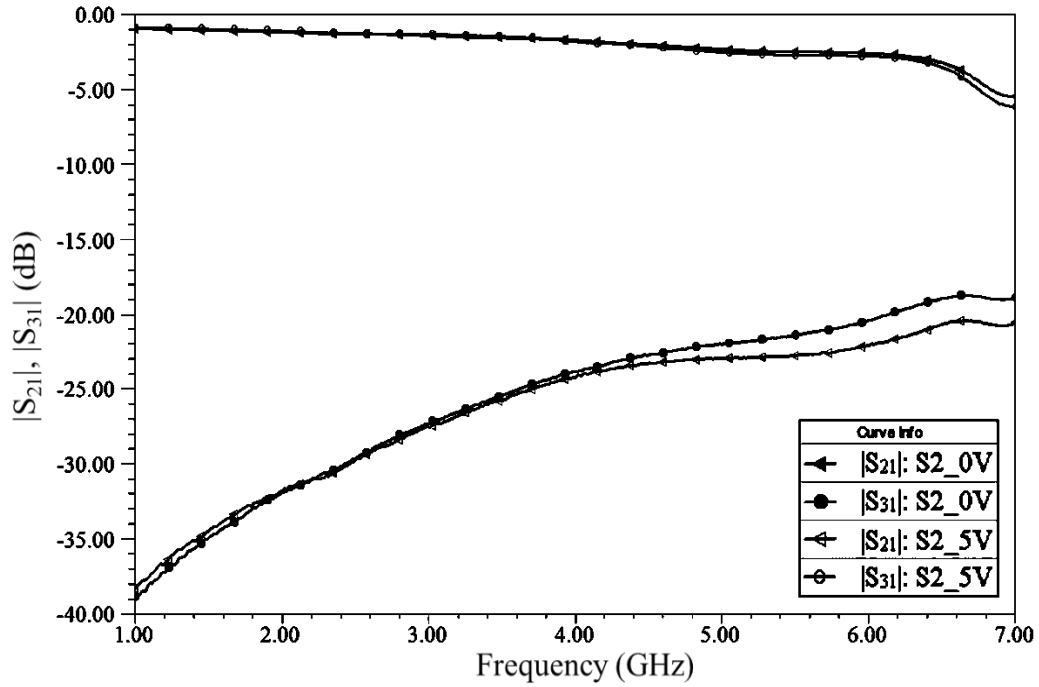
Fig. 5-17: Measured $|S_{21}|$ and $|S_{31}|$ for S1.
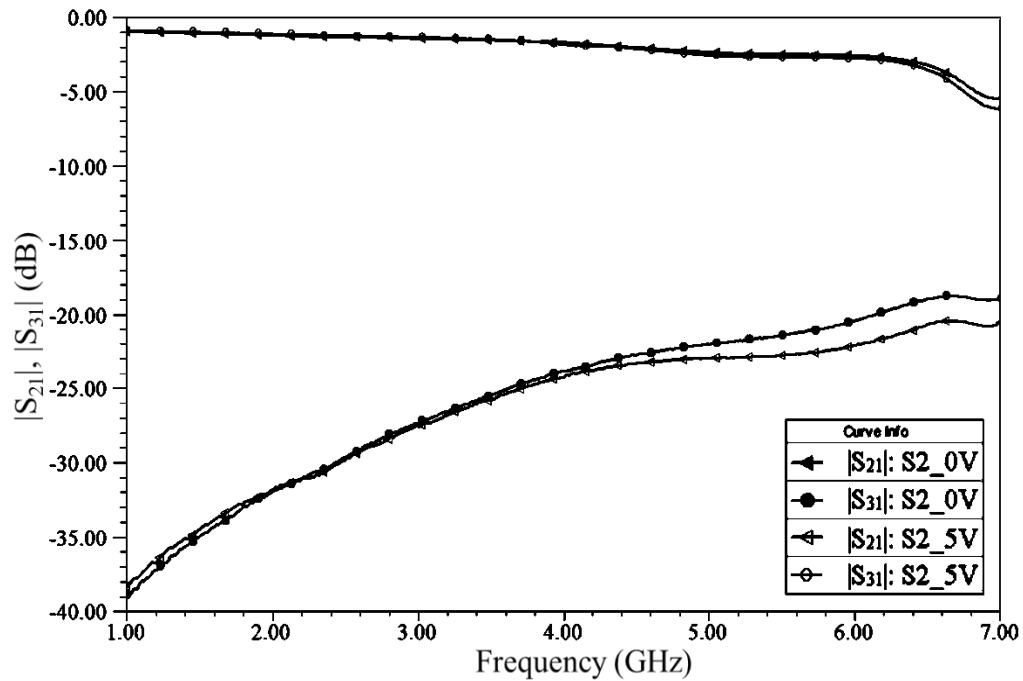
Fig. 5-18: Measured $|S_{21}|$ and $|S_{31}|$ for S2.
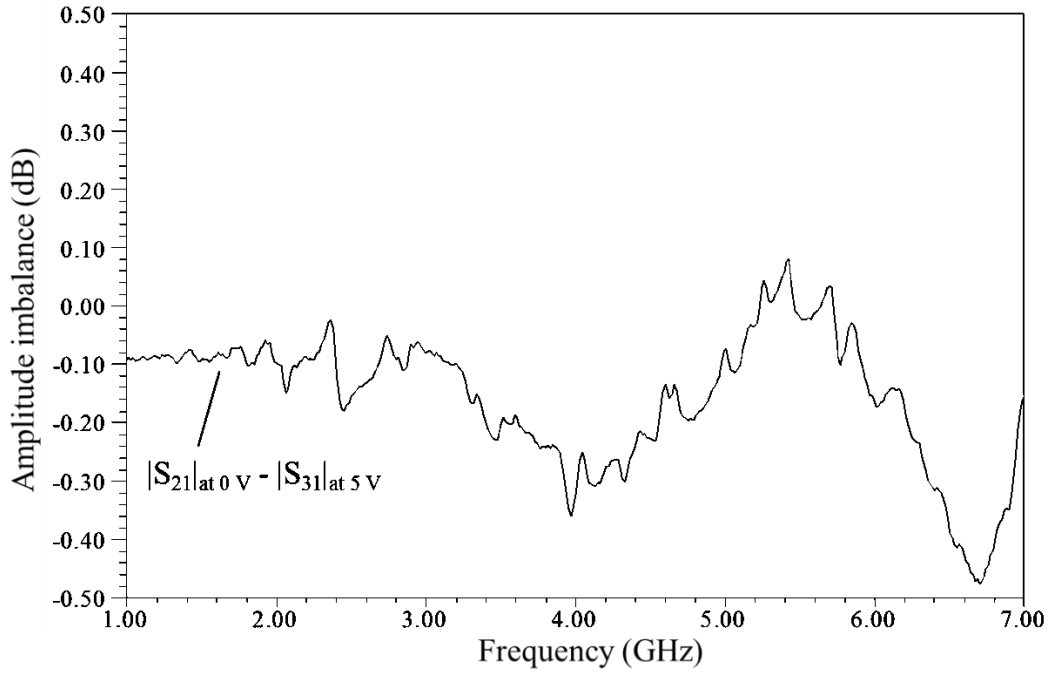
Fig. 5-19: Amplitude imbalance between $|S_{21}|$ at 0 V and $|S_{31}|$ at 5 V for S1.
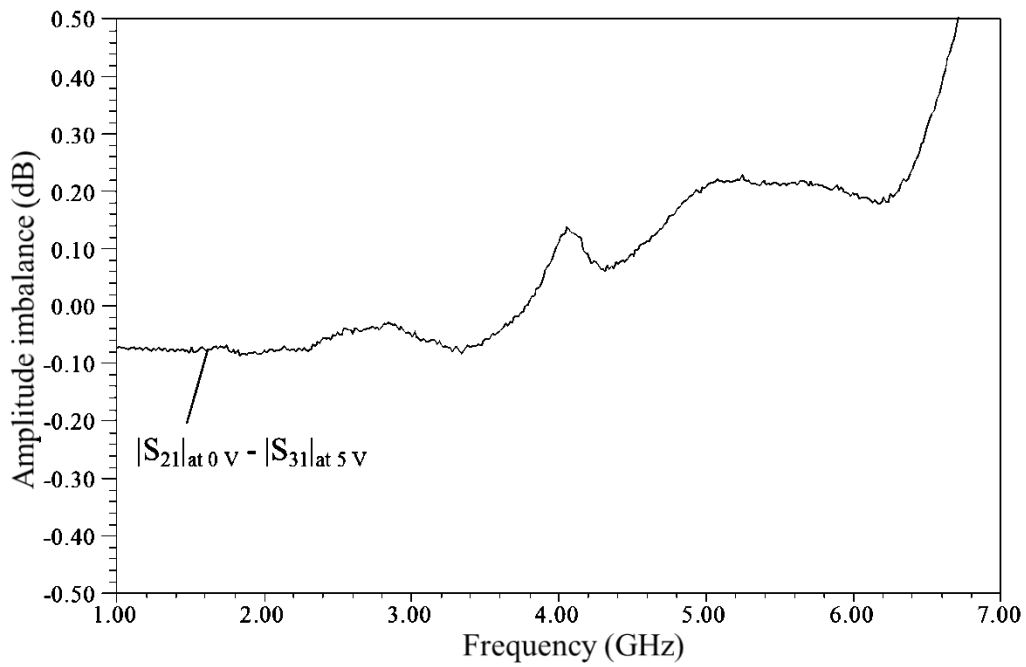
Fig. 5-20: Amplitude imbalance between $|S_{21}|$ at 0 V and $|S_{31}|$ at 5 V for S2.
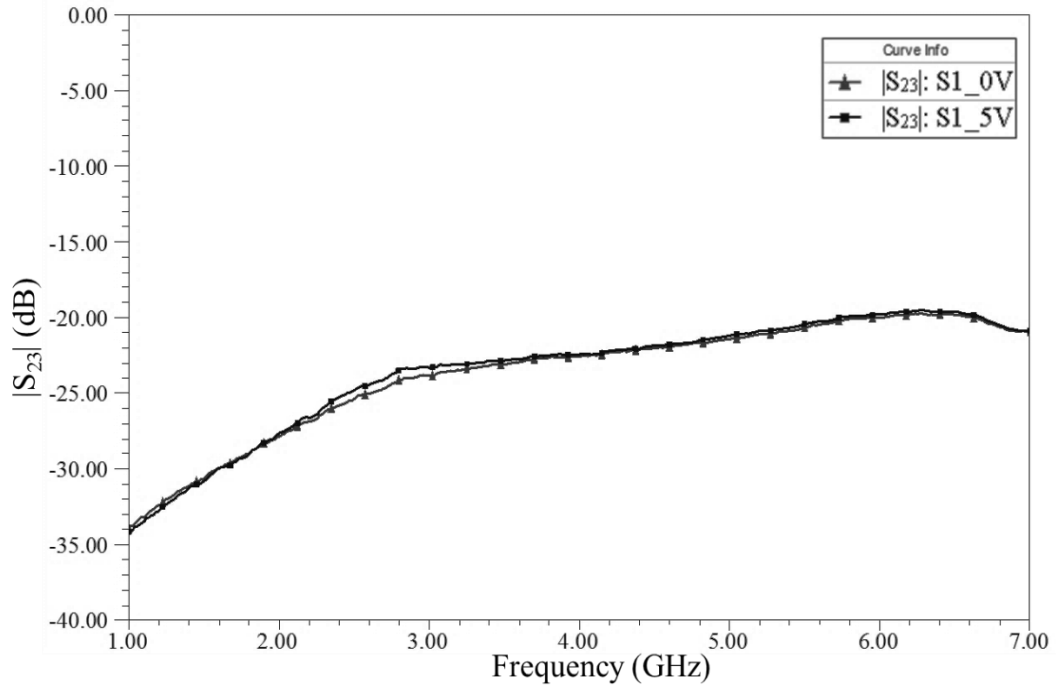
Fig. 5-21: Measured $|S_{23}|$ for S1.
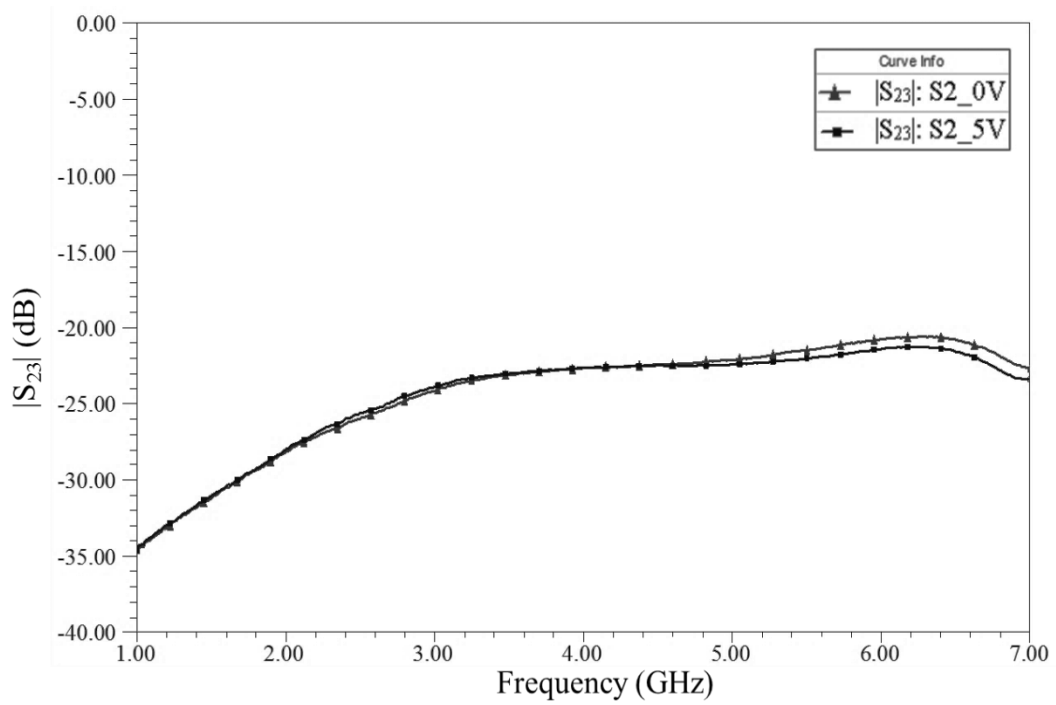
Fig. 5-22: Measured $|S_{23}|$ for S2.
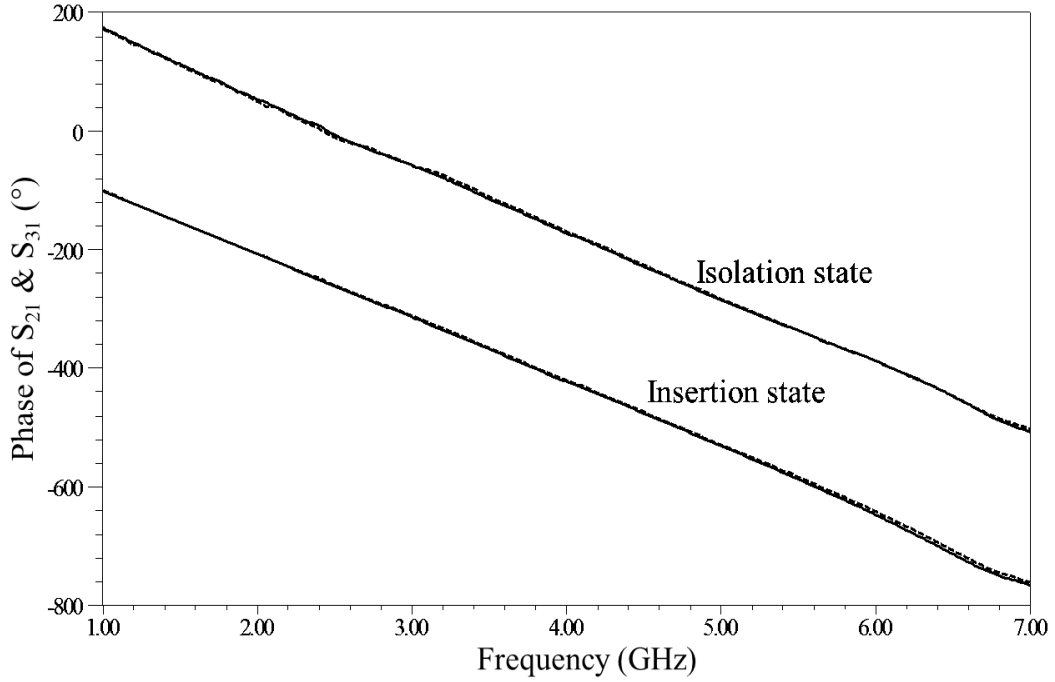
Fig. 5-23: Measured S_{21} (dotted line) and S_{31} (solid line) phase response for S1.
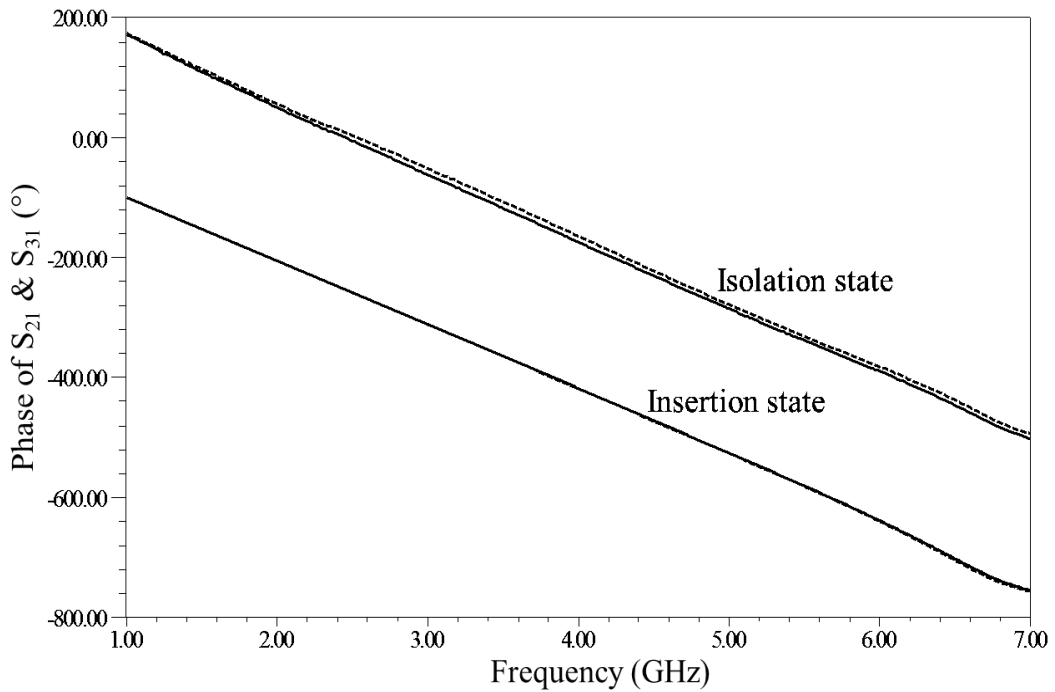
Fig. 5-24: Measured S_{21} (dotted line) and S_{31} (solid line) phase response for S2.
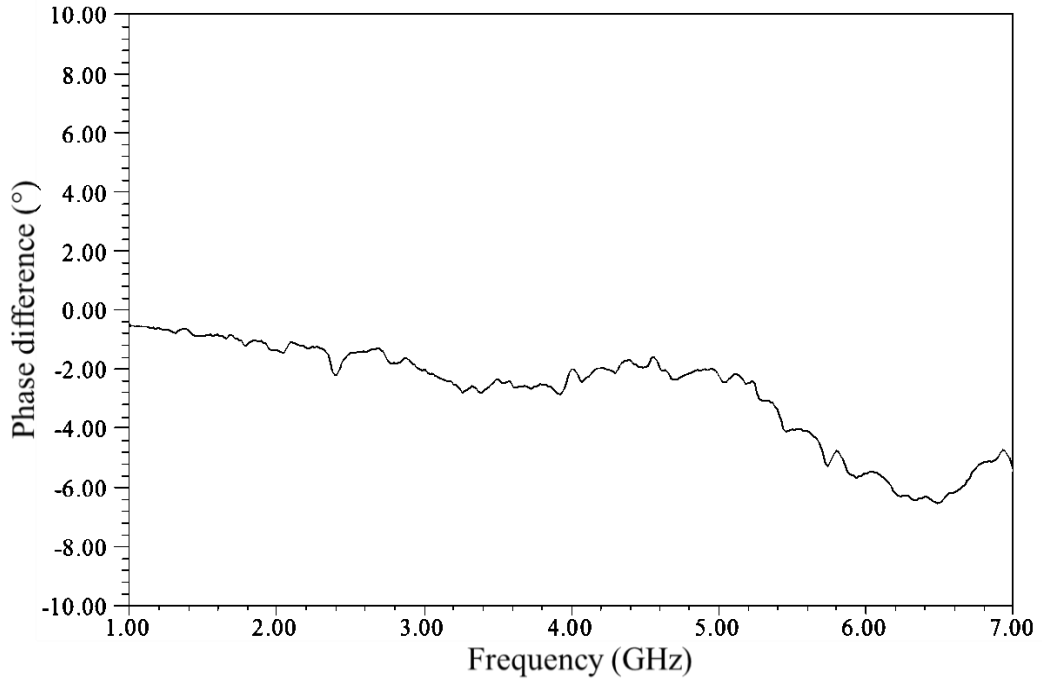
Fig. 5-25: Phase difference of insertion states for S1.
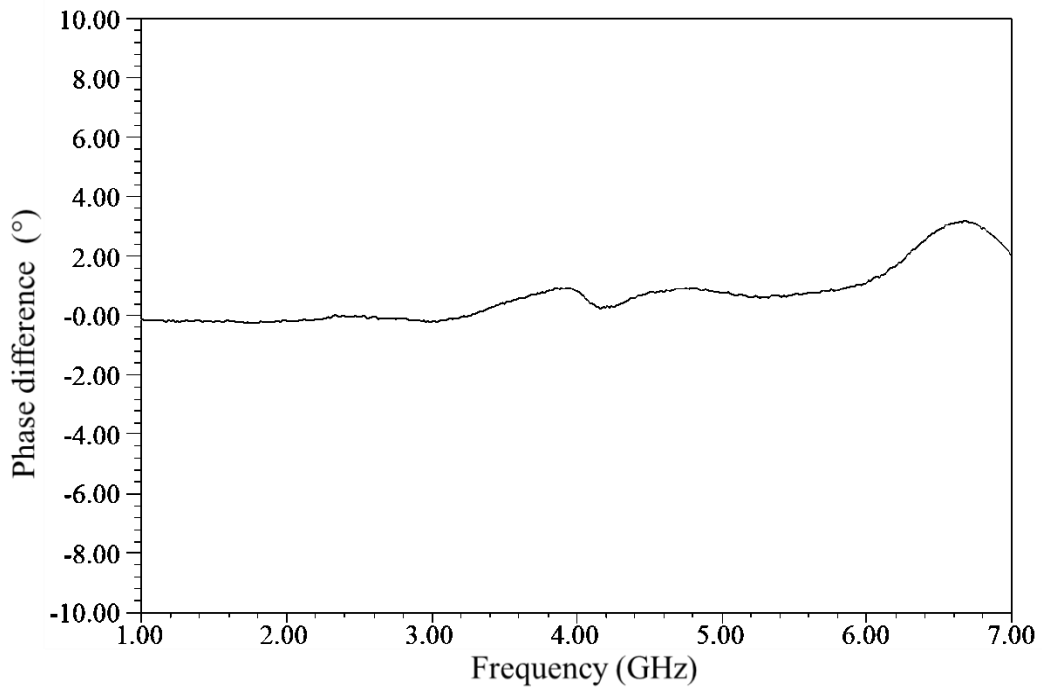
Fig. 5-26: Phase difference of insertion states for S2.

Some discrepancies were observed between the measurement results and the data given in the data sheet. The poorer return loss may be attributed to the improper ground for the IC chip. As plated through via cannot be done in-house, a thin wire was used to connect the ground between the top layer and bottom layer. This will degrade the performance of the ground. In addition, the prototype uses microstrip as the input/output transmission line, instead of co-planar line as recommended by the data sheet. This will account for the differences in the observed results too.

5.4   Conclusions

The prototype circuits for both VGA and RF switch have successfully verified their respective performance. Though some discrepancies between the measured results and that reported in the datasheet were observed, the differences are mainly due to the in house fabrication quality of the prototype. With proper fabrication process, especially the vias connecting the circuits with the ground plane, the IC chips will work well in the final circuit. The objective to verify the components performance and mitigate any potential risk is achieved.

Chapter 6 Implementation and measurement

6.1 Introduction

After all the sub-components have been separately validated using individual prototypes, an integrated PCB based on the proposed vector sum phase shifter architecture was built and implemented. The circuit is targeted to cover 2 GHz to 6 GHz. In this chapter, the implemented circuit and the measured results are shown.

6.2 Fabricated PCB board

The printed circuit board (PCB) is implemented in microstrip line. The substrate used is 32 mils RO4003. The size of the PCB is 134 mm by 80 mm. Fig. 6-1 shows the top metal layer of PCB layout. The bottom layer is fully covered with metal. A three-stage Wilkinson power divider is used to split the input signal equally. Broadband variable gain amplifiers, Avago VMMK-3503, are used to vary the magnitude of the signals. The two signals are then vector summed by the Quadrature Magic-T. As the vector sum circuit can only produce a phase difference from 0 to 180°, two broadband 90° phase shifters are used to extend the phase difference coverage to full 360°. Four RF single-pole double-throw (SPDT) switches, SKY13286-359LF, are used to select either the reference path or the phase shift path.

For the Quadrature Magic-T, the input branch was redesigned to bend to one side so to better connect with the Wilkinson power divider. The section for tuning the quadrature phase is meandered. The area with thicker substrate is also indicated. Some ground islands were also included in the PCB for troubleshooting purpose. To integrate the circuit easily, the impedance of the interconnections between different components is maintained at 50 Ω. Therefore they are able to be directly connected together without problem. To avoid introducing unwanted phase difference, the RF path of the circuit was designed as symmetrical as possible.
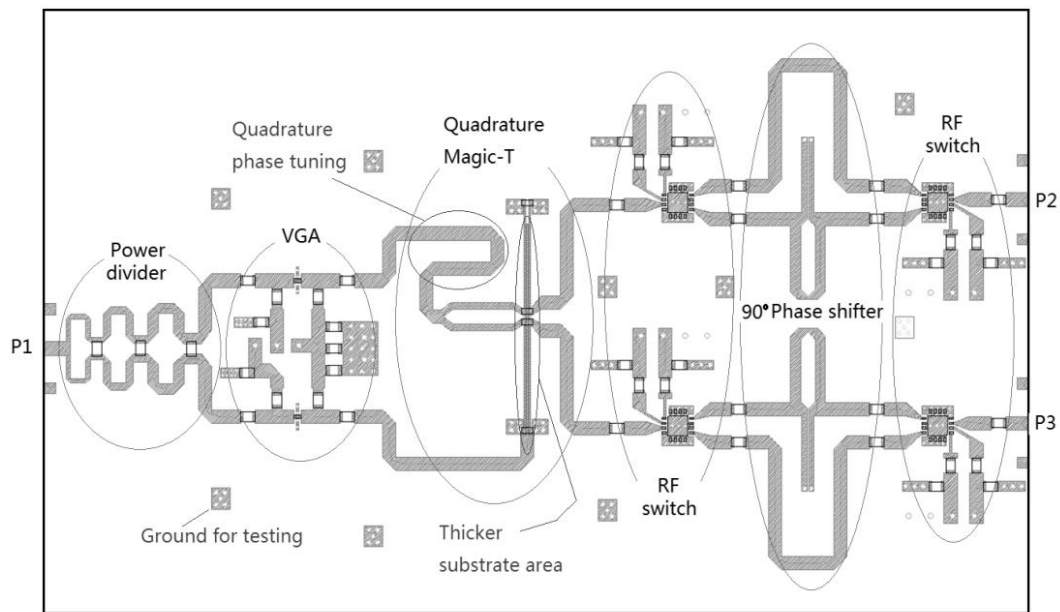
Fig. 6-1: PCB layout of the two-way vector sum phase shifter.
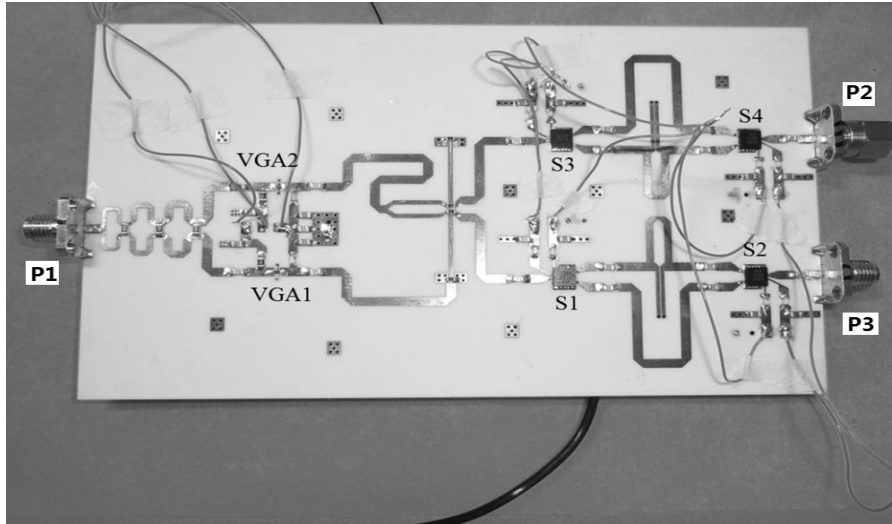
Fig. 6-2: Photo of the fabricated polarization controller circuit.

Fig. 6-2 shows the fabricated circuit. It was fabricated using photolithography technique, so the dimensions of the circuit are more accurate than that of the individual prototype circuits shown in the previous chapters. A minimum gap width of 0.08 mm can be achieved. Plated through vias are also used for all the connections from top layer to bottom layer. The active components were soldered to the PCB under ESD-protection environment using a reflow process.

During the measurement, five independent voltage sources with shared grounds were used to control the circuit. One power supply is for the V_{dd} of all the active components to provide the required 5 V DC power. To prevent interference due to sharing of the same power supply and to prevent the RF signals from flowing into the voltage sources, capacitors are used to remove and block unnecessary signals. Two power sources, one for VGA1 and another for VGA2, are used to control the gain of each amplifier. The switch S1 and S3 share one

90

control voltage; switch S2 and S4 share the other control voltage. When 0 V is applied to S1 and S3 and 5 V is applied to S2 and S4, the upper branches of 90° broadband phase shifters are selected. The lower branches of the 90° broadband phase shifters are selected when 5 V is applied to S1 and S3 while the 0 V is applied to S4 and S2.

6.3 Measurement results and analysis

The S-parameters of this circuit are measured. The VGAs are varied from 0.5 V to 1.8 V with a step size of 0.1 V. Two switches setting are measured. Case A and case B refer to and correspond to the two different switches settings shown in Table 6-1.

Table 6-1: Switch settings and the corresponding phase output.

	S1	S2	S3	S4	Phase coverage
Case A	0 V	5 V	0 V	5 V	-90° to 90°
Case B	5 V	0 V	5 V	0 V	90° to 270°

Fig. 6-3 to Fig. 6-12 show the measurement results of the two-way vector sum phase shifter at 4 GHz. Fig. 6-3 shows the phase difference between the output ports. As VGA1 and VGA2 change, the phase difference between the two output ports varies from -90° to 270°. Fig. 6-4 shows the amplitude balance of the circuit. A non-zero amplitude imbalance is observed and the imbalance varies with the control voltages.

91
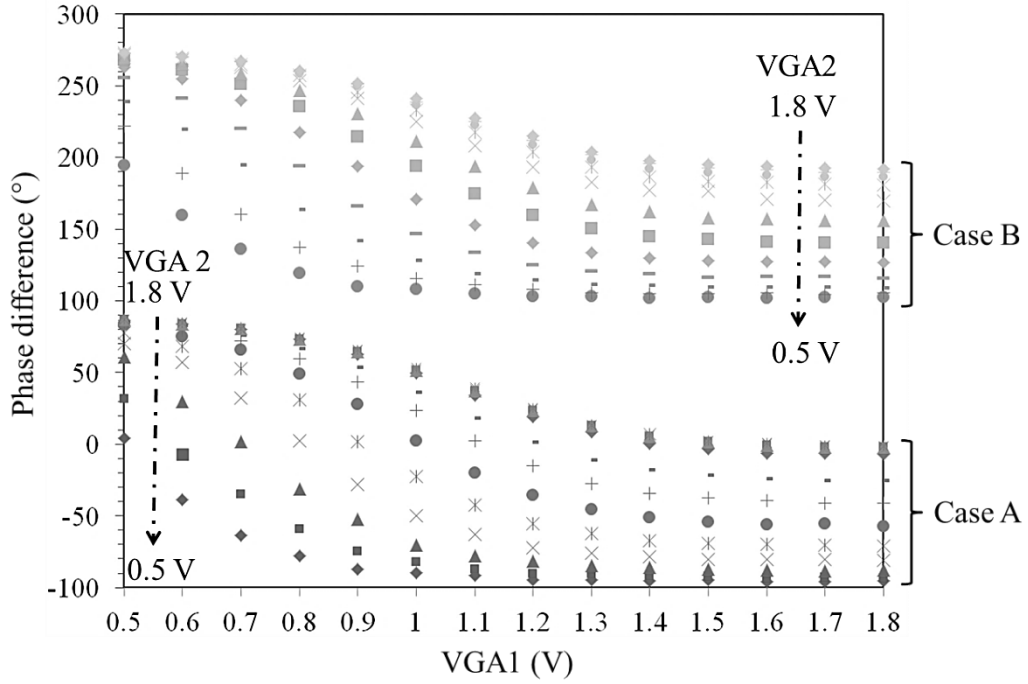
Fig. 6-3: Measured phase difference at 4 GHz.
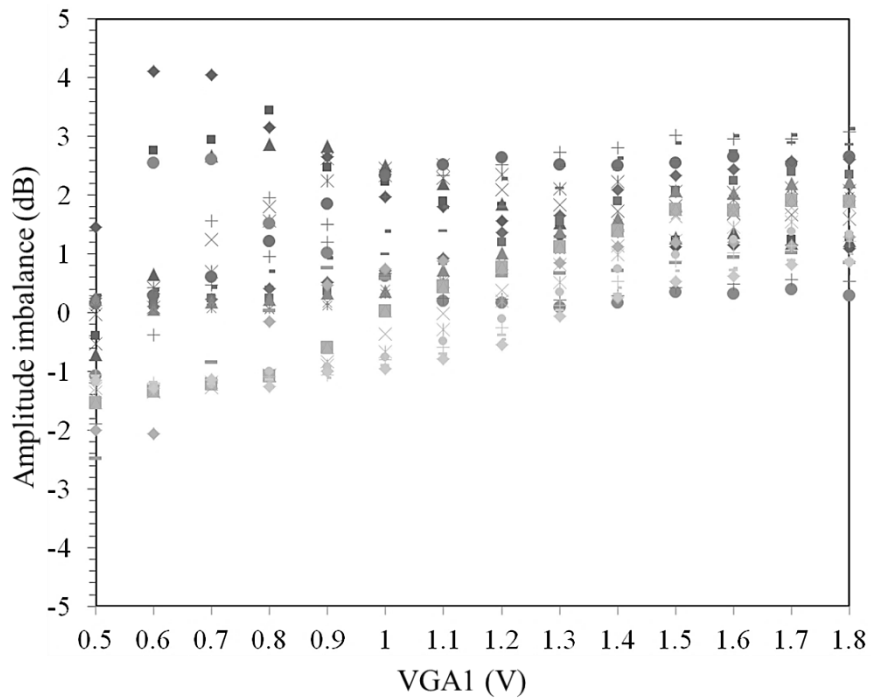
Fig. 6-4: Measured amplitude imbalance for both Case A and B at 4 GHz.

92
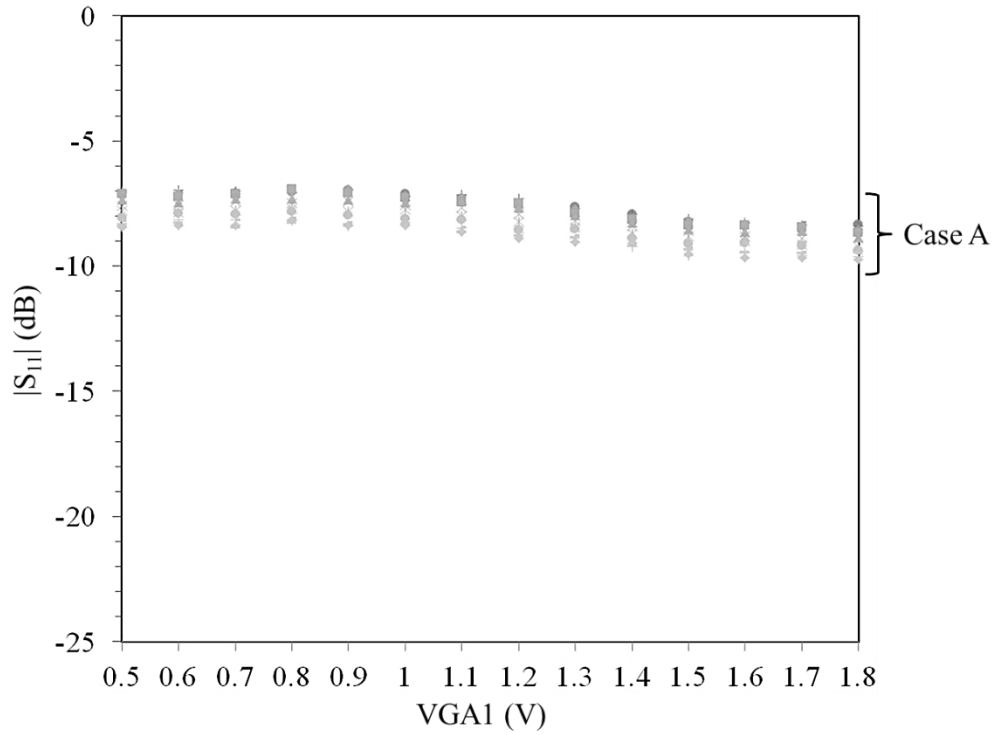
Fig. 6-5: Measured $|S_{11}|$ for Case A at 4 GHz.
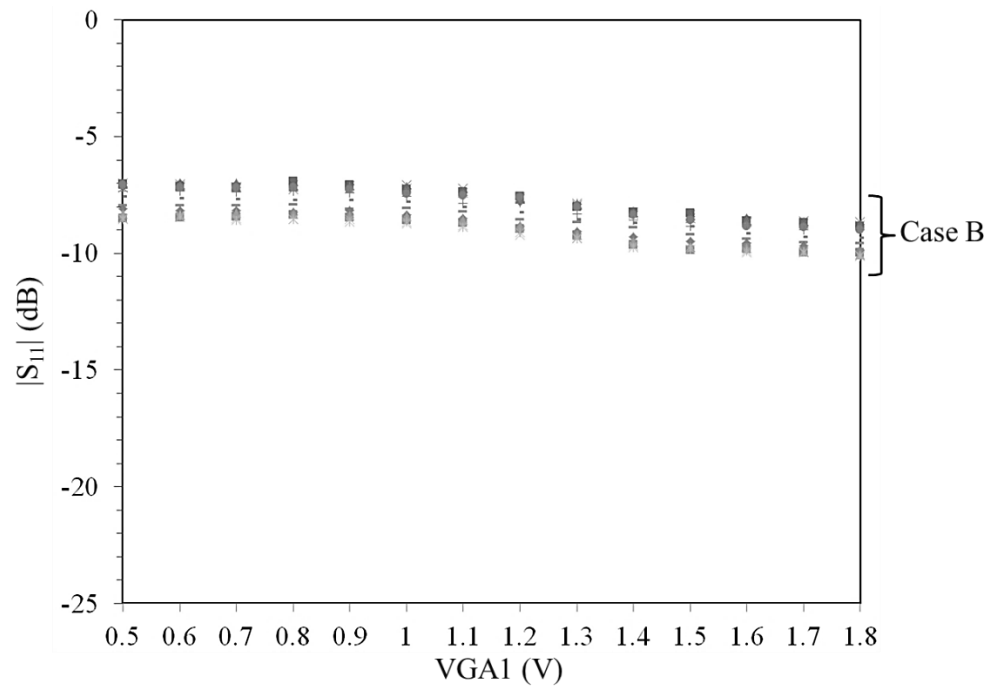
Fig. 6-6: Measured $|S_{11}|$ for Case B at 4 GHz.

93
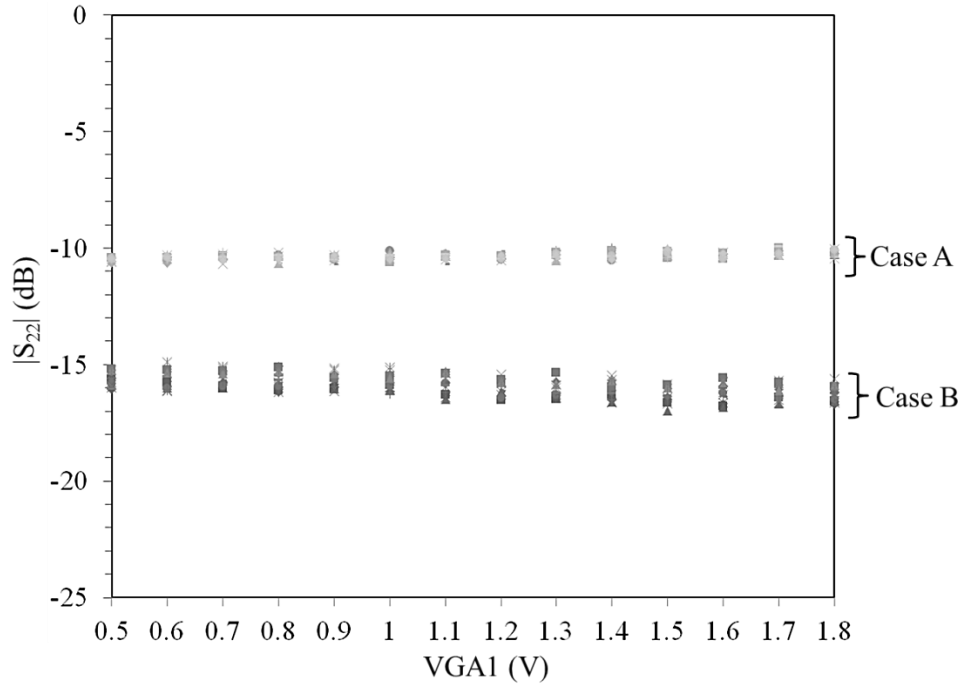
Fig. 6-7: Measured $|S_{22}|$ for Case A and B at 4 GHz.
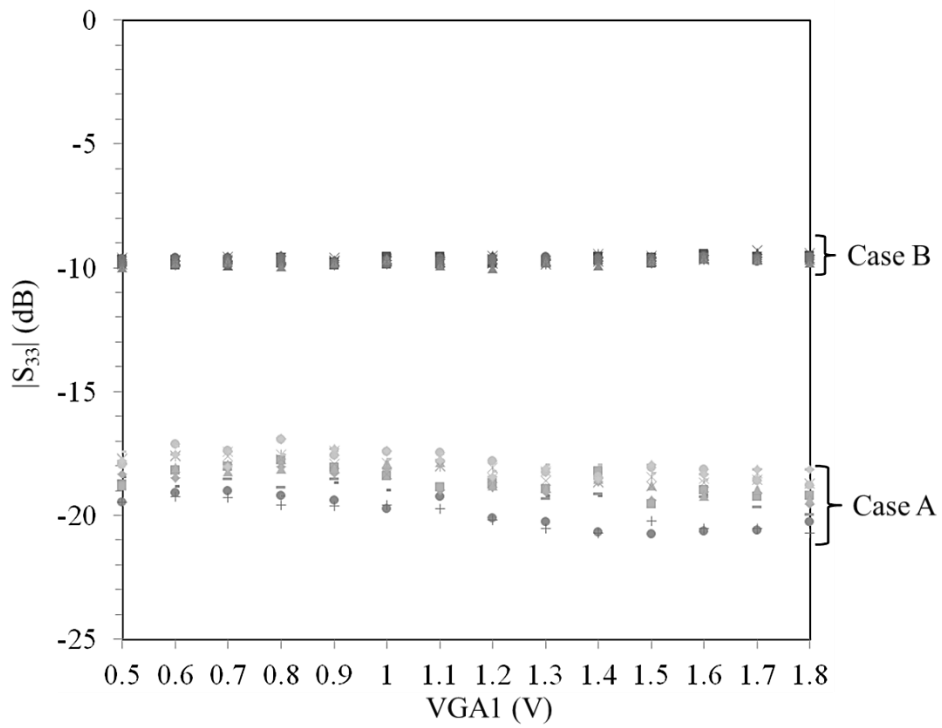
Fig. 6-8: Measured $|S_{33}|$ for Case A and B at 4 GHz.
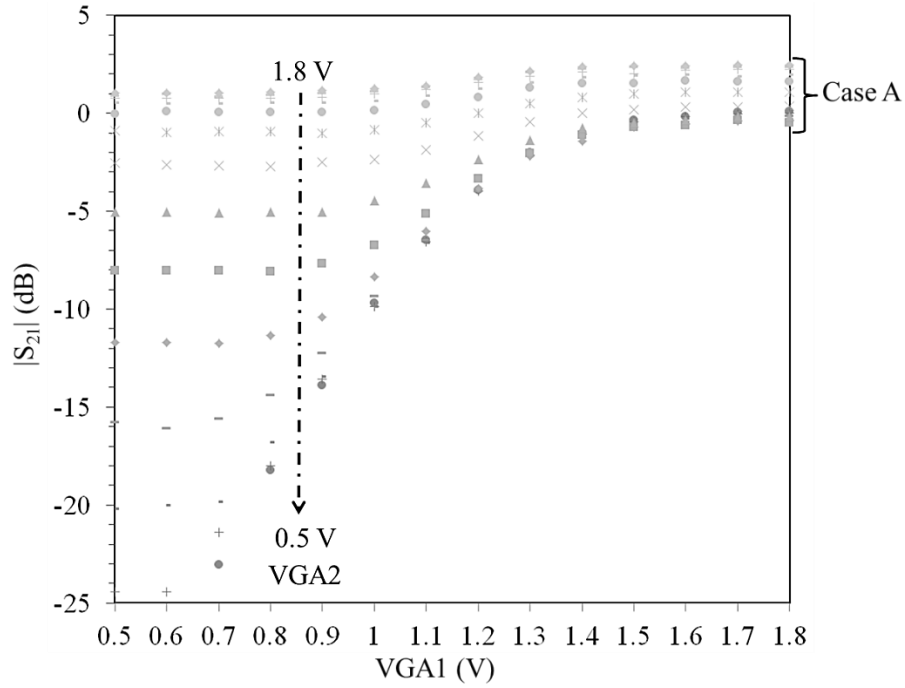
Fig. 6-9: Measured $|S_{21}|$ for Case A at 4 GHz.
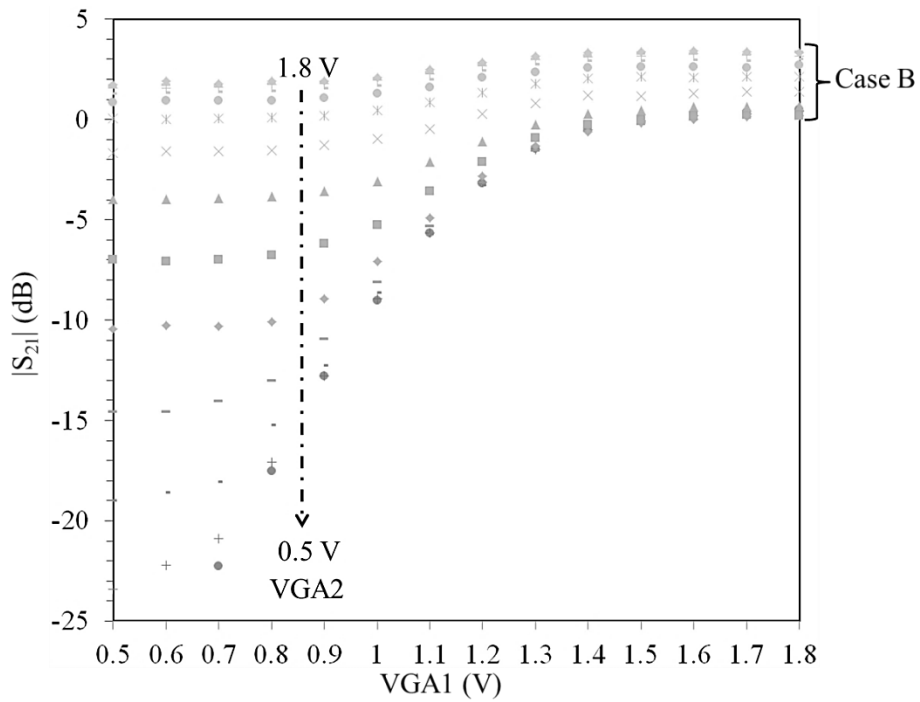
Fig. 6-10: Measured $|S_{21}|$ for Case B at 4 GHz.
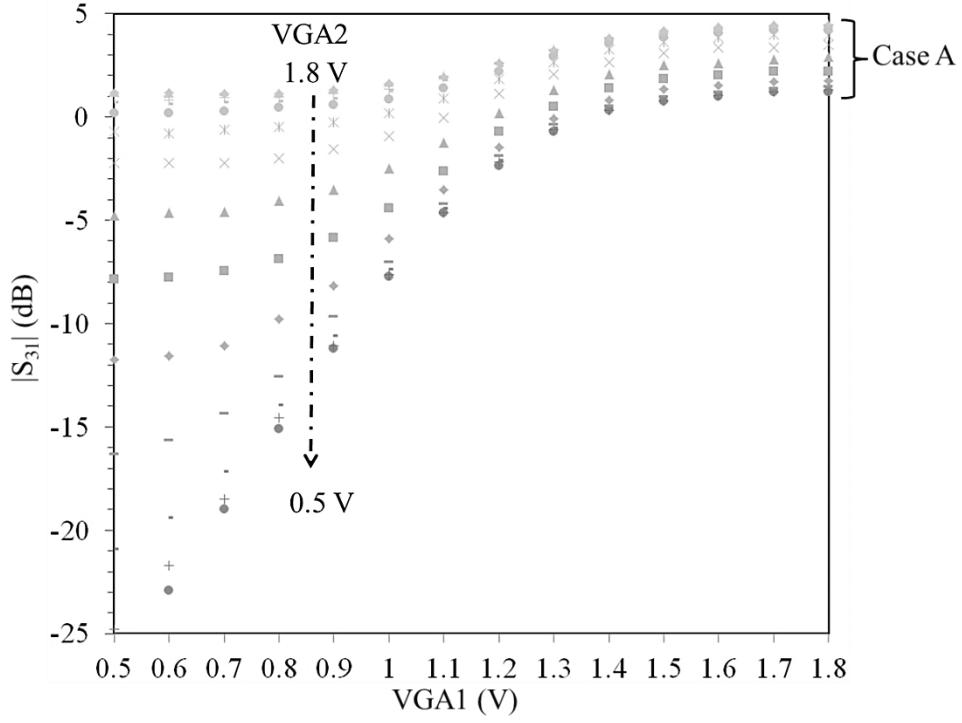
Fig. 6-11: Measured $|S_{31}|$ for Case A at 4 GHz.
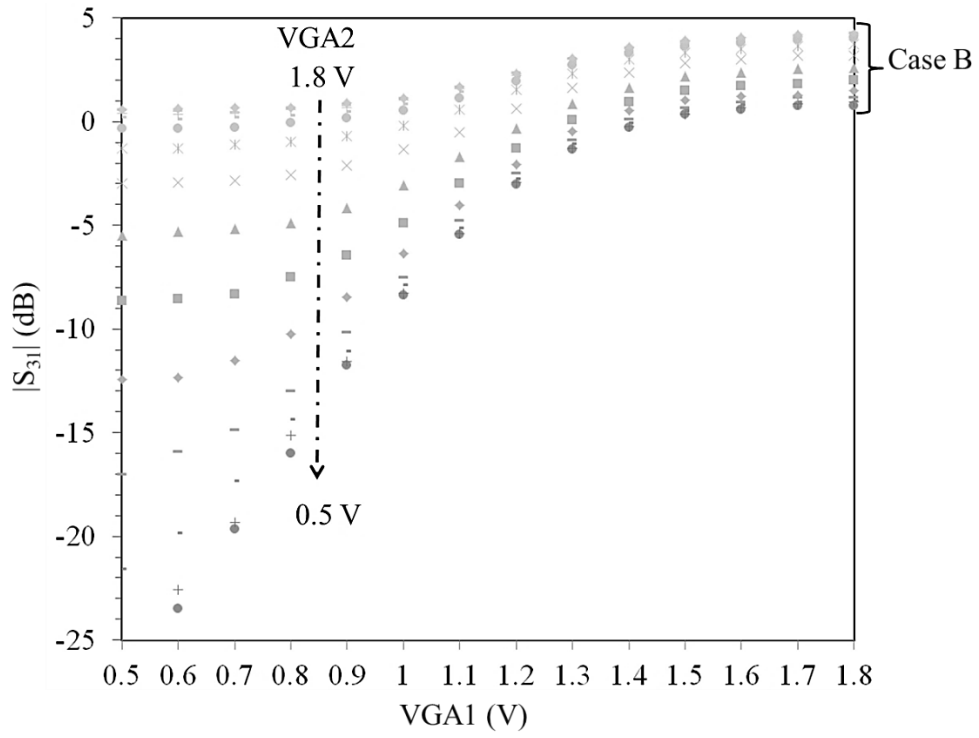
Fig. 6-12: Measured $|S_{31}|$ for Case B at 4 GHz.

Fig. 6-5 and Fig. 6-6 show the $|S_{11}|$ of the circuit. The return loss is only greater than 7 dB. This is because the input return losses of the VGA chips are not well matched to 50 Ω. Fig. 6-7 and Fig. 6-8 show the $|S_{22}|$ and $|S_{33}|$ for the output ports. The port 2 and port 3 return losses for Case A and Case B are different. Though the phase delay line of the 90° phase shifter has achieved a return loss of better than 15 dB, the mismatch will further degrade when connected to the rest of the circuit. As such, different return losses are observed at the output ports when the phase delay line or 50 Ω reference line is connected. Fig. 6-9 to Fig. 6-12 show the $|S_{21}|$ and $|S_{31}|$ of the circuit. As expected, the output insertion losses vary with the gain of the VGAs.

Fig. 6-13 to Fig. 6-16 are the measurement results of the circuit from 2 GHz to 6 GHz. Fig. 6-13 are the return losses of the ports for both Case A and Case B switch settings. The port 1 return loss is larger than 6 dB for both cases and it improves as the control voltages of the VGAs increase. At low control voltages, the VGAs are barely switched on. As such, most of the signals are reflected back to the input ports. Port 2 and port 3 have return losses larger than 7 dB. A comparison between Case A and Case B return losses shows that the return losses curve will interchange when the reference line or the phase delay line of the 90° is connected. This phenomenon is also observed in Fig. 6-7 and Fig. 6-8. As the circuit is formed by cascading different components, any mismatch will therefore cause the return loss to degrade drastically. The return losses will improve with better matched switches and VGAs.

Fig. 6-14 and Fig. 6-15 show the $|S_{21}|$ & $|S_{31}|$ results. The gain of the circuit changes with the voltage change. As the input signal is -30 dBm, a large amount of noise can be observed in the output when the gain of the VGA is low. When the gain increases, the insertion loss curves become smoother. Fig. 6-16 shows the amplitude imbalance of the circuit. Excluding the outlier values, the amplitude imbalance is between -2 dB to 5 dB. Ideally, the insertion loss at the output ports should be equal. However, the insertion loss for one of the ports tends to be higher. A likely reason is that the quadrature magic-T is not splitting the signal equally or the losses in the switch are different.

Fig. 6-17 show the phase change when the voltages of the VGAs are varied. For Case A, the phase coverage is from $-90°$ to $90°$. For Case B, the phase coverage is from -270° to -90°. There are also overlaps of traces which mean that there is more than one combination of VGA control that can produce the same phase difference.
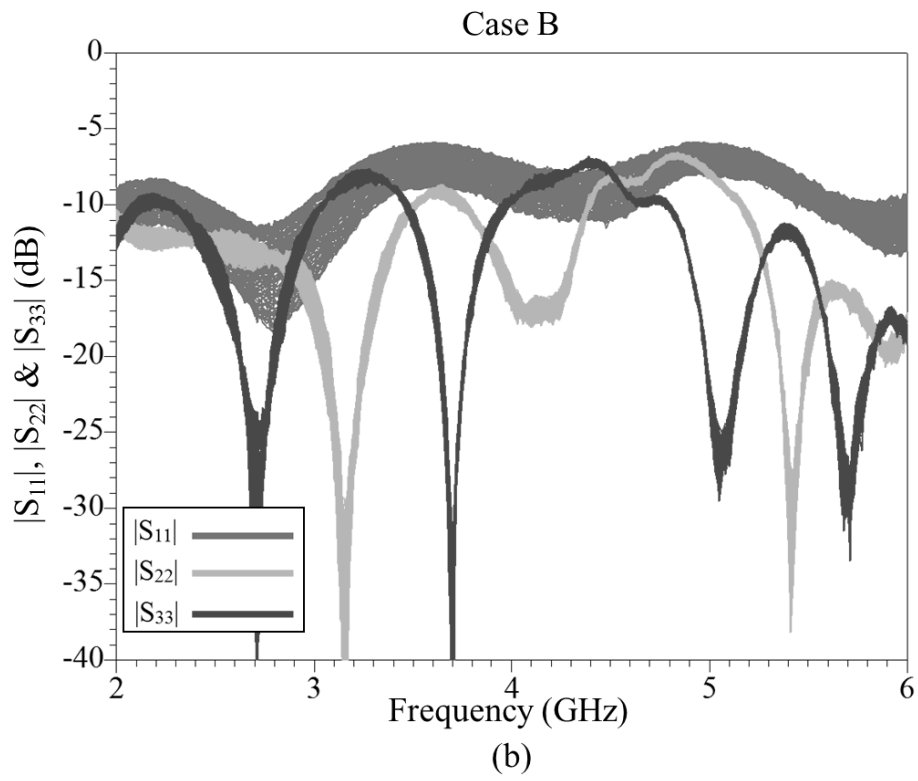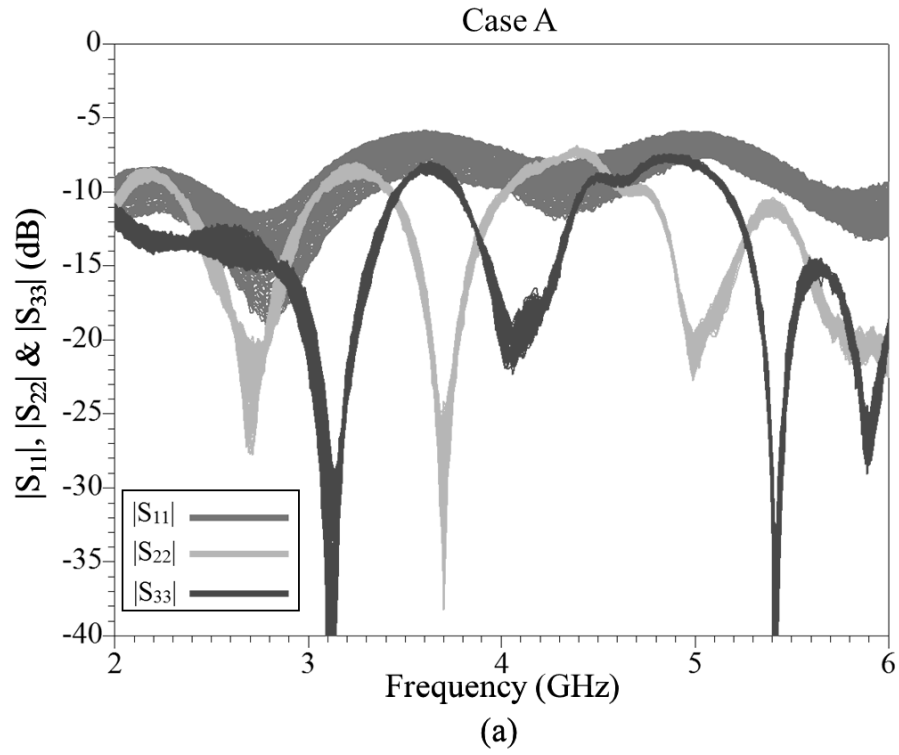
Fig. 6-13: Measured $|S_{11}|$, $|S_{22}|$ and $|S_{33}|$ for (a) Case A and (b) Case B.
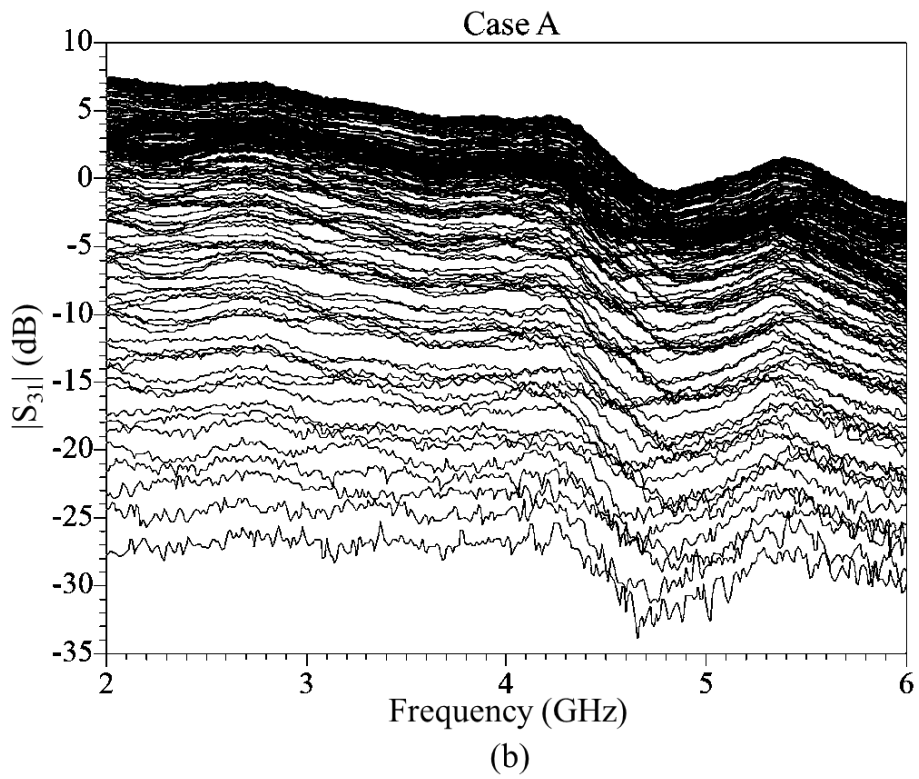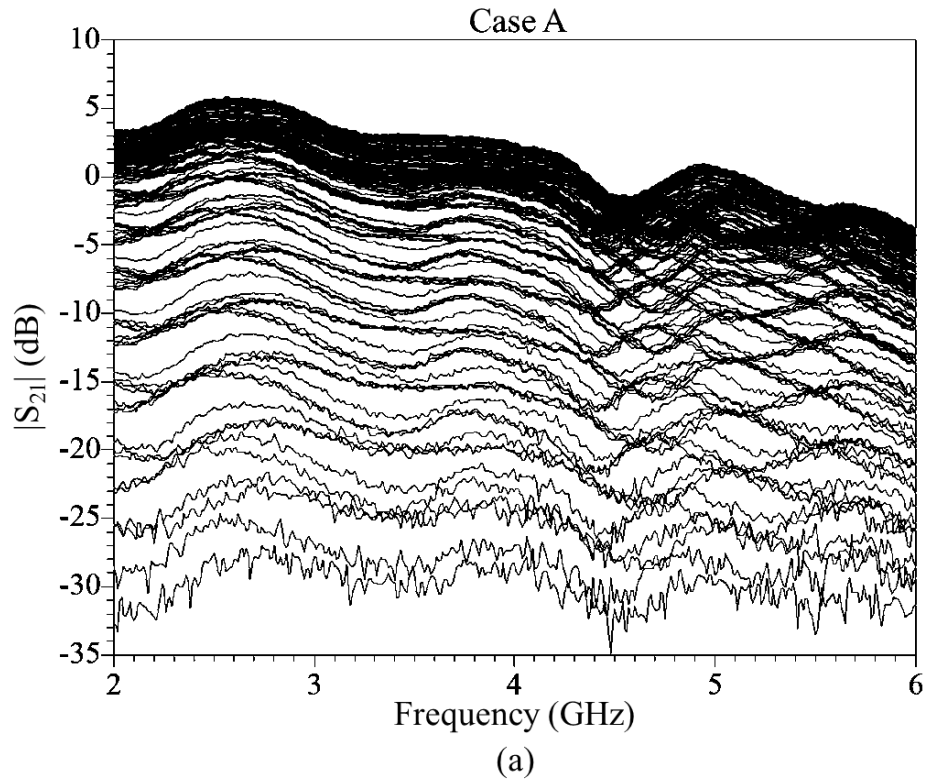
Fig. 6-14: Measured (a) $|S_{21}|$ and (b) $|S_{31}|$ Case A.

100
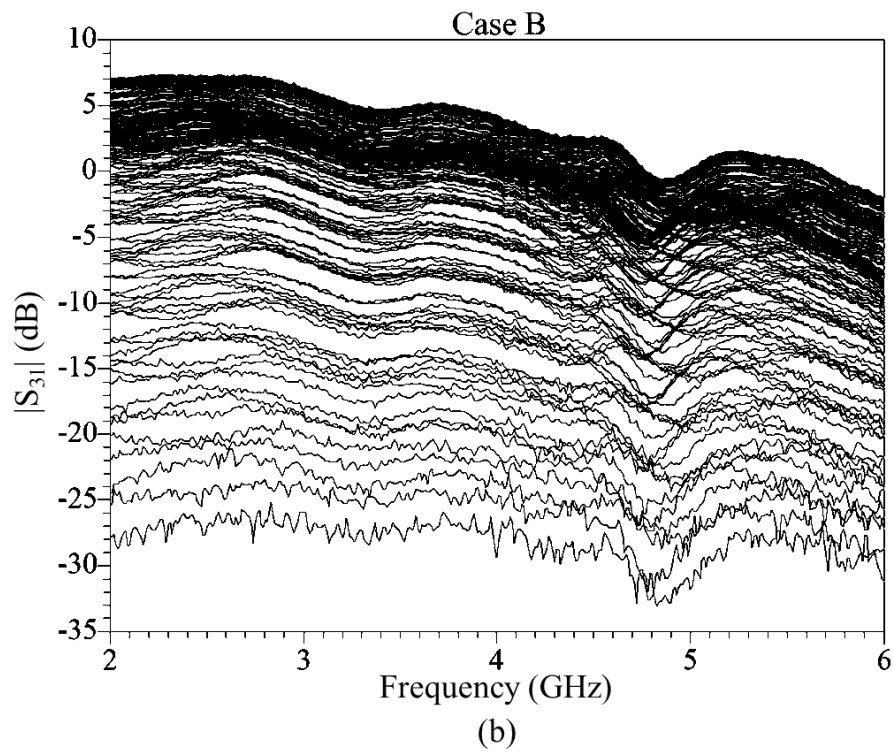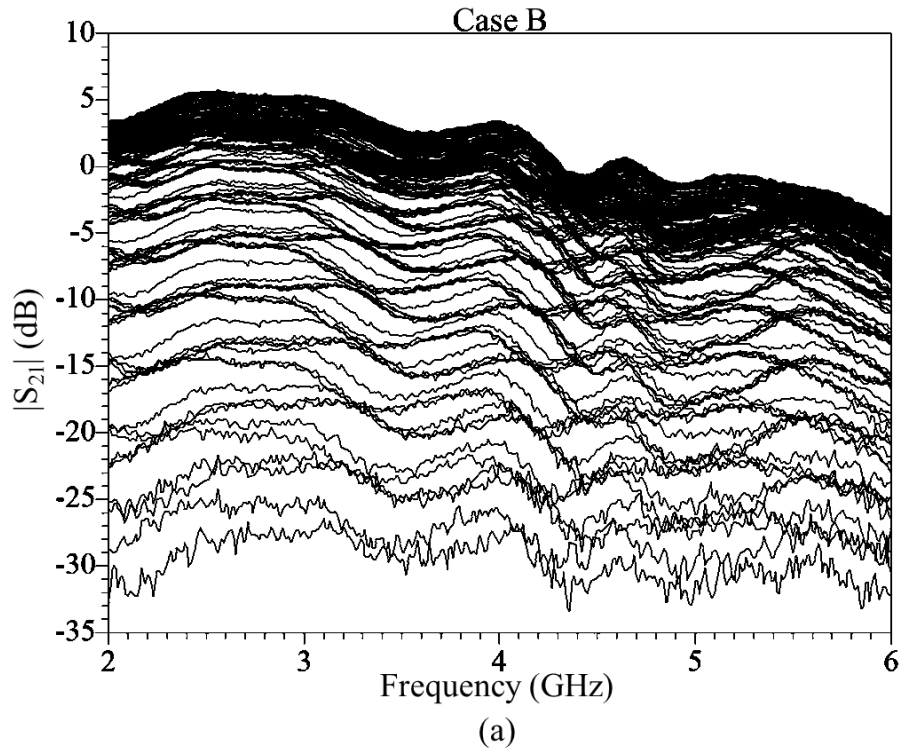
Fig. 6-15: Measured (a) $|S_{21}|$ and (b) $|S_{31}|$ Case B.

101
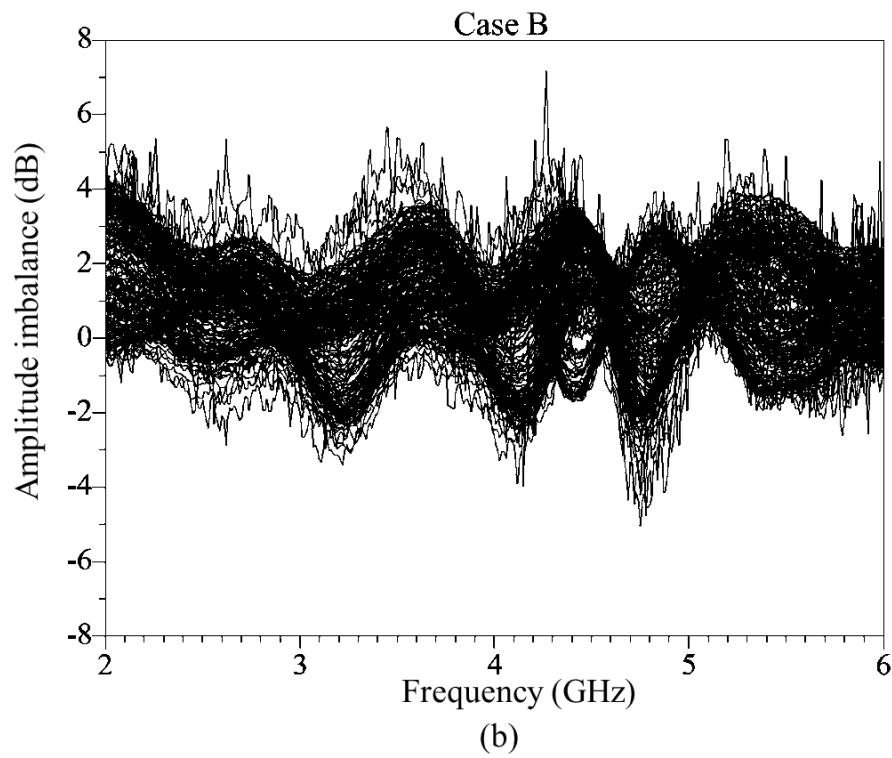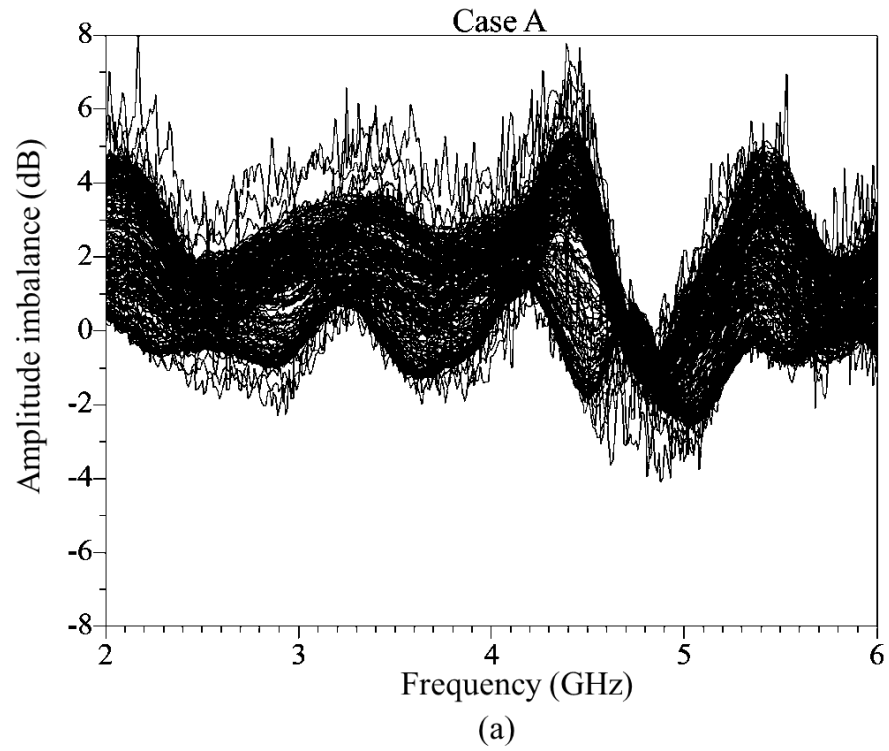
Fig. 6-16: Measured amplitude imbalance for (a) Case A and (b) Case B.
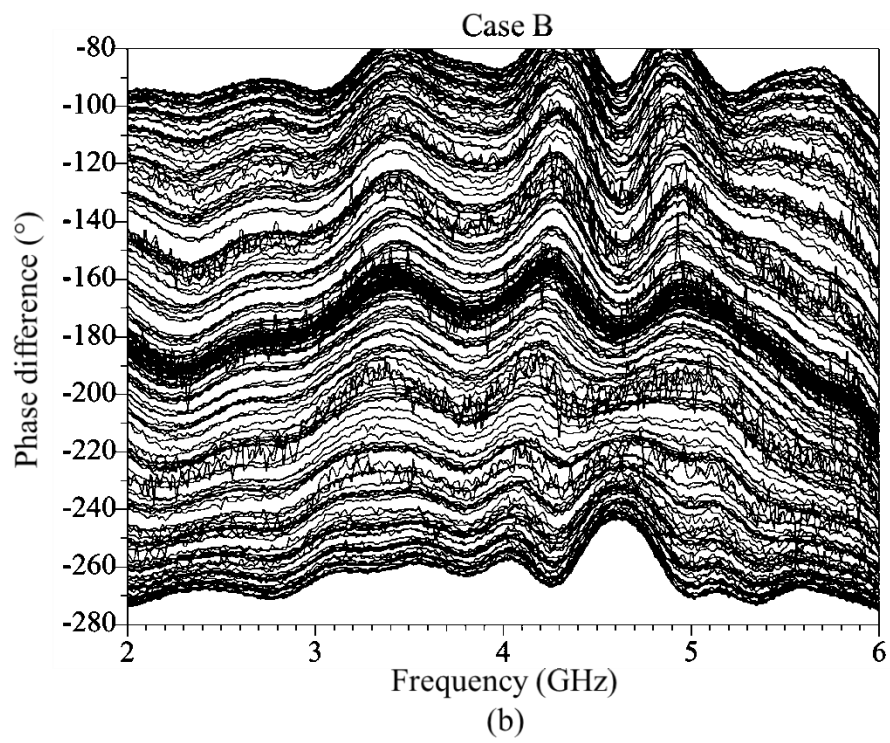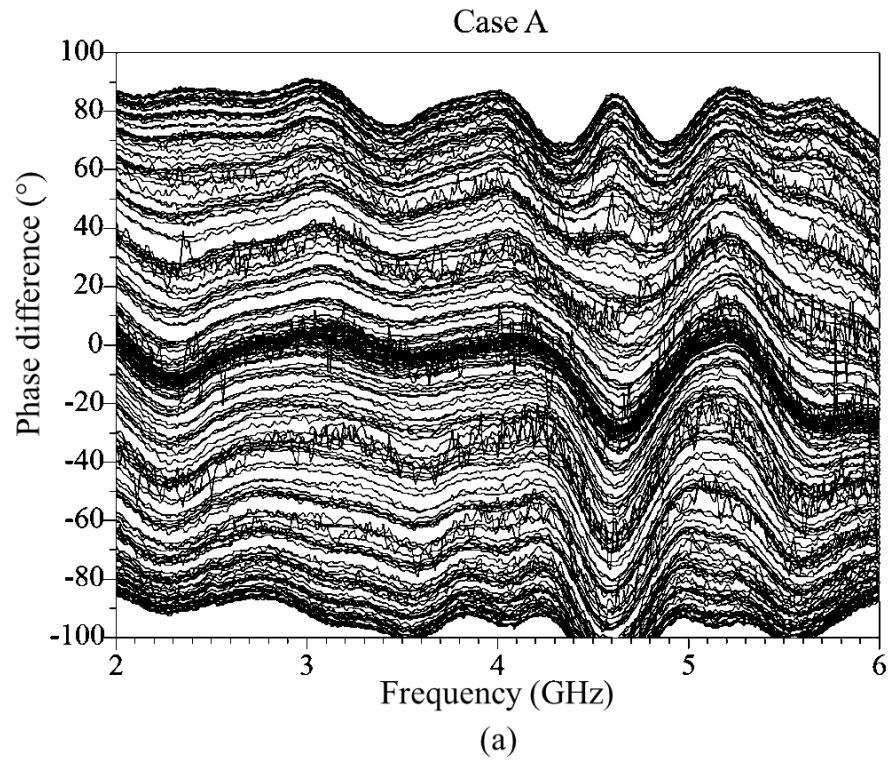
Fig. 6-17: Measured phase difference for (a) Case A and (b) Case B.

103

The mean phase differences between the two outputs are calculated for frequencies between 2 GHz to 6 GHz. Fig. 6-18 shows the mean phase difference for the different applied voltages at the VGAs. It can be observed that it is possible to change the phase difference with one control voltage, i.e. fix one VGA to a fixed voltage while varying the other VGA. As the control voltages increase, the increase in gain drops until the maximum gain of the VGA is reached. This results in compression in the phase difference being observed. Fig. 6-19 shows the RMS phase error of the circuit. For Case A, the RMS phase error is less than 9°. For case B, the RMS phase error is less than 11°. The RMS phase error will improve if the bandwidth decreases or the outlying values are discarded. In addition, improving the matching between the cascaded components will help to reduce the phase error as the phases of the signals are affected by the weighted average of the amplitude at the vector sum stage.
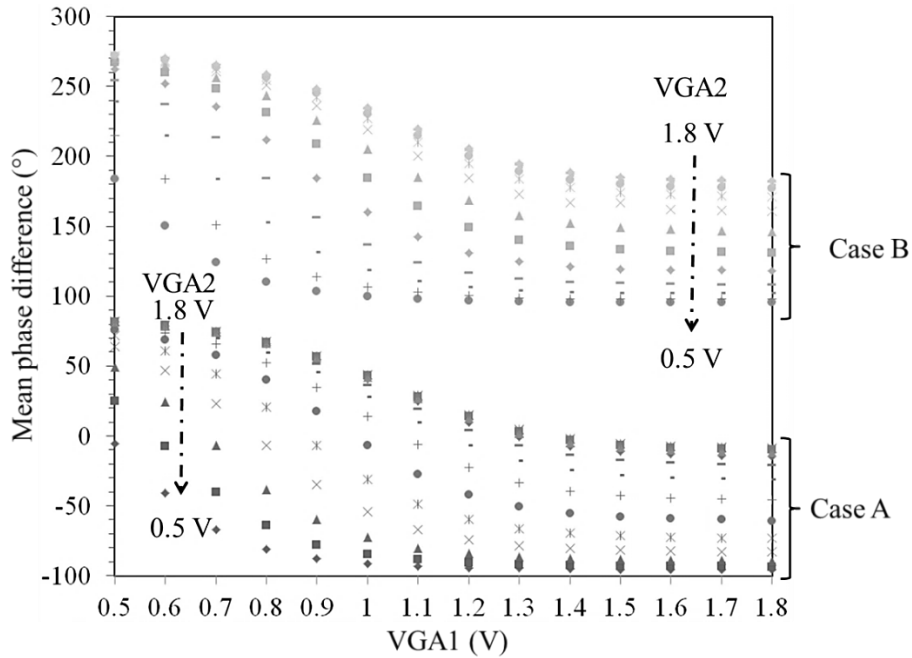
Fig. 6-18: Mean phase difference for 2 GHz to 6 GHz.
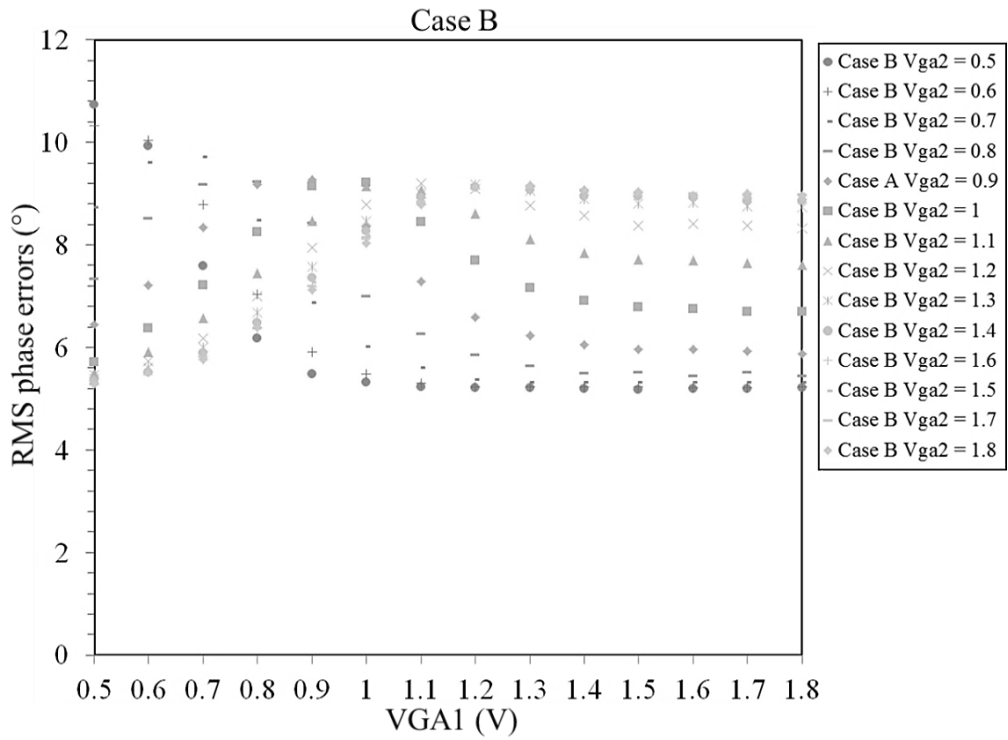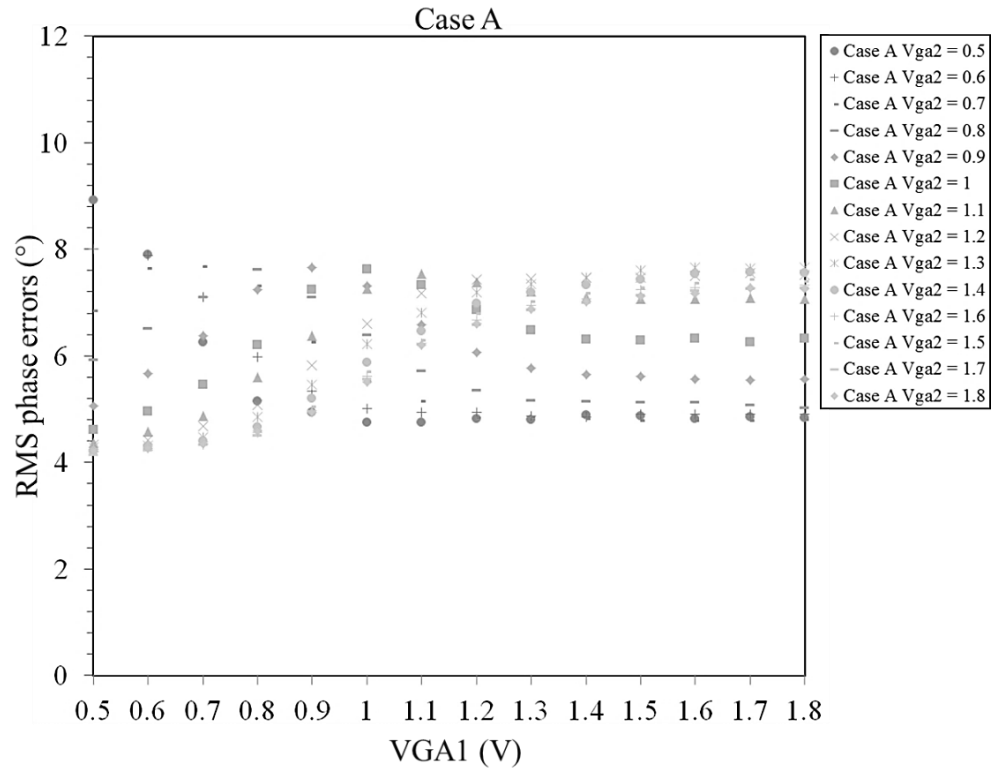
Fig. 6-19: RMS phase error for 2 GHz to 6 GHz.

105
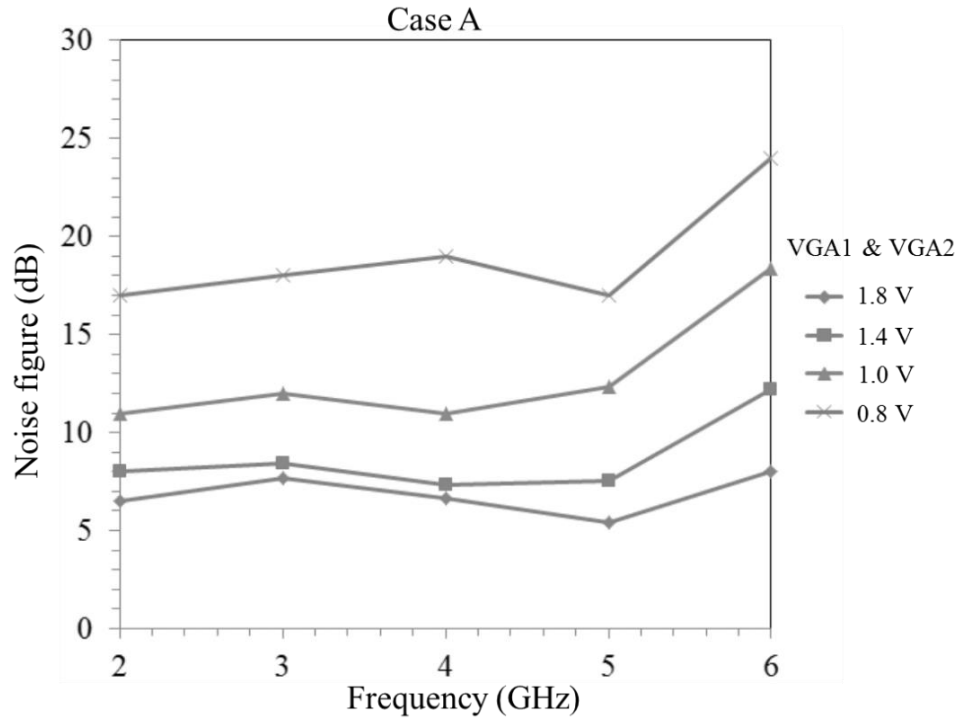
Fig. 6-20: Noise figure of the path between port 2 and 1 (Case A).
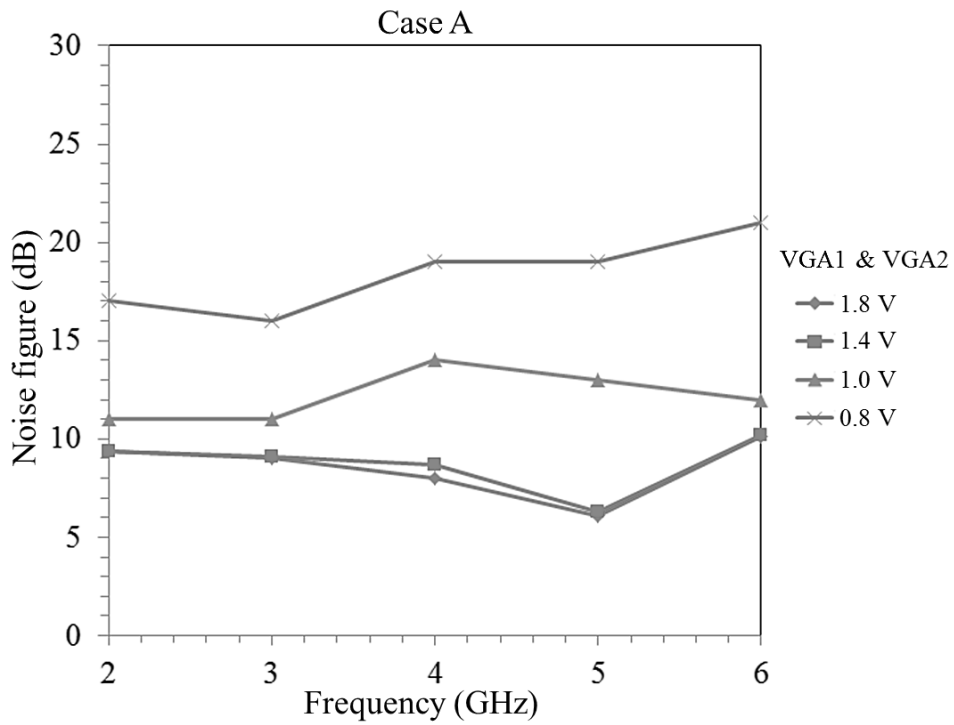
Fig. 6-21: Noise figure of the path between port 3 and 1 (Case A).
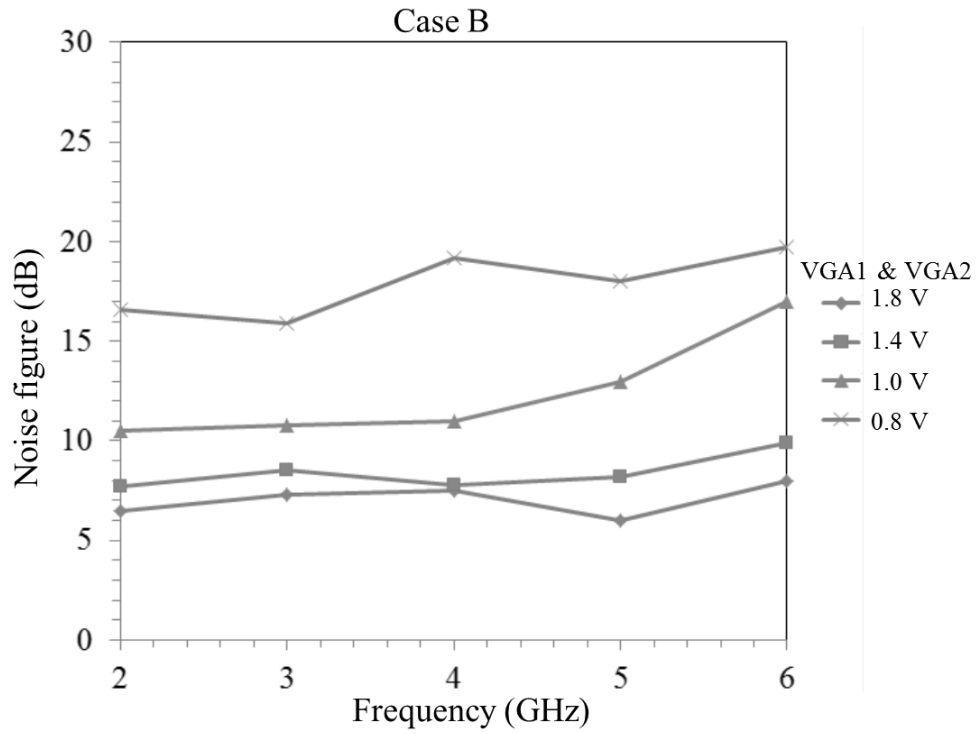
Fig. 6-22: Noise figure of the path between port 2 and 1 (Case B).
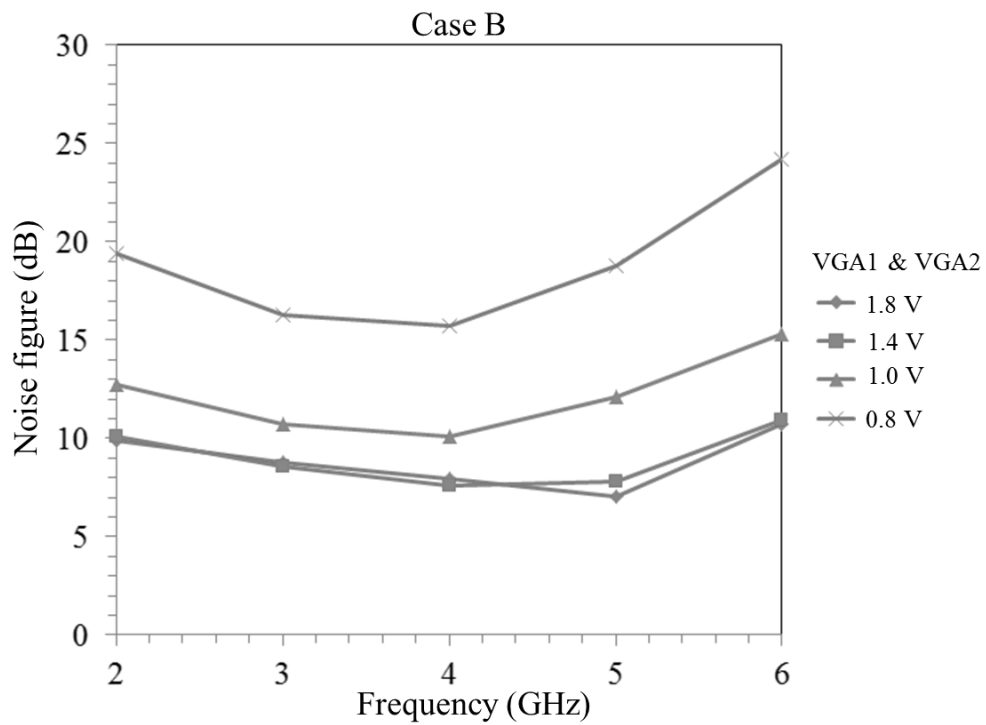
Fig. 6-23: Noise figure of the path between port 3 and 1 (Case B).

A HP 8971C noise meter test set is used to measure the noise figure of the circuit. The noise figures between the input port and output ports are measured. Fig. 6-20 to Fig. 6-23 show the measured results. Fig. 6-20 and Fig. 6-21 correspond to the Case A settings while Fig. 6-22 and Fig. 6-23 correspond to the Case B settings shown in Table 6-1. The noise figure increases as the gain of the variable amplifiers decreases. This is similar to the trend reported in the data sheets of the variable gain amplifiers. The variable gain amplifiers are reported having a noise figure of 4.2 dB at 1.8 V and 19 dB at 0.65 V. At 6 GHz, the measured noise figure tends to be higher. A possible reason is that the insertion losses of the RF switches increase at 6 GHz.
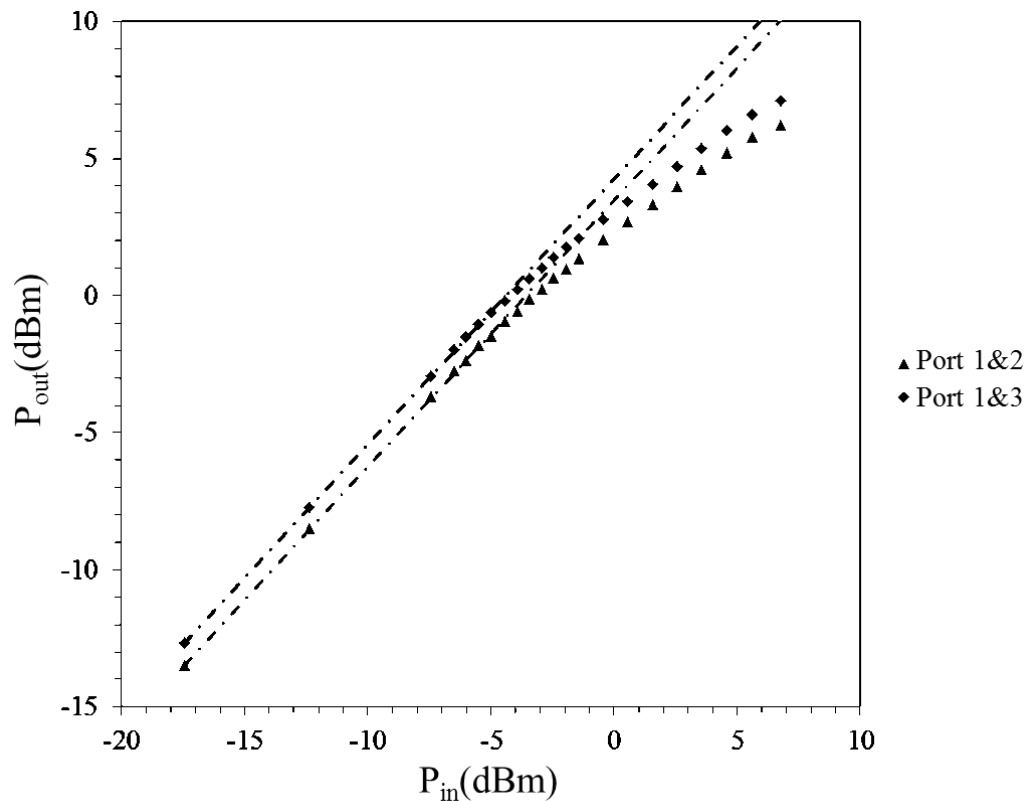
Fig. 6-24: Measured input and output power at 4 GHz (VGA1 = VGA2 = 1.8 V).

The input power and output power of the circuit are measured using Agilent E8257D signal generator and Rohde & Schwarz power meter. The input power is varied from -15 dBm to 10 dBm. The measured input power to the circuit is from -17.45 dBm to 7.75 dBm. The output power is measured using power meter. Fig. 6-24 shows the measured input power and output of the circuit at 4 GHz when the VGAs voltages are set to 1.8 V. From the figure, the predicted 1 dB compression point occurs at around -0.44 dBm.

Table 6-2: A performance comparison of the 360° phase shifters.

Method	Freq. (GHz)	Phase range	RMS phase error (°)	RMS amplitude error (dB)	P1dB (dBm)	Technology	Ref.
Vector sum	2.3 – 4.8	360°	1.4	1.1	1.8	0.18 μm CMOS	[12]
Switched network	2.5 – 3.2	360°	2	-	12/2 (Tx/Rx)	0.18 μm CMOS	[36]
Vector sum	5 – 18	360°	10	1.7	-5.4	0.13 μm CMOS	[37]
Vector sum	6 – 18	360°	5.6	1.1	-	SiGe BiCMOS	[38]
Vector sum	2 – 3	360°	5	1.2	-13.5	0.18 μm CMOS	[11]
Switched network	9 – 15	360°	<12	<2.2	-	0.18 μm CMOS	[39]
Vector sum	2 – 6	360°	<11	1.3	-0.44	PCB	This work

Table 6-2 compares the performance of the proposed phase shifter with the other reported phase shifters. Except for the RMS phase error, the proposed circuit has achieved a performance that is comparable with its competitors. It is possible to lower the RMS phase errors by avoiding settings that result in high errors since more than one VGA settings can be used to achieve the same phase shift.

It is important to point out that while Table 6-2 is useful in gauging the performance of the proposed phase shifter, it has its limitation. A full comparison, which considers the return losses, the insertion losses, the total power consumption and the size of the phase shifters, is needed before the merit of the proposed phase shifter design can be accurately determined. Additionally, most of the vector sum phase shifters are implemented as integrated circuits and are two-port devices. The proposed phase shifter, on the other hand, is implemented on PCB and is a three-port device. As such, the comparison in Table 6-2 is not a one to one comparison and caution has to be exercised. Nevertheless, the comparison has provided some insights to the potential of the circuits.

6.4 Conclusions

The functionalities of the two-way vector sum phase shifters using Quadrature Magic-T have been verified with the measurement results of the fabricated circuit. The circuit is able to achieve 360° phase shifting between the outputs. An unequal amplitude imbalance is observed which is probably due to an unequal power split at the Quadrature Magic-T. This can be compensated by the

power amplifiers at the next stage. The overall performance of the circuit can be improved by designing the circuit as a whole. Nevertheless, the phase control between the two outputs is shown.

Chapter 7 Polarization controller architecture

7.1   Introduction

Considering the pros and cons of the control circuits for the existing polarization controllers, the two-way vector sum shifter has been proposed for application in polarization control. In this chapter, the integration between the circuit and the antenna to achieve different polarizations will be analyzed. In addition, a comparison of the proposed circuit performance with the circuit proposed in [9] is made.

7.2   Proposed polarization controller architecture

Fig. 7-1 shows the proposed connection between the vector sum phase shifter and the dual polarized antenna. The circuit can be divided into three parts.
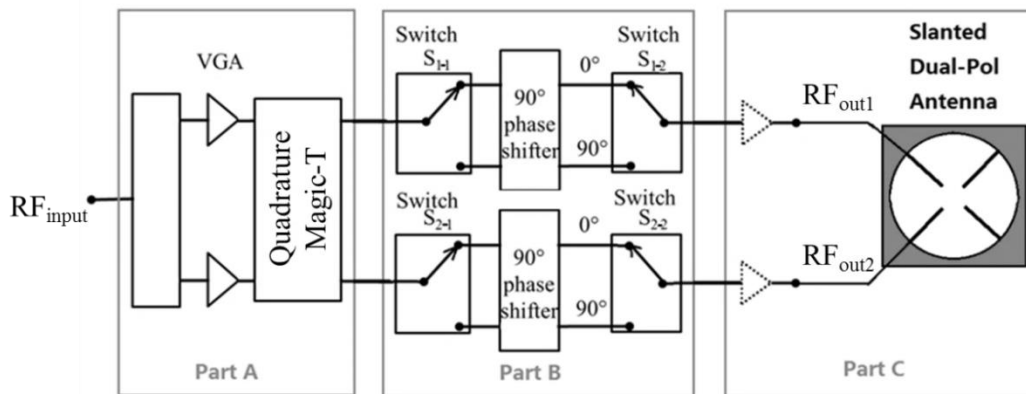
Fig. 7-1: Proposed polarization controller block diagram.

Part A and Part B are the two parts of the vector sum phase shifter proposed in Chapter 2. Part C illustrates the potential connection between the

vector sum phase shifter (polarization controller) and the dual-polarized antenna. The output signals from Part B are fed to the power amplifiers as what is normally done in a transmitter. However, the amplified signals, instead of being combined by another hybrid circuit as shown in Fig. 1-5, are directly fed to the two feeds of the dual polarized antenna. The radiated signals will be vector-combined in space to achieve the required polarization. Without the extra hybrid, the power efficiency can be improved as the circuit dissipates less power. In addition, the amplitude and phase error can also be improved as less error is introduced.

The polarization that can be achieved by the circuit is also dependent on the placement of the dual polarized antenna. Assuming the two radiators of the antenna are arranged in slant -45° and +45° direction respectively, four main polarizations, V, H, RHCP and LHCP, can be achieved with full power when the phase difference between the two signals is 0°, 180°, 90° and 270° respectively. With this configuration, slant +/- 45 polarizations can only be achieved with half of the total power by switching off one of the power amplifiers. Table 7-1 lists the achievable main polarizations.

Table 7-1: Achievable polarizations through spatial power combining.

Excitation to dual polarization antenna			Resultant polarization	Remark
Slant – 45°	Slant +45°	Phase difference (°)		
1	1	0	V	Full power
1	1	180	H	Full power
1	1	90	LHCP	Full power
1	1	-90	RHCP	Full power
1	0		Slant -45°	Half power
0	1		Slant +45°	Half power

7.3 Comparison of the polarization control circuits

The circuit in [9] is compared with the proposed circuit. The circuit proposed in [9] achieves polarization control by varying the amplitude of the signals fed to the V-pol and H-pol of the dual polarized antenna. The amplitude of the signals is varied by adjusting the phase settings of the phase shifters. From equations (1-3) and (1-4), it can be observed that the amplitude of the output signals depends on the phase difference between the phase shifters. When both phase shifters have the same phase shift, the amplitudes of the two output signals are equal. When the phase shift is 45°, the signal at one of the outputs is maximum while the other is at 0. The equations have also shown that both output signals have the same insertion phases.

For the circuit proposed in this work, the polarization control is achieved by controlling the phase difference between the signals fed to the antenna ports. The phase difference between the output signals is adjusted by the gain of the variable gain amplifiers. From equations (2-3), (2-4) and (2-5), it can be observed that the phase difference between the signals is dependent on the gain of the VGAs. When the gains are equal, the phase difference will be 0° or 180° depending on the switch state of the RF switches. When either of the amplifier is switched off, the phase difference will be 90° or -90°. The equations have shown that both outputs have the same amplitudes.

As the output from the circuit in [9] only varies in the amplitude, it is suitable for linear polarizations control. The circuit proposed in this work is able to achieve linear (slant -45°), circular and elliptical polarizations.

When used in phased arrays, the circuit proposed in [9] has the advantage of varying the insertion phase of the signals without introducing any phase difference between the output ports nor affect the amplitude difference. As such, that circuit can be used to control the phasing of the phased array as each array unit can be separately adjusted to achieve different phase output.

For the proposed circuit, the phasing control and the polarization control for the phased array have to be implemented separately. However, this design is able to maintain the same phase difference between the ports while varying the amplitude of the output signals. This is useful for scenarios where amplitude tapering is needed to reduce the sidelobes.

In terms of implementation, the proposed circuit uses vector sum phase shifters which can easily achieve a continuous phase shift. The circuit in [9] uses lumped components and discrete phase states are realized. For lumped component implementation, fixed phase shifters which are compact in size, wide in bandwidth and large in phase shift values are needed. For vector sum phase shifters, wideband variable gain amplifiers with matched ports and linear performance are required. Both implementations have their own merits and challenges.

The Lange coupler is commonly used for wide band performance. However, it is less suitable for implementation on PCB. In addition, an 180° phase shifter is needed. The Quadrature Magic-T is slightly easier to implement on PCB compared to the Lange coupler. In addition, it removes the need to implement a 180° phase shifter separately. However, it is less compact in design compared to the Lange coupler.

In the proposed circuit, EM signals from power amplifiers are combined spatially. This reduces the circuit losses that will occur if another Lange coupler is being used. The proposed circuit can be implemented on a chip. Its size is expected to shrink with the increase in frequency. Table 7-2 is a summary of the key differences of the two polarization circuits.

Table 7-2: A comparison of the polarization control circuits.

	Circuit in [9]	Proposed circuit
1	Amplitude difference between the output ports varies with the phase shifter settings	Phase difference between the output ports varies with variable gain amplifier settings
2	For the same amplitude imbalance, the insertion phase may be different	For the same phase difference, the amplitude of the output signals can be varied
3	Phase shifters uses lumped component implementation	Vector sum phase shifter are used
4	Lange coupler for 90° vector summation	Quadrature Magic-T used for vector summation
5	The EM signals are combined using Lange coupler	The EM signals are combined using spatial combining

7.4   Polarization control circuits in phased arrays

Fig. 7-2 shows the proposed phased-array control circuits. The circuit is Fig. 7-2 (a) controls the polarization and the phase simultaneously. In Fig. 7-2 (b), the phase and the polarization are controlled separately; the first two levels of the circuit control the phase difference among the antenna elements while the third level of circuits controls the polarization.

(a)

(b)
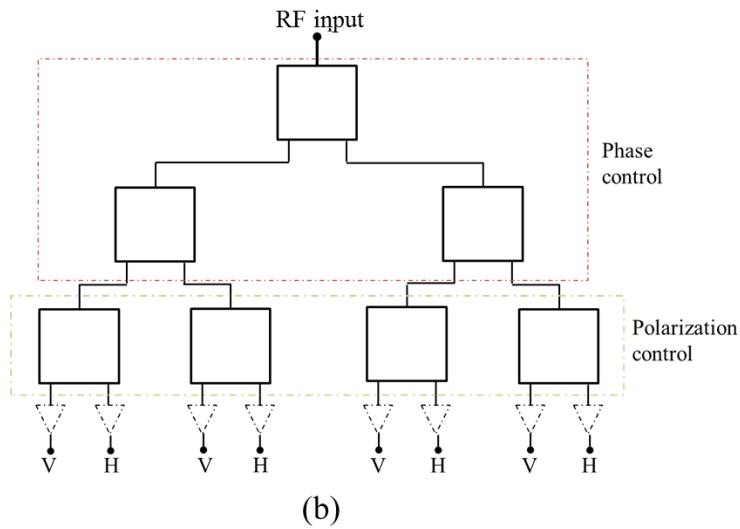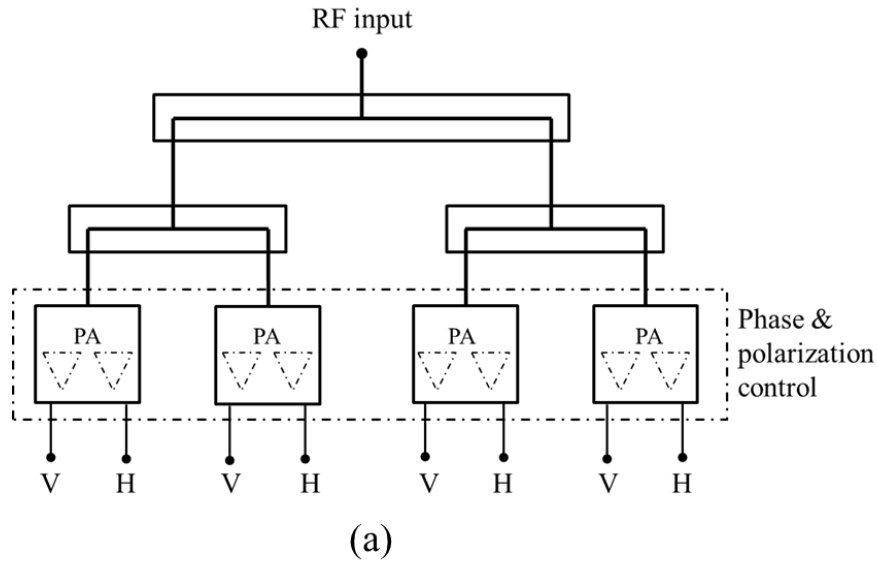
Fig. 7-2: Proposed feeding network (a) using circuit in [9] and (b) using proposed circuit.

On the schematic level, the architecture in Fig. 7-2 (a) is simpler than that of Fig. 7-2 (b). However, the difficulty will increase as the number of antenna elements increases due to the need to set all the phase shifters. Fig. 7-2 (b) controls the phases row by row. In addition, the signals are amplified by the

variable gain amplifiers. As such, there is no need to include extra amplifiers to boost the signal.

7.5   Conclusions

A polarization controller circuit is proposed. It uses a two-way vector sum phase shifter proposed in this work and the concept of spatial power combination. The two-way vector sum phase shifter is made up of a novel magic T circuit, broadband 90° phase shifters and VGAs. It can achieve continuous 360° phase shift. Spatial power combination has the merit of reducing power loss due to the circuit. When dual polarized antenna is used together with the vector sum phase shifter, polarization control can be achieved. Besides achieving polarization control, the circuit can be used for phase control too.

Chapter 8 Conclusions and recommendations

8.1 Conclusions

The polarization of electromagnetic waves has important applications in communication and radar. When a dual polarized antenna is used, it is possible to achieve different polarization of the electromagnetic wave by changing the magnitude and the phase of the signals feed to the antenna. In this work, an alternative polarization controller architecture using a two-way vector sum phase shifter is proposed. Using this architecture, it is possible to achieve ±slant 45°, circular and elliptical polarization.

The proposed two-way vector sum phase shifter consists of a power divider, two variable gain amplifiers, a Quadrature Magic-T, four RF switches and two 90° phase shifters. The circuit is able to achieve 360° continuous phase tuning between the two output signals while maintaining the amplitude of the signals are equal. During the implementation of the vector sum phase shifter, the subcomponents are designed and tested.

For the vector summation, instead of choosing the commonly used Lange coupler, Quadrature Magic-T is used. Quadrature Magic-T is a planar 180° hybrid that has an extra section of quarter-wavelength transmission line added to the sum port. This design allows it to retain the characteristics of 180° hybrid while acquiring the phase characteristics of a quadrature hybrid. In addition, when compared to a typical 180° hybrid, the slope of the insertion phases is aligned

over a larger bandwidth for the Quadrature Magic-T. For the fabricated circuit, the phase difference between Port 2 and Port 3 is between 178° and 180° from 2 GHz to 5.4 GHz when the delta-port is excited; the phase difference is between -1.1° and 0.824° when the sum-port is excited. When both the sum- and delta-ports are excited in phase and simultaneously, the phase difference of the two signals at Port 2 is between 83° and 92° from 2 GHz to 5.4 GHz; the phase difference at Port 3 is between 87° and 97°.

The broadband 90° phase shifter is designed and implemented. The structure of the phase shifter is similar to that of Schiffman phase shifter except that it has a bandpass and all-pass topology. The phase shifter is able to achieve greater than 15 dB return losses from 2 GHz to 6 GHz. The phase shift that can be achieved is 90° and with a phase error of about ±7.5° from 2 GHz to 6 GHz.

A prototype of the two-way vector sum phase shifter using PCB is fabricated and measured. The circuit has demonstrated full phase coverage from 2 GHz to 6 GHz. Across the whole frequency band, the maximum RMS phase error measured is 11°.

8.2   Recommendations

The mathematical analysis has shown that the polarization of the dual polarized antenna can be controlled by varying the phase difference between the two input signals. The fabricated circuit has demonstrated the feasibility of the proposed two-way vector sum phase shifter to achieve broadband, continuous 360° phase tuning. However, further work to improve its performances such as return

losses and reduce its size is needed before the circuit can be used in real communication or radar systems.

The prototype of the circuit is built by simply cascading individually designed components. The performance of the circuit will improve if the whole circuit is designed as one. This is because the phase and amplitude compensation can be added. In addition, the matching of the circuit can be adjusted for optimum performance.

While the performance of the Quadrature Magic-T is relatively wide, it is insufficient to cover the whole bandwidth. Further work to improve the bandwidth of the circuit is needed.

Though this two-way vector sum phase shifter is designed for polarization controller, its 360° continuous phase control between the two ports allows it to be used as the phase control in phase arrays. The possible architecture for the phasing circuit has been shown in Section 0. Further work to combine the sub circuits into a phasing circuit can be explored.

Bibliography

[1]   J. L. Blanton, "Device and method for polarization control for a phased array antenna," U. S. Patent US7436370 B2, Oct. 14, 2005.

[2]   EMS Techonolgies Inc. (2003, March). Application Note POL-1 Phased Array Polarization Switches, [Online]. Available: http://www.dandsmicrowave.com/papers/Williams-Brunasso_Phased%20Array%20Polarization%20Switches.pdf.

[3]   S. Hirotoshi and U. Toshiaki, "Clutter signal suppression radar," U.S. Patent US3918055 A, Nov. 4, 1975.

[4]   Y. Chang, Y. Li, W. Wang and S. Xiao, "New target detection method in strong active jamming background for polarimetric radar," in *IEEE 10th Int. Conf. on Signal Processing (ICSP),* Beijing, Oct. 2010, pp. 1947-1950.

[5]   U. A. Bakshi and A.V. Bakshi, Electromagnetic Wave Theory, Pune: Technical Publisher Pune, 2009.

[6]   D. Adamy, Introduction to Electronic Warfare Modeling and Simulation, North Carolina: Scitech Publishing Inc., 2006.

[7]   J. Lu, C. Y. Poh, Y. P. Lim and P. Bhandari, "Compact wideband array with dual-polarization," in *2011 IEEE Int. Symp. on Antennas and Propagation (APSURSI),* Spokane, WA., July 2011, pp 612-615.

[8]   D. W. Corman, R. Zienkewicz and D. R. Saunders, "Multi-Beam active phased array architecture with independant polarization control," U.S. Patent US20130088391A1, April 11, 2013.

[9]   G. van der Bent, T. S. de Boer, R. van DijK, M. W. van der Graaf, A. P. de Hek, and F. E. van Vliet, "X-band phase shifting dual-output balanced amplifier MMIC," in *Proc. 39th European Microwave Conf. (EuMIC2009),* Rome, Sept 2009, pp 1665-1668.

[10]   S. J. Kim and N. H. Myung, "A new active phase shifter using a vector sum method," *IEEE Microw.and Guided Wave Letters,* vol. 10, no. 6, pp. 233-235, June 2000.

[11]   Y. Zheng and C. E. Saavedra, "Full 360 vector-sum phase-shifter for microwave system applications," *IEEE Trans. on Circuits and Systems,* vol. 57, no. 4, pp. 752-758, April 2010.

[12] A. Asoodeh and M. Atarodi, "A full 360° vector-sum phase shifter with very low RMS phase error over a wide bandwidth," *IEEE Trans. Microwave Theory and Tech.,* vol. 60, no. 6, pp. 1626 -1634, June 2012.

[13] P. J. Peng, J. C. Kao and H. Wang, "A 57-66 GHz vector sum phase shifter with low phase/amplitude error using a wilkinson power divider with LHTL/RHTL elements," *IEEE Compound Semiconductor Integrated Circuit Symp. (CSIC)*, pp.1-4, Oct. 2011.

[14] L. Bui, K. Ghorbani and A. Mitchell, "Multi-channel vector sum phase shifter," *Optics Letters,* vol. 31, no. 5, pp. 577-579, 2006.

[15] H. Erkens, R. Wunderlich, and S. Heinen, "A Comparison of two RF vector-sum phase shifter concepts," *German Microwave Conference, Munich*, March 2009, pp. 1-5.

[16] D. M. Pozar, Microwave Engineering, 4th Edition, Wiley Global Education, 2011.

[17] E. G. Cristal and L. Young, "Theory and tables of optimum symmetrical TEM-mode coupled transmission line directional couplers," *IEEE Trans. Microwave Theory Tech,* vol. 13, no. 5, pp.544 -558, Sept. 1965.

[18] S. M. H. Javadzadeh, S. M. S. Majedi and F. Farzaneh, "An ultra-wideband 3-dB quadrature hybrid with multisection broadside stripline tandem structure," in *Mobile Multimedia Communications*, Springer Berlin Heidelberg, 2012, pp. 672-681.

[19] S. March, "Phase Velocity Compensation in Parallel-Coupled Microstrip," in *1982 IEEE MTT-S Int. Microwave Symp. Dig.*, Dallas, 1982.

[20] M. Dydyk, "Accurate design of microstrip directional couplers with capacitive compensation," in *1990 IEEE MTT-S Int. Microwave Symp. Dig.*, Dallas, TX., May 1990, pp. 581-584.

[21] K. S. Ang and Y. C. Leong, "Converting baluns into broad-band impedance-transforming 180° hybrids," *IEEE Trans. Microwave Theory and Tech.,* vol. 50, no. 8, pp. 1990-1995, Aug. 2002.

[22] I. Robertson and S. Lucyszyn, "Phase Shifters," in *RFIC and MMIC Design and Technology*, London, IET, pp. 381-428, 2001.

[23] X. Tang and K. Mouthaan, "Loaded-line phase shifter with enlarged phase shift range and bandwidth," in *Proc.40th European Microwave Conf.,* Paris, Sept. 2010, pp. 818-821.

[24]   W. Li, Y. Kuo, Y. Wu, J. Cheng, T. Huang and J. Tsai, "An X-band full-360° reflection type phase shifter with low insertion loss," in *Proc. 42nd European Microwave Conf.,* Amsterdam, Oct.-Nov. 2012, pp. 1134-1137.

[25]   K. Miyaguchi, M. Hieda, K. Nakahara, H. Kurusu, M. Nii and et. al., "An ultra-broad-band reflection-type phase-shifter MMIC with series and parallel LC circuits," *IEEE Trans. Microwave Theory and Tech.,* vol. 49, no. 12, pp. 2446-2452, Dec 2001.

[26]   X. Tang and K. Mouthaan, "Design Considerations for Octave-Band Phase Shifters Using Discrete Components," *IEEE Trans. Microwave Theory and Tech.,* vol. 58, no. 12, pp. 3459-3466, Dec. 2010.

[27]   J. Quirarte and J. Starski, "Novel Schiffman phase shifters," *IEEE Trans. Microwave Theory and Tech.,* vol. 41, no. 1, pp. 9-14, Jan. 1993.

[28]   Y. X. Guo, Z. Y. Zhang and L. C. Ong, "Improved wide-band Schiffman phase shifter," *IEEE Trans. Microwave Theory and Tech.,* vol. 54, no. 3, pp. 1196-1200, March 2006.

[29]   H. K. Oh, W. Y. Lim and K. K. Chan, "Compact Single Layer Planar Wideband 180° Balun Networks," *IEEE Antennas and Propagation Society Int. Symp.*, 2010.

[30]   J. K. Hunton, "New Differential Phase Shift Networks Combining All-Pass and Band-Pass Elements," in *1981 IEEE MTT-S Int. Microwave Symp. Dig.*, Los Angeles, June 1981, pp. 223-225.

[31]   Z. Hu and K. Mouthaan, "A 2–6.5 GHz CMOS variable gain amplifier for vector-sum phase shifters," in *2012 Asia-Pacific Microwave Conference Proceedings (APMC),* Kaohsiung, Dec. 2012, pp. 94-96.

[32]   Hittite Microwave Corporation, "GaAs MMIC Analog Variable Gain Amplifier," 2013. [Online]. Available: http://www.hittite.com/content/documents/data_sheet/hmc972lp5.pdf.

[33]   Avago Technologies (2012, Dec. 26), "VMMMIK-3503 0.5 - 18 GHz Variable Gain Amplifier in SMT Package,". [Online]. Available: http://www.avagotech.com/docs/AV02-2918EN.

[34]   R. Cory (2009, May), "RF/Microwave Solid State Switches," [Online]. Available: http://www.skyworksinc.com/downloads/press_room/published_articles/MPD_052009.pdf.

[35] Skyworks Solution (2012, Aug. 9). "SKY13286: 0.1 to 6 GHz High Isolation SPDT Absorptive Switches," [Online]. Available: http://www.skyworksinc.com/uploads/documents/200570H.pdf.

[36] M. Meghdadi, M. Azizi, M. Kiani, A. Medi, and M. Atarodi, "A 6-bit CMOS phase shifter for S-band," *IEEE Trans. Microwave Theory and Tech.*, vol. 58, no. 12, pp. 3519–3526, Dec 2010.

[37] K. J. Koh and G. M. Rebeiz, "0.13-um CMOS phase shifters for X-, Ku-, and K-band phased arrays," *IEEE J. Solid-State Circuits*, vol. 42, no. 11, pp. 2535–2546, Nov. 2007.

[38] K. J. Koh and G. M. Rebeiz, "A 6–18 GHz 5-bit active phase shifter," in *2010 IEEE MTT-S Int. Microwave Symp. Dig.*, Anaheim, May 2010, pp. 792–795.

[39] D. W. Kang, H. D. Lee, C. H. Kim, and S. Hong, "Ku-band MMIC phase shifter using a parallel resonator with 0.18-um CMOS technology," *IEEE Trans. Microwave Theory and Tech.,* vol. 54, no. 1, pp. 294–301, Jan. 2006.